# DISSERTATION

**Entitled**

# A STUDY OF THE MAGNESITE MINERALISATION AND ITS POTENTIAL ENVIRONMENTAL IMPACT IN THE TSHIPISE MAGNESITE FIELD, LIMPOPO PROVINCE OF SOUTH AFRICA


**Submitted by**

**Lutendo Desmond Mutshaine**
**Student No: 55362125**


**In fulfilment of the degree**

## MSc in Environmental Management

**Within the**


**Department of Environmental Sciences**
**College of Agriculture and Environmental Sciences**
**University of South Africa**

**Supervisor: Professor Baojin Zhao**
**Co-Supervisor: Dr Lindani Ncube**
**Co-supervisor: Mrs Helena J. van Niekerk**


**Date: February 2021**

# DECLARATION

I, Lutendo Desmond Mutshaine (student number 55362125), declare that “A study of the magnesite mineralisation and its potential environmental impact in the Tshipise magnesite field, Limpopo Province of South Africa**”** is my own work and that all the sources that I have used or quoted have been indicated and acknowledged through complete references.

11/11/2021

…… ……

SIGNATURE DATE

Mr. L.D. Mutshaine

# ABSTRACT

This study sought to determine the mineralisation of magnesite in the Folovhodwe, Venmag and Nyala Mines in the Tshipise area of the Limpopo Province in South Africa. The main aims of the study were to characterise the geology of the discussed mines, and to estimate the economic potential of extracting magnesite from the waste dump rocks and the impact of the Venmag Mine on environmental soil and surface water. Data were collected using the following methodologies: Field observation, Sampling and Laboratory work that comprised microscopy, X-Ray Diffraction (XRD), X-Ray Fluorescence (XRF) and Inductively Couples Plasma-Optical Emission Spectrometry (ICP-OES).

The study focused specifically on: (1) The source rocks of the magnesite ore; (2) The mineralisation type of magnesite; (3) The role of the dolerite dykes, sills, and structures on the mineralisation of magnesite; (4) The economic potential of the *in situ* magnesite and re-use of the waste rock dumps; and (5) The quality of environmental water and soil.

The researcher found that: (1) The magnesite host rock is ultramafic, rather than doleritic, as previously thought; (2) The magnesite mineralisation occurs as veins and is controlled by structures such as bedding plans and joints; (3) The geological sequential order is generalised as ultramafic rocks → dolerite dykes and sills → thermal water circulation → formation of magnesite veins; (4) The resource evaluation indicates mineable magnesite, both *in-situ* and from the waste rock dumps; (5) The waste dump rocks may be used for neutralising acid mine drainage due to their high alkalinity, or for road construction and bricks making due to their physical characteristics; (6) The water quality from the Venmag Mine pits and the Nwanedi River were not significantly impacted by magnesite mining activities during the season of this study; and (7) There was no major contamination of heavy metals from the waste rock dumps and their surrounding soil at the time of the study.

The researcher recommends that a study be done for the age of the magnesite mineralisation as well as the doleritic rocks, and reprocessing of the magnesite waste

rock dumps economically and technically in the Nyala, Venmag and Folovhodwe Mines.

# ACKNOWLEDGEMENTS

I would like to thank God Almighty in Heaven who has enabled me to complete this research project. Honour and Glory are his. I would also like to extend my appreciation to the following people who played a vital role during my dissertation writing journey:

- Prophet M.R. and Prophetess T. Sehlwane for their encouragement;

- My parents, Mr T.S. and Mrs L.C. Mutshaine for their support throughout my life;

- My supervisors Prof. B. Zhao, Dr. L. Ncube and Mrs. H. J. Van Niekerk for their guidance and incredible patience;

- The community of Folovhodwe and its Chief Mr. Nefolovhodwe for kindly allowing to carry out my research in their community; and

- Finally, yet very importantly, I would like to thank my family members - my brothers M. Mutshaine and T. Khomola for assisting me during my field work, and my wife and son for all their support.

# TABLE OF CONTENTS

# LIST OF FIGURES

# LIST OF TABLES

# LIST OF ABBREVIATIONS

| | |
|---|---|
| AUG: | Augite |
| BPG: | Best practice guidelines |
| CHL: | Chlorite |
| CPX: | Clinopyroxene |
| Cd: | Cadmium |
| Cl: | Chloride |
| Cu: | Copper |
| CZ: | Central Zone |
| DWA: | Department of Water Affairs |
| DWS: | Department of Water and Sanitation |
| DOL: | Dolomite |
| DMR: | Department of Mineral Resources |
| EC: | Electrical conductivity |
| EN: | Enstatite |
| F: | Fluoride |
| Fe: | Iron |
| Fm: | Formation |
| FM: | Folovhodwe Mine |
| FO: | Forsterite |
| GPS: | Global positioning system |
| GT: | Goethite |
| ICP-OES: | Inductively coupled plasma-optical emission spectrometry |
| IIM: | IImenite |
| K: | Potassium |
| Kt: | Kilotonnes |

| | |
|---|---|
| LMB: | Limpopo Mobile Belt |
| LZ: | Lizardite |
| M: | Molar |
| Mg: | Magnesium |
| MgO: | Magnesia |
| Mgs: | Magnesite |
| Mt: | Magnetite |
| Mt: | Million Tonnes |
| MC: | Microcline |
| Mn: | Manganese |
| MS: | Muscovite |
| NLTZ: | North Limpopo Thrust Zone |
| OL: | Olivine |
| OR: | Orthoclase |
| OPX: | Orthopyroxene |
| Pb: | Lead |
| PI: | Plagioclase |
| PPM: | Parts per million |
| QZ: | Quartz |
| SA: | South Africa |
| SASV: | South African Screening Values |
| SMZ: | Southern Marginal Zone |
| SD: | Siderite |
| SME: | Smectite |
| TLC: | Talc |
| TDS: | Total dissolved solids |
| TH: | Total hardness |

| | |
|---|---|
| VM: | Venda Magnesite Mine |
| WHO: | The World Health Organisation |
| Wt%: | Weight percentage |
| XRD: | X-ray diffraction |
| Zn: | Zinc |

# CHAPTER 1 - INTRODUCTION

## 1.1 Background

Magnesite ore is a natural mineral mainly composed of magnesium carbonate (MgCO3) and the primary source for the production of magnesium (Mg) and its compounds. Magnesium can be formed in numerous ways, such as the substitution of Iron (Fe) in siderite ($FeCO_3$) to form magnesite, carbonation of olivine in the presence of water and carbon dioxide and carbonation of magnesium serpentine to form talc, magnesite and water (Wang *et al.,* 2011; Sibanda *et al.,* 2013).

Abu-Jaber and Kimberley (1992) further explained the formation of magnesite from an evaporation process of sedimentary rocks, and the replacement of magnesium (Mg)-rich ultramafic rocks as hydrothermal veins. The mineral chemistry of magnesite consists of MgO (47.6 wt%) and $CO_2$ (52.4 wt%) and this depends on the environment where it was formed (Parente *et al.,* 2004). It has a hardness between 3 to 5 and a specific gravity between 3 and 3.2, a crystalline structure from rhombohedral to hexagonal and the colour of magnesite ranging from white, yellowish, orange, red and brown to grey depending on the chemical components (Parente *et al.,* 2004).

Magnesite ore is composed of serpentine, quartz-based silica, opal and limestone, and the $SiO_2$, $Fe_2O_3$, CaO and $Al_2O_3$ contents are important in determining the quality of magnesite ore as economic evaluation is done according to these values (Möller, 1989). It is important to note that although Mg is found in over 60 minerals, only a few minerals such as dolomite, magnesite ($MgCO_3$), brucite ($Mg(OH)_2$), carnallite ($KMgCl_3.6H_2O$), and olivine ($(MgFe)_2SiO_4$) are of commercial importance (Hess, 1908). Of these minerals, magnesite ($MgCO_3$) and dolomite ($MgCO_3.CaCO_3$) are the major sources of Mg and Mg compounds (Möller, 1989).

Magnesium is the eighth most abundant element in the Earth's crust, its abundance and its usefulness by many industries (Hess, 1908; Möller, 1989). The largest consumer of magnesia (MgO) in the world is the refractory industry that, in 2004, consumed about 56% of the magnesia in the United States, with the remaining 44% being used in agricultural, chemical, construction, environmental and other industrial

applications (Shand, 2006). Magnesite has multiple uses: it is used to prepare cement, decolouring agents, fertilizer, animal feed as well as refractory products (Sibanda *et al*., 2013). It can also be used as a slag-former in steel making to protect the lining of the furnace as well as a catalyst and filler in the production of synthetic rubber and the preparation of magnesium chemicals and fertilizers. In addition, it can also be burned in the presence of charcoal to produce magnesium oxide products and it can be used in the uranium treatment process (Hess, 1908). Magnesite is also used for the amendment of agricultural soil (Masindi, 2016).

Although magnesite is said to be abundant, minimal information or data exist on the extent of global magnesite resources. According to Wilson (2012), the most important countries for the production of magnesite include China, North Korea and Russia, each of which have approximately 20% of the global resources, followed by Slovakia (10%) and Brazil (7%).

In South Africa, however, the main magnesite deposits are in Mpumalanga and Limpopo Provinces (Masindi, 2016) where they occur as an alteration product of ultramafic rocks, which has high magnesium estimated at 18 million tonnes (Mt) of total reserves (Jeleni *et al.,* 2012; Sibanda *et al*., 2013; Masindi, 2016). In Mpumalanga Province, magnesite deposits are found in Malelane and Lydenburg and to the north of the Southernburg areas while in Limpopo Province, they are found in the Burgersfort, Giyani and Folovhodwe areas (Masindi, 2016).

Magnesite mining in South Africa dates back to the early 1960s (Wilke, 1965), where some of the magnesite mines in the Limpopo Province include Syferfontein (still operational) and the Venmag and Nyala Mines (both abandoned) (Sibanda *et al.,* 2013). Viljoen and Viljoen (1969) confirmed that the Strathmore mines in the vicinity of Malelane have been abandoned.

Although active mining of magnesite still takes place in South Africa, there are a significant number of abandoned magnesite mines, including the Folovhodwe, Venmag and Nyala Magnesite Mines (Coetzee *et al*., 2008). These mines are the focal point of this study, which extend about 50 km east-northeast of Tshipise Aventura Resort. They consist of large deposits of amorphous magnesite occurring in

weathered sheets of olivine dolerite, intruding into the basal portion and the limburgitic/basalts in the Letaba Formation of the Karoo Supergroup (Strydom, 1998).

Magnesite deposits around the Folovhodwe area are suitable for artisanal mining due to the fact that they occur as a soft clay-like matrix above the water table (Paul *et al.,* 1997). The abandoned Nyala Magnesite Mine, in turn, is situated 5 km west of Klein Tshipise in the village of Zwigodini (Sibanda *et al.,* 2013; Mhlongo and Amponsah-Dacosta, 2014). The main magnesite body occupies an area of 1060 m by 200 m and it occurs down to a depth of around 200 m (Strydom, 1998). The deposit is amorphous in nature and is hosted by metamorphosed ultrabasic and calcareous rocks of the Limpopo Mobile Belt (Viljoen and Viljoen, 1969).

Mhlongo and Amponsah-Dacosta (2014) explained that magnesite miners in the Nyala Mine left two large volumes, unrehabilitated of waste rock dumps exposing spoil materials and excavations which are hazardous to the environment. This points to the fact that there are many potential impacts associated with the abandoned mines on the environment and, hence, the need to explore their potential impacts.

Mining excavation and mine dumps have various effects on the terrain, including the destruction of vegetation cover and contamination of water and soil (Narayanan and Devarajan, 2011; Fu *et al.,* 2011; Wang *et al.,* 2015). Balamurugan and Balakumaran (2015) added that environmental impacts are usually related to loss of soil quality, increased soil alkalinity and leaching of metals into water systems. The Department of Mineral Resources (DMR) is concerned about pollution associated with abandoned mines as their waste rock dumps, especially in arid areas, are the main source of dust pollution in local communities and the surrounding environment (Coetzee *et al*., 2008). This means that abandoned mines affect surrounding communities.

Fu *et al.* (2011) and Wang *et al.* (2015) observed similar effects on soil following Chinese magnesite mining were, compared with soils from farmlands, magnesite waste rock dumps and surrounding soil were seriously degraded and were highly alkaline (pH >9.3). Furthermore, these authors revealed that the soil samples had a high ratio of soluble magnesium and calcium concentration which affected water absorption during plant growth (Fu *et al.,* 2011). This shows that the problem of the

negative impact of abandoned magnesite mines is a global phenomenon and requires the attention of researchers to find mitigating and management measures.

Whilst abandoned magnesite mines are usually associated with negative effects, there are potential positive impacts as well. Paul *et al.* (1997) explained that magnesite mining in the Limpopo Province involved small-scale, mechanical excavation and trucks to transport the ore. This means that a large portion of the Fallershall farm around the Folovhodwe Magnesite Mine still has the potential for economic mining (Strydom, 1998). Thus, surrounding communities can still benefit from these mines and Sibanda *et al.* (2013) suggested that the magnesite waste rock dumps may provide more extractable magnesite. In addition, Sibanda *et al.* (2013) explained that the hand sorting method was used to select grain sizes of magnesite ore greater than 25 mm only and anything smaller were put in waste rock dumps. Due to the method of hand sorting, there are still many magnesite resources left in waste rock dumps, which might be economically valuable (Paul *et al.,* 1997).

From this discussion, it is clear that abandoned mines can be exploited for the benefit of surrounding communities. Sibanda *et al.* (2013) sum up that Venmag, Nyala, and Folovhodwe Magnesite Mines left several waste rock dumps within communities, which increased waste materials to be potentially considered for brick making and for neutralising acid mine drainage, and to be used for road construction materials. In light of the discussion above, it is important to investigate the formation of magnesite and its potential impacts on different environments.

## 1.2 Problem statement

This research investigated the formation of magnesite in the Tshipise Mines field and the impact of mining in this area. Previous studies on magnesite mineralisation in the Tshipise hold the view that magnesite formed in the mafic rock, that is, dolerite dykes and sills of the Karoo Supergroup (Van Zyl *et al.,* 1942; Wilke, 1965; Michael and Carey, 1989; Strydom, 1998; Mbedzi, 2014). This, however, has not been proven conclusively, and hence, there is a need to investigate these phenomena to understand the formation of magnesite in this area.

Additionally, as shown in the background section, there are many abandoned mines in the Limpopo Province, which have the capacity to impact the natural environment and socio-economic environment positively and/or negatively. Whilst this is the case, there is little information about the economic potential of the magnesite resources, both *in situ* and in mine waste rock dumps, pointing to the need for further research. Sibanda *et al.* (2013) focussed on the status of the Nyala Mine and showed the environmental impacts on soil and surface water, as well as the potential value exploitable in the Nyala Mine waste dump rocks. However, these aspects of the Venmag Mine and the Nwanedi River, and the waste rock dumps left unrehabilitated within the communities of Zwigodini and Folovhodwe. This suggests the potential to re-mine, re-use and re-extract the waste rock dumps at those mines for the benefits of the surrounding communities.

## 1.3 Aims and Objectives

### 1.3.1 Aims

This study aims to investigate the economic geology, mineral resources and the potential impact of magnesite mining on the environment surrounding magnesite mines near Tshipise villages, Limpopo Province, South Africa.

### 1.3.2 Objectives

The objectives of the study are as follows:

- To characterise the economic geology and formation of magnesite at three abandoned magnesite mines in the Tshipise area, Limpopo Province. This should include an analysis of the ore bodies, the host rocks, the source of metals and hydrothermal fluids and the mechanism of magnesite mineralisation;
- To evaluate the magnesite in the abandoned magnesite mines in the Tshipise area and to estimate the potential for reprocessing of the waste rock dumps; and
- To assess the impact of magnesite mining on the soil and surface water in and around the Venmag Magnesite Mine in the Tshipise area.

## 1.4 Locality

The study area is located in the Musina Local Municipality in the Vhembe District in the far north of Limpopo Province. The Tshipise magnesite field is located in the far eastern side of the Tshipise Forever Resort, extending towards the Tshikondeni Coal Mine, and has three magnesite operations, i.e., the Nyala, Venmag and Folovhodwe Magnesite Mines (Figure 1.1).

The Nyala Magnesite Mine is located at Zwigodini Village, 5 km west of the Sagole Spa at latitude 22˚31'45.10 S and longitude 30˚37'43.89" E. The Folovhodwe Magnesite Mine is located in the northern part of the Folovhodwe Village within the Fallershall farm along the R525 road to Tshikondeni Coal Mine at latitude 22˚30'23.15 S and longitude 30˚22'20.15 E. The Venmag Magnesite Mine is located at the Folovhodwe Village on the eastern side of the Nwanedi Nature Reserve at latitude 22˚40'25'' S and longitude 30˚21'0'' E, adjacent to the Ziska 122 farm (Figure 1.1).

### 1.4.1 Climate

Annually, the area receives about 400 mm to 600 mm, mainly during mid-summer between 15 November and 20 March. The lowest rainfalls are in the months between May and September. Monthly mean temperatures vary from 35°C in December to 15°C in June while the daily summer temperatures range from 30°C to 40°C (South African Weather Services, 2017).

### 1.4.2 Topography and drainage

The elevation of Tshipise ranges from 500 m to 670 m above sea level. The Nwanedi River flows northwards from the north-eastern slopes of the Soutpansberg Mountains and drains into the Limpopo River at Three Crook's Corner (Ramulwela *et al.,* 2013).

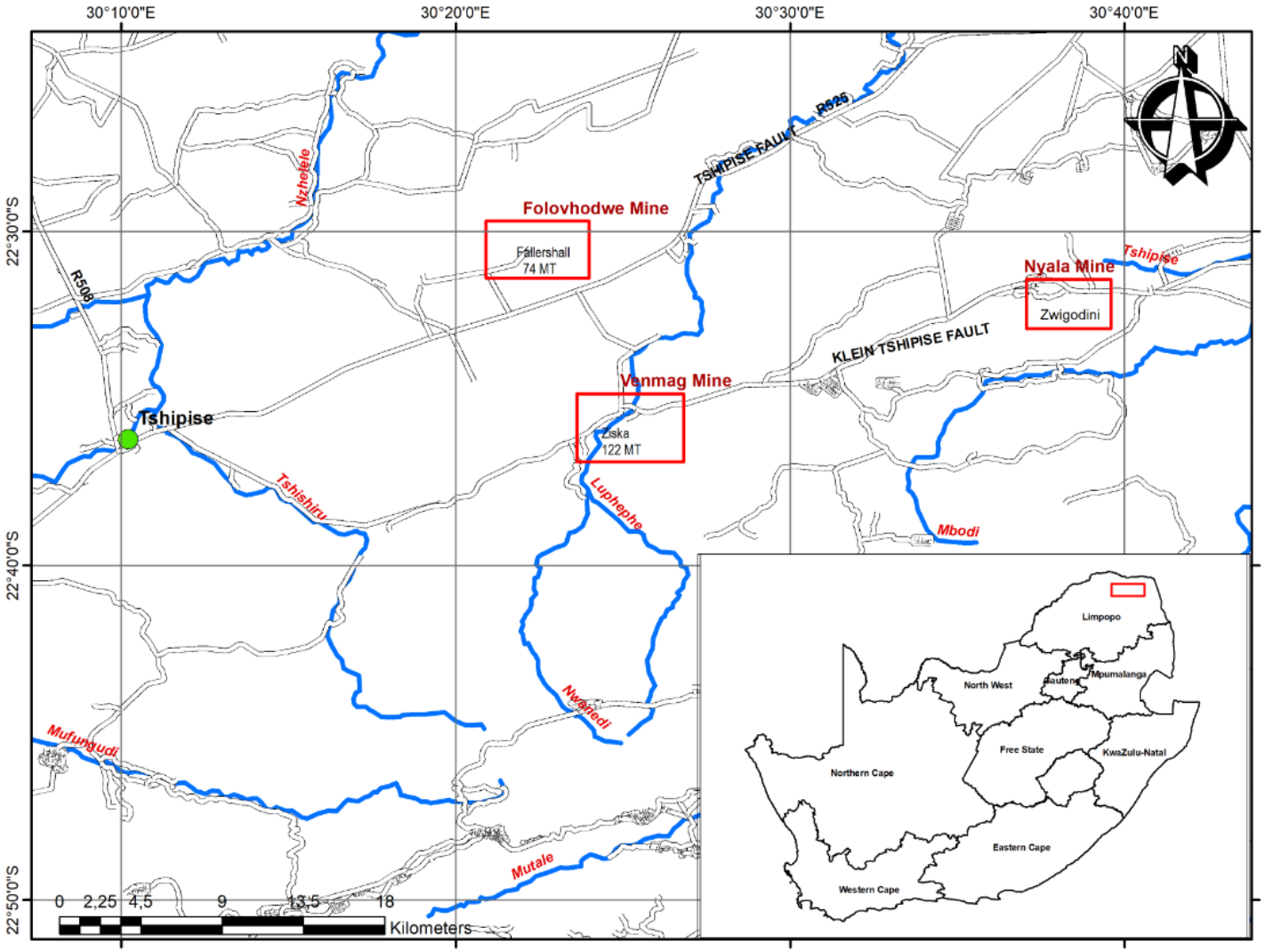


Figure 1.1: Map indicates the study sites. Modified from Paul *et al.* (1997).

## 1.5 Chapters of the dissertation

This dissertation comprises five chapters. Chapter 1 provides the general background information of the study area, problem statement, aims, objectives and the outline for the dissertation. Chapter 2 reviews previous studies and provides background information on geology, stratigraphy, lithology, structural geology, thermal events, mineralisation, and the history of magnesite mining. Chapter 3 outlines the methods used to collect and analyse data and these include field observation, sampling and laboratory analyses such as x-ray diffraction (XRD), x-ray fluorescence (XRF) and inductively coupled plasma-optical emission spectrometry (ICP-OES). Chapter 4 presents the collected data and findings on economic geology, mineral resources from residue and waste rock dumps and analysis on collected water samples. Chapter 5 discusses the results from this study. Chapter 6 presents the conclusions drawn from the study and provides recommendations for potential future work. Lastly, a list of references and appendices are presented.

# CHAPTER 2 - LITERATURE REVIEW

This chapter reviews previous studies and provides background information on geology, stratigraphy, lithology, structural geology, thermal events, mineralisation and the history of magnesite mining. This is done in line with the objectives of the study, which are to investigate the formation of magnesite in the Tshipise mining field and to determine the potential beneficial exploitation of magnesite and rocks remaining in three abandoned magnesite mines as well as an analysis of the impact of the mines on the environment. The chapter will begin by providing background information on the Limpopo Mobile Belt, the area where the Tshipise magnesite mines are located.

## 2.1 Tectonic setting

This section discusses the Limpopo Mobile Belt and the cratons which form the basement of magnesite deposits that are relevant to this study.

### 2.1.1 Limpopo Mobile Belt

The Limpopo Mobile Belt is located between Zimbabwe and Kaapvaal Cratons along the boundary of South Africa in the south and Zimbabwe in the north (Van Reenen *et al.,* 1992; Rollinson, 1992). The first systematic geochronological study of the Limpopo belt was undertaken by Fripp (1983), who revealed a complex sequence of tectono-thermal events with major age groupings at around 2000 Ma and 2650 Ma.

The Limpopo Mobile Belt (LMB) is a major zone of high-grade metamorphic tectonites which separates the Archaean granite-greenstone terrains of the Rhodesian and Kaapvaal Cratons. It extends along an ENE axis for over 560 km and varies in width between 240 km and 320 km (Fripp, 1983). The belt is divided into three zones based on structural characteristics and lithology: (1) The Northern Marginal Zone (NMZ); (2) The Central Zone (CZ); and (3) The Southern Marginal Zone (SMZ). The NMZ and a small portion of the CZ are located in Zimbabwe while the rest are in South Africa (Van Reenen *et al.,* 1992). According to Barton *et al.* (1992), the CZ is characterised by a unique succession of leucocratic, granitic, and high-grade, commonly migmatitic, quartzofeldspathic rocks and supracrustal lithologies (quartzite and calc-silicate, carbonate, metapelitic, and para-amphibolitic rocks) separated by the wide Palala-

Zoetfontein and Triangle shear zones from two marginal zones. Barton *et al.* (1992) further adds that the SMZ consists of high-grade, intensely deformed and metamorphosed, tonalitic, and trondhjemitic rocks with minor greenstones that were interpreted as reworked rocks of the Kaapvaal Craton (Van Reenen *et al.,* 1987; Van Reenen *et al.,* 1992), whereas the NMZ is dominated by enderbite and enderbitic orthogneisses with very minor green stones and few granitic rocks (Van Reenen *et al.,* 1987; Van Reenen *et al.,* 1992).

The three zones of the Limpopo Mobile Belt are thought to have been formed under granulite-facies conditions and subsequently overprinted under retrograde conditions (Van Reenen *et al.,* 1987; Van Reenen *et al.,* 1992). Their lateral extent to the east and west is poorly defined because they are covered by younger sedimentary and volcanic rocks (Barton *et al.,* 1992). This study will focus on the SMZ in South Africa because it is more relevant to the mineralisation of the magnesite in terms of geographical locality.

The SMZ is bound by the Sunnyside-Palala shear zone towards the north and by the orthoamphibole isograd to the south, and shearing occurs to the south along the Kaapvaal Craton interior and the Thabazimbi shear zone (Du Toit *et al.,* 1983). The SMZ is underlaid by strongly deformed ortho- and paragneisses at the granulite and upper amphibolite grades of regional metamorphism, and its rocks are broadly subdivided into the following: (1) The Bandelierkop Formation comprising metavolcanic and metasedimentary supracrustal rock; and (2) The grey migmatised tonalitic to trondhjemitic gneisses (Du Toit *et al.,* 1983). Eglington and Armstrong (2004) explain that the Banderlierkop Formation is subdivided into the ultramafic, mafic and pelitic members. Michael and Carey (1989) clarified that the ultramafic member rocks were formed as discontinuous lenses and ponds and they are covered by leucogranite that intrudes in the fractures. That being the case, several pod-like ultramafic bodies consisting of peridotite, pyroxenite, dunite, and hornblendite occur as variably sized xenoliths in the Banderlierkop Formation these rocks are considered to represent the high-grade metamorphosed equivalents of Archaean Greenstone Belt lithologies occurring within granitoid gneisses on the northern edge of the Kaapvaal Craton (Du Toit *et al.,* 1983).

The peridotite and dunite are serpentinised and consist of large relic crystals of olivine and enstatite in a matrix of antigorite/lizardite and magnetite (Brandl and De Wit, 1997). All the ultramafic rocks are relatively MgO-rich with values ranging from 28 wt% to 35 wt%, suggesting a lherzolitic precursor (Van Reenen, 1992; Brandl and De Wit, 1997). The age of these ultramafic rocks is not known, but they are older than the granulite facies Matok Granite dated between 2667 Ma and 2664 Ma (Barton *et al.*, 1992). The study area is found within the margins of the Kaapvaal Craton.

### 2.1.2 Kaapvaal Craton

The northern Kaapvaal Craton comprises the Murchison, Pietersburg and Sutherland Greenstone Belts and surrounding granitoids (Viljoen and Viljoen, 1969). According to Vearncombe *et al.* (1988), the Sutherland Belt comprises metavolcanic schists of ultramafic and mafic rocks, but the little felsic composition with subordinate banded iron formation, quartzite, politic schist and minor dolomite. In contrast, south-directed thrusting in the Sutherland and Murchison Belts is geometrically related to the Limpopo deformation and interpreted as an integral part of the Limpopo event (McCourt and van Reenen, 1992; Vearncombe *et al.,* 1988).

There are layered ultramafic intrusives in the Kaapmuiden-Malelane region of the Barberton Greenstone Belt which are rich in olivine mineral, and most of them occur in the Onverwacht Group (Viljoen and Viljoen, 1969) while the Malelane magnesite deposits have been deposited within the ultramafic rocks of the Bushveld Complex formed at 2.0 Ga (Hamilton *et al.,* 1977; Walraven *et al.,* 1990; Cawthorn *et al.,* 1981). The ultramafic intrusions in the region are host rocks to both chrysolite asbestos and magnesite (Viljoen and Viljoen, 1969; Strydom, 1998).

## 2.2 Stratigraphy

The Banderlierkop Complex consists of ultramafic rocks, forming a Giyani Greenstone Belt formed about 3.5 Ga (Bahnemann, 1972; Hamilton *et al.,* 1977; Kamo and Davis, 1994; Lahaye *et al.,* 1995; De Ronde and Kamo, 2000) which comprises ultramafic,

pelite and mafic rocks and it is part of the Archean basement rocks (Michael and Carey, 1989) (Table 2.1).

Table 2.1: Informal lithostratigraphic column of the Tshipise area. Modified from Michael and Carey (1989).

| | **GROUP** | **PRINCIPAL LITHOLOGY** |
|---|---|---|
| Karoo supergroup | Lebombo Group | Syenite, picrite, olivine dolerite sills, basalt/Limburgite |
| | Stormberg Group | Dolerite dykes and sills, Basaltic lava |
| | Beaufort Group | Sandstone |
| | Ecca Group | Sandstone |
| Archean Basement | Bandelierkop Complex | Ultramafic (pyroxenite and peridotite, usually associated) /Mafic/Pelite |
| | Giyani Group | Ultramafic/Mafic/Pelite |

## 2.3 Structural geology

Van Zyl *et al.* (1942) found that exposure of both the intrusive and extrusive (volcanic) rocks in the Tshipise area are controlled by three major east-northeast-striking fault systems, namely the Klein Tshipise, the Bosbokpoort and the Tshipise faults, which might have contributed during the mineralisation of the magnesite deposits (Figure 2.1).

## 2.4 Thermal events

Thermal springs originate either from recent plutonic activity (volcanic origin) or from rainwater that percolates into the ground through permeable rocks or via conduits such as joints, faults and fracture zones in less permeable rocks (meteoric origin) (LaMoreaux and Tanner, 2001). With regard to South Africa, since there is no evidence of recent volcanic activity (Olivier *et al*., 2008), it is generally assumed that

all thermal springs in South Africa are of a meteoric origin (Rindl, 1916; Kent, 1949; Kent, 1969; Hoffmann, 1979; Ashton and Schoeman, 1986; Visser, 1989; Diamond and Harris, 2000).

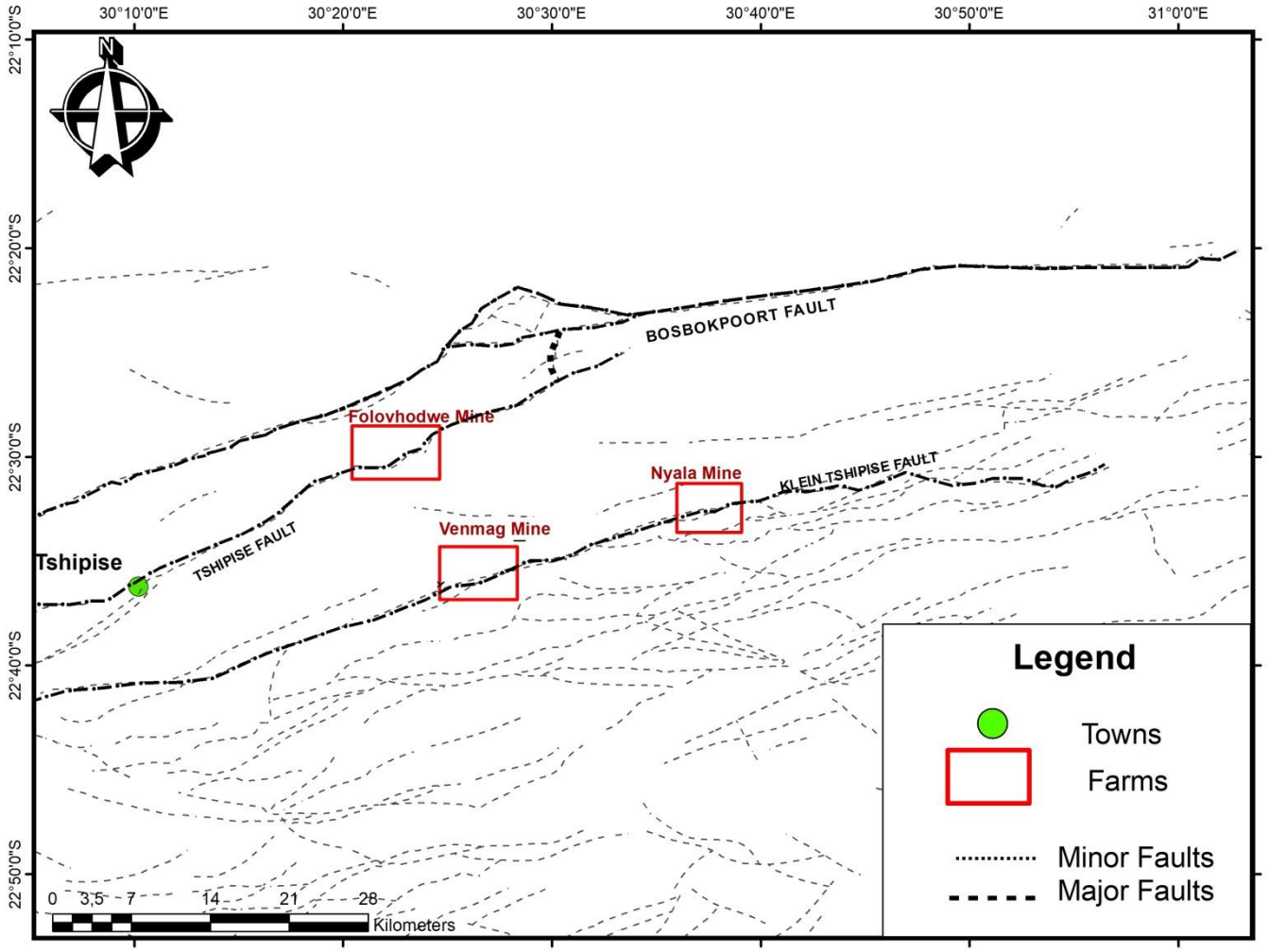


Figure 2.1: Structural geology showing faults associated with the magnesite fields (produced by Arc Gis software).

Two well-known hot springs (the Tshipise and Sagole) are found near the study area. The farm on which they are found is located within the Honnet Nature Reserve, approximately 36 km from Musina, just off the R525 road. The latter, previously known as Klein Tshipise, is situated at Sagole village, approximately 57 km to the east of Tshipise Aventura (Nature Reserve). Thick growths of algae cover submerged rocks and the sides of the watercourse (Olivier *et al.,* 2011). The water from the spring flows northwards into the Tshipise River and geological studies have shown conclusively that the origin of each thermal spring can be attributed to the local presence of deep geological structures such as folds, fractures, faults, and dykes that provide a means for the circulation to depth and the return of the heated waters to the surface (Olivier *et al.,* 2011).

## 2.5 Magnesite mineralisation

According to Zachmann and Johannes (1989) and Scott *et al.* (2013), the following are the four ways in which magnesite can form:

- During regional, contact or hydrothermal metamorphism of peridotites or serpentine rocks, often resulting in cryptocrystalline magnesite;
- During regional, contact or hydrothermal metamorphism of limestone, magnesium-rich solutions may cause alteration of carbonate rocks such as limestone;
- Epigenetic magnesite may occur in sedimentary environments. Solutions of carbonic acid may make it easier for the formation of magnesite within the regolith of rocks rich in magnesium such as ultramafic rocks; and
- Precipitation in veins, fissures and fractures occurring in carbonates and ultramafic rocks. The resulting magnesite ores are often known as stock magnesite, characterised by a texture of unevenly intersecting thin veins and veinlets.

According to Strydom (1998), the magnesite in the Tshipise area resulted from the alteration of the high magnesia-rich pyroxenite in the basal zones. In contrast, magnesite deposits in the Mooketsi in the Giyani area are associated with the Giyani Greenstone Belt (Van Zyl *et al.,* 1942). Magnesite deposits in the Gravelotte are associated with the Murchison Greenstone Belt and the Mica magnesite deposits

occur in the same geological environment as those in the Giyani Group (Wilke, 1965; Strydom, 1998).

Previous researchers reported that the mineralisation of magnesite occurs in a low ridge, formed from black and feldspathic sandstone of the Ecca Group and alteration of olivine ultramafic rocks (Van Zyl *et al.,* 1942; Wilke, 1965; Strydom, 1998). Mineralisation occurred along the joints and fracture planes of the basalt rocks and the magnesite is zebra-type with the magnesite capping being, in some places, completely covered by deposits of red sand and gravels (Strydom, 1998).

According to Van Zyl *et al.* (1942), mineralisation of the magnesite occurred within the north olivine dolerite dykes along the Fallershall farm in the north, and in the south olivine dolerite dyke of the Tshipise area extending from Klein Tshipise to the east of the Folovhodwe and the Nyala Magnesite Mines that operated at the Amonda 161 farm portion. Strydom (1998) indicated that mineralisation in this mine occurred in the low ridge which has formed black and light-coloured, hard, flinty and with metamorphosed shales and feldspathic sandstone of the Ecca Group, and altered olivine dolerites.

### 2.5.1 Local geology in the Tshipise area

Magnesite deposits in the Tshipise area were deposited within the dolerite dyke of the Karoo Supergroup (Strydom, 1998). Furthermore, the mineralisation of magnesite occurred within the mafic and ultramafic rocks, forming part of the metamorphosed volcano-sedimentary supracrustal rocks (Van Zyl *et al.,* 1942; Wilke, 1965; Michael and Carey, 1989; Strydom, 1998; Mbedzi, 2014). Near the base of the formation, there are fairly commonly seen agate, red jasper and clasts (Barker *et al.,* 2006). Sedimentary rocks such as shale were reported to comprise a few thin scattered layers of limited strike length (Bumby *et al.,* 2002).

### 2.5.2 Mechanism of magnesite formation

The mechanism of magnesite formation depends on environmental conditions (Van Zyl *et al.,* 1942; Wilke, 1965). Formula 1 is the illustration of magnesite formation from an alteration of ultramafic rocks, being typically represented by olivine (such as Chrysolite):

$$2\ Mg_3Si_2O_5(OH)_4 + 3\ CO_2 \rightarrow Mg_3Si_4O_5(OH)_4 + 3\ MgCO_3 + 3\ H_2O$$

Chrysolite Serpentine Magnesite (1)

### 2.5.3 Background information on magnesite mining

Currently, South Africa has two operating magnesite mines: Chamotte Holdings (Pty) Ltd in Mpumalanga Province near the town of Malelane as well as Syferfontein Calcite (Pty) Ltd near the town of Musina in Limpopo Province. ln, the Tshipise magnesite field, mining took place on the following farms: Graandrik 162, David 160 and Frampton 72 farms (Van Zyl *et al.,* 1942; Wilke, 1965). The magnesite occurrences can be found in the westerly extensions of a dolerite dyke extending from Amonda 161 towards Rynie 158, Martin 157 and Septimus 156 farms (Wilke, 1965). The largest deposit found is the Nyala Magnesite Mine that is situated 6.5 km west of Klein Tshipise, which is now called Sagole Spa. According to Mhlongo and Amponsah-Dacosta (2014), the magnesite deposits in the Tshipise area are all mined using open cast mine due to their shallow nature and the direct use of heavy excavators to mine without the need for blasting. This applies to the Folovhodwe, Venmag and Nyala Magnesite Mines.

Previously, the magnesite ore in the Tshipise magnesite mines was recovered by hand-sorting so that 300 Kt of magnesite was mined out to a depth of 22 m for about two years between 1961 and 1962 in the Nyala Magnesite Mine while the Venmag Mine produced approximately 45 Kt of magnesite over the same period at 20 m (Strydom, 1998).

Those waste rocks and magnesite ore less than 25 mm in size were transported to waste rock dumps (Wilke, 1965) while the fine magnesite was left in the wastes (Sibanda *et al.,* 2013). Furthermore, these authors indicated that since the magnesite waste rock dumps were left unrehabilitated, no reprocessing has been attempted in order to recover the remaining ore and further reuse of the wastes for either road construction or brick making.

Reuse and reprocessing of magnesite waste rock is commonly practiced in Africa. In the north-western parts of Rwanda, local industry uses volcanic rocks for building materials and so the employment offered in their reuse has benefited the local communities. Such volcanic rocks have high compressive strength and improved permeability, essential characteristics for building construction as subsurface layers and for brick making (De Dieu *et al.,* 2016).

## 2.6. Water quality

This study will compare the impact of magnesite mining on water resources against the guidelines of the Department of Water and Sanitation (DWS) (previously known as the Department of Water Affairs and Forestry (DWAF)). The DWS has developed best practice guidelines (BPG) for water quality particular industrial processes and emphasise the following water quality parameters; total dissolved solids (TDS), pH, redox potential, salinity, alkalinity, hardness, and other variables (DWAF, 1996). The DWS Water Quality Guidelines make provision for 5 water-use categories according to the quality of the water, which are recommended for industrial use as well as domestic purposes and are indicated in Table 2.2.

Table 2.2: DWAF water quality standards. Source: DWAF (1996).

| | | | | | |
|---|---|---|---|---|---|
| Status | Class 0 | Class I | Class II | Class III | Class IV |
| Elements | Ideal | Good | Marginal | Poor | Dangerous |
| Calcium (Ca) (mg/L | 0-80 | 80-150 | 150-300 | >300 | |
| Magnesium (Mg) (mg/L) | <30-70 | 70-100 | 100-200 | 200-400 | >400 |
| Sodium (Na) (mg//L) | <100 | 100-200 | 200-400 | 400-1000 | >1000 |
| Potassium (K) (mg/L) | <25 | 25-50 | 50-100 | 100-500 | >500 |
| Sulphate (SO4) (mg/L) | <100-200 | 200-400 | 400-600 | 600-1000 | >1000 |
| Chloride (Cl) (mg/L) | <100 | 100-200 | 200-600 | 600-1200 | >1200 |
| pH | 5-9.5 | 4.5-5 & 9.5-10 | 4-4.5 & 10-10.5 | 3-4 & 10.5-11 | < 3 & >11 |
| Total dissolved solids (TDS) (mg/L) | <450 | 450-1000 | 1000-2400 | 2400-3400 | >3400 |
| Electrical conductivity (EC) (Ms/m) | <70 | 70-150 | 150-370 | 370-520 | >520 |
| Carbonate alkalinity (mg/L) | 0-200 | 200-300 | 300-600 | >600 | |
| Iron (Fe) (mg/L) | <0.01-0.5 | 0.5-1.0 | 1.0-5.0 | 5.0-10.0 | >10 |
| Nitrate ($NO_3^-$) (mg/L) | <6 | | | 20-40 | >40 |
| Fluoride (F) (mg/L) | <0.7 | 0.7-1.0 | 1.0-1.5 | 1.5-3.5 | >3.5 |

## 2.7 Hydrochemical facies

The hydrochemical facies is the chemistry of water like Piper and Stiff diagrams that are used to show the proportion of ionic concentration in individual samples. Significant characteristics of hydrochemical facies can be illustrated by methods similar to those used in lithofacies studies trilinear diagrams that show the facies present in an area or in formations, fence diagrams that show the facies distribution and maps that show isopleths of chemical constituents within certain formations (Kumaresan and Riyazuddin, 2006).

Piper trilinear diagram (Piper, 1944) evaluates the evolution of the river water and the relationship between rock types and water composition while the Durov diagram is advantageous over the Piper diagram in revealing some geochemical processes that could affect the groundwater genesis (Lloyd and Heathcoat, 1985).

Trilinear and similar diagrams have long been used to study the chemistry of water. Emmons and Harrington (1913) used two triangles, one for cations and one for anions, with each vertex representing 100% of a particular ion or groups of ions, as is often used in petrographic studies. Hill (1940) published a trilinear diagram which added to the original two triangles a diamond shaped area in which the two points plotted in the triangles are projected into the diamond and are plotted as a single point as illustrated in Appendix G.

# CHAPTER 3 - METHODOLOGIES

The study includes a desktop study, field work, sampling, and laboratory analyses. These features of the study are presented as a flow diagram in Figure 3.1.

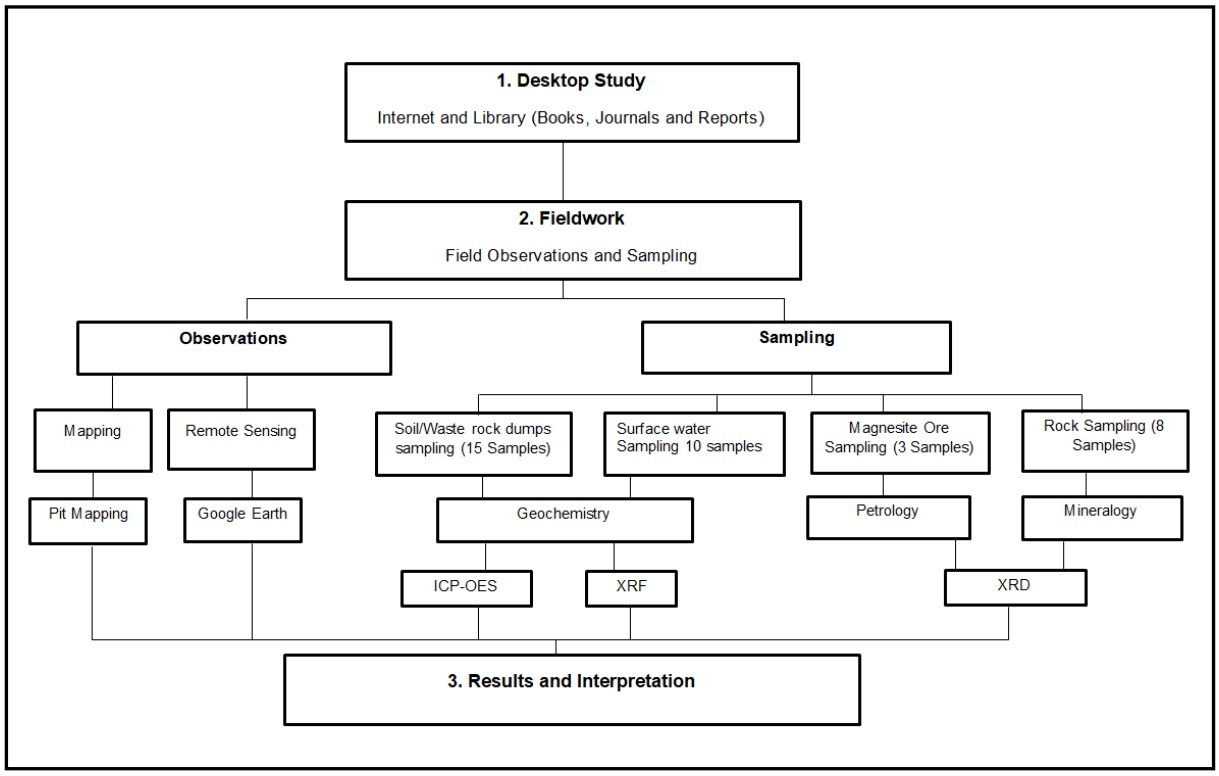


Figure 3.1: Flow chart summary of the methodologies used in this study.

## 3.1 Desktop study

A desktop study was initially conducted to make a preliminary assessment of the site conditions, the conceptual design of the project and to review the literature on geology and the impacts of magnesite mining on the environment and water quality. This was done to acquire relevant information before field work commenced.

## 3.2 Field work and sampling

Field work involved field observation, pit mapping as well as soil, water, rock and magnesite sampling. The collected rock samples were washed to remove impurities and thereafter, were sent to Geolabs Global (Centurion, South Africa) for analysis. All these methods are discussed below.

### 3.2.1 Field mapping

Field mapping and observations were conducted along the mine pits in the study area to characterise the economic geology of the mine sites. This was done to achieve the following:

- Understand magnesite deposits and mineralisation of the source rock and host rocks;
- Investigate structural control of mineralisation such as the influence of dolerite dykes and sills, the structural distribution as well as structural control such as bedding and joints within the dyke and ultramafic rock;
- Measure the parameters of dykes and sills, strata of ultramafic rocks, magnesite ore bodies, strikes and dips on the face of the mine pits;
- Relate mineralisation with its potential host rock/s such as dolerite dyke or ultramafic rock and any other possible sources;
- Trace the directions of the dykes within the area to understand the stress field concerning mineralisation;
- Understand the stress/pressure type within the area to investigate whether normal joints or compressional joints occur; and
- Produce a mine geological map.

### 3.2.2 Water sampling

Water samples were collected from the Venmag Mine pit and also from sites along the Nwanedi River. Only two samples of water were taken from the Venmag Mine pit (W1 and W2) and all of the eight other samples were collected from the Nwanedi River (W3 to W10). Water analysing, testing was conducted to determine physical water quality parameters such as pH, electrical conductivity (EC) (µS/m), temperature (ºC), total dissolved solids (TDS) (mg/L), total hardness (mg/L) as well as chemical parameters including Calcium (Ca), Magnesium (Mg), Sodium (Na), Potassium (K), Sulphate ($SO_4$), Chloride (Cl), Iron (Fe), Nitrate (N), Fluoride (F), and Carbon Alkalinity (mg/L). Each water sample collection site was identified using GPS (Appendix C).

Before collecting the samples, the sampling polypropylene bottles were soaked overnight with a dilute nitric acid solution (1.0 M $HNO_3$) before they were washed using

a non-phosphate laboratory detergent. Thereafter, the bottles were thoroughly rinsed twice using double-distilled water. During sampling, initially collected water samples were used to rinse each of the respective sampling polypropylene bottles. Mine pit water was collected by dipping a polyethene sampling bottle into the stagnant water and the bottle was filled to excess and capped immediately to prevent oxidation and other chemical changes before laboratory testing. Samples were stored in a cube of cooler box ice to keep the water samples below 4$^{o}$C (Appelo and Postma, 2005).

### 3.2.3 Rock sampling

Rock samples were taken from the host rocks of magnesite, i.e., dolerite dykes and ultramafic rocks. Samples (VR1, VR2 and VR3) were collected from the Venmag Mine; FR1, FR2 and FR3 from the Folovhodwe Mine; and NR1, NR2 and NR3 from the Nyala Magnesite Mine. The samples were used for thin section and whole-rock geochemistry. The collection position of each sample was marked with GPS coordinates (Appendix C).

### 3.2.4 Magnesite ore sampling

Three magnesite ore samples were collected directly from the Venmag Mine pit for analysis of whole-rock geochemistry. The relative standard deviations (RSD) concentration level was used to evaluate the samples to confirm that they complied with the certified values (Table 3.1).

Table 3.1: Validation method against soil certified values.

| Metal | Concentration level (ppm± RSD*) | Certified values (ppm) |
|---|---|---|
| As | 0.086 ± 5.69 | 11,00 |
| Cu | 0.04 ± 2.72 | 12,00 |
| Ni | 0.144 ± 3.13 | 8,00 |
| Pb | 0.036 ± 1.84 | 40,00 |
| Zn | 0.053 ± 2.25 | 264,00 |

### 3.2.5 Soil sampling

A systematic, unaligned sampling pattern method was used to collect soil samples. The field was divided into cells (Gridlines) using a coarse grid, each with a width of 15 m and a length of 20 m. A sampling point was then identified on each grid. Several

individual soil cores were collected over the designated area using an auger. A total of 15 soil samples were collected from the surface soil and transferred into labelled fresh sampling bags named from S-1 to S-15 (Figure 4.21). Samples from the waste rock dumps were separated from the soil samples collected outside the locality of the waste rock dumps. The GPS coordinates for each sample was noted (Appendix D).

Soils were sampled from the centre of the magnesite waste rock dumps and its surrounding area using the following sample identification S1 to S15. The following samples were taken from the waste rock dumps (S1, S2, S6, S11, S12 and S14) and the associated soil (S3, S4, S5, S7, S8, S9, S10, and S15) (Figure 4.16). The soil samples that were taken from the field were analysed for the following major oxides ($SiO_2$, $Al_2O_3$, $Fe_2O_3$, $TiO_2$, CaO, MgO, $Na_2O$, $K_2O$, MnO, and $P_2O_5$) and for further investigation of the trace elements (Fe, P, Ba, Cr, Cu, Ni, V, Zn, Li, Nb, Sn, Ta, Rb, and W) using x-ray fluorescence (XRF) spectrometry.

**Internal control data**

A total of three soil samples were analysed for background levels. These samples were collected from the centre of the waste rock dumps inside the Venmag Mine area to the surrounding environment.

## 3.3 Laboratory work

This section focused on microscopy, x-ray diffraction (XRD), x-ray fluorescence (XRF) and inductively coupled plasma-optical emission spectrometry (ICP-OES).

### 3.3.1 Microscopy

The microscopy study was used to determine the mineralogy and petrology and also used to supplement the XRD analysis. It involved the use of both transmitted and reflected light microscopy, and eight representative samples of different host rocks were selected for double-polished thin section analysis of the MSA Group (Randburg, South Africa). All thin sections were prepared following the procedure described by Murphy (1986).

### 3.3.2 X-ray diffraction (XRD)

The collected rock samples were washed with distilled water to remove impurities and left to dry at room temperature, after which the samples were crushed and then oven-dried at 75ºC. Then, 500 g of the powder of the whole rock samples were separated and kept for future use (Lavina *et al.,* 2014).

All rock samples and ore minerals were detected using XRD analysis according to the method described by Lavina *et al.* (2014) to detect minerals that are not identifiable by physical analysis of hand specimens and those not clearly distinguishable using petrographic studies. In this technique, conventional x-rays are generated in a cathode ray tube. Free electrons are produced by heating a filament, called the cathode (similar to the filament in a conventional incandescent electric light bulb) to a high temperature, and these negatively charged electrons are accelerated to high energy by applying a voltage of several tens of kilovolts between the filament and the target or anode (Artioli, 2017).

In practice, a representative portion of each sample (500 g) was analysed by XRD to obtain its bulk composition. A Siemens D500 diffractometer (PANalytical Products, Randburg, South Africa) was used, with a step size of 0.02º and a counting time of 1 second per step, being applied over a range from 5ºC to 80ºC.

For quality control, detection limit, and method validation, the results of selected metals for certified soil value material are given in Table 3.1. Analysis of diluted standard metal solutions provided calibration values with correlation coefficients in the ranges as follows: As (0.54 to 0.86), Cu (0.28 to 0.45), Ni (0.57 to 0.144), Pb (0.23 to 0.36) and Zn (0.26 to 0.53). The calibration curves per metal had the following R-values: Cu (0.9995), Ni (0.9888), and Zn (0.9948) with detection limits being obtained for As (0.04 ppm), Cu (0.02 ppm), Ni (0.02 ppm), Pb (0.02 ppm) and Zn (0.02 ppm).

### 3.3.3 X-ray fluorescence (XRF)

The XRF spectrometer functions in a similar way to the electron microprobe but with two significant differences. Firstly, the characteristic x-ray spectra of the elements in the sample are excited by the high-energy continuous spectrum of an electron beam

and this minimizes the amount of continuous spectrum produced by the sample. Secondly, heterogeneous samples such as rocks must be either finely ground or fused before being analysed (Nesse, 2012).

The whole-rock geochemical analysis was done at Geolabs Global (Centurion, South Africa) using a PANalytical Axios (PANalytical Products, Randburg, South Africa) XRF instrument.

In practice, a sample of rock powder was sieved to pass through a 75 µm sieve and pressed using a PVA (polyvinyl alcohol) binder. The powder pellets were analysed for major oxide elements MgO, $Fe_2O_3$, $SiO_2$, MnO, $TiO_2$, $K_2O$, $Al_2O_3$, and CaO. The detection limit for major oxides was 0.01 wt% while for trace elements, it was 0.2 ppm for Br, Pb and Ba (1 ppm), Cr (0.3 ppm), Cd (0.005 ppm), Cl (0.001 ppm), Zn (0.2 ppm), F (0.001 ppm), Cu (0.02 ppm), Mn (0.2 ppm), Ni (0.08 ppm) and Fe (0.002 ppm). The calibration of the spectrometers as well as the detection limits, accuracy, precision of the analyses and the analysis of all samples were as described by Lavina *et al.* (2014).

Testing of water sampling was conducted for the following physical parameters: pH, Electrical Conductivity (EC) (µS/m), Temperature (ºC), Total Dissolved Solids (TDS) (mg/L), Total Hardness (mg/L), and cations including Calcium (Ca), Magnesium (Mg), Sodium (Na), Potassium (K), Sulphate ($SO_4$), Chloride (Cl), Iron (Fe), Nitrate (N), Fluoride (F) as well as Carbon Alkalinity (mg/L). The GPS coordinates of each water sampling site were recorded (Appendix C).

### 3.3.5 Inductively coupled plasma-optical emission spectrometry (ICP-OES)

The soil geochemical composition was determined using ICP-OES. According to Boss and Fredeen (2004), particular soil sample preparation depends on the physical and chemical characteristics of the soil and could involve only a simple dilution or a complex array of chemical reactions and other preparation steps. The following heavy metals were analysed using ICP-OES: Al, As, B, Ba, Bi, Ca, Cd, Co, Cr, Cu, Fe, Li, Mn, Ni, P, Pb, Se, Sr, Ti, Tl, V and Zn. This study adopted the analytical method involving digestion of soil samples using ultra-pure acids in high microwave vessels as described by Shackley (2018).

All the collected soil samples were sieved through a 20 µm mesh sieve. Then, approximately 0.25 g of each soil sample was weighed into the respective digestion tubes. Thereafter, 9 ml of nitric acid, 3.0 ml of concentrated hydrochloric acid and 1.0 ml of hydrogen peroxide were added to each soil sample. The final digests were transferred to respective 50 ml polypropylene tubes before being diluted to 50 ml with ASTM® Type I water (from a Millipore® filtration system). Four multi-element standards were prepared such that every wavelength had at least one standard for calibration. The resultant aliquot was determined for trace elements and major oxides (Boss and Fredeen, 2004).

The collected water samples were analysed using ICP-OES for the following parameters, including hardness, conductivity, TDS, alkalinity and trace elements (Cr, Cu, Zn, Pb, Mn, Fe, Cl, Ni, Cd, K, Ca, S and Mg). The pH and EC were measured on site using a WTW pH 526 meter (Labotec, Midrand, South Africa) fitted with IDS ORP pH electrodes while the later was displayed on a WTW 330i conductivity meter (Labotec, Midrand, South Africa, with TetraCon® 325-4 electrodes. The TDS was measured using a TDS-3 meter (Nham *et al.*,1991).

### 3.3.6 Single contamination index method

The level of metal contamination in the examined soil samples was quantified using the Single Contamination Index method. A brief description of the applied index is as follows: (1) The Contamination Index (**P *f***) is the ration obtained by dividing the concentration of the metal over the background value; and (2) The concentration levels of the metals may be classified based on the Single Contamination Index (**P *f***) scale ranging from A to F (A-Very low, B-Low, C-Medium, D-High, E-Very high, and F-Super high) (Wei *et al.,* 2011).

# CHAPTER 4 - RESULTS

This chapter discusses the results of the analysis of samples collected at three abandoned South African magnesite mines regarding (1) their economic geology aspects, including interpretation of the old map information obtained from the Council for Geoscience, field observations, mapping of the host rocks, controlling structures, the ore body types and the relationship to the surrounding lithologies of magnesite mineralisation, (2) estimation of economic potential following reactivation of the mines or treatment of the mine dumps, and (3) environmental impacts of the disused mines and their dumps on water quality and soil in the study area.

## 4.1 Economic geology

This section provides results from the study regarding economic geology aspects including: (1) Distribution of magnesite deposits and mines; (2) Magnesite mineralisation; and (3) The petrology mineral geochemistry of the host and the relevant rocks in the Venmag, Folovhodwe and Nyala Mines.

### 4.1.1 Distribution of magnesite deposits and mines

The magnesite mines in the Tshipise area are the Venmag, Folovhodwe and Nyala Magnesite Mines. It is important to note that all those mines currently have ceased operations due to economic challenges and market demand issues. For this study, most of the field work was carried out at the Venmag Mine for more detailed surface and pit mapping while the Folovhodwe and Nyala Mines were mapped to a lesser extent for comparison of characteristics of economic geology (Figure 4.1).

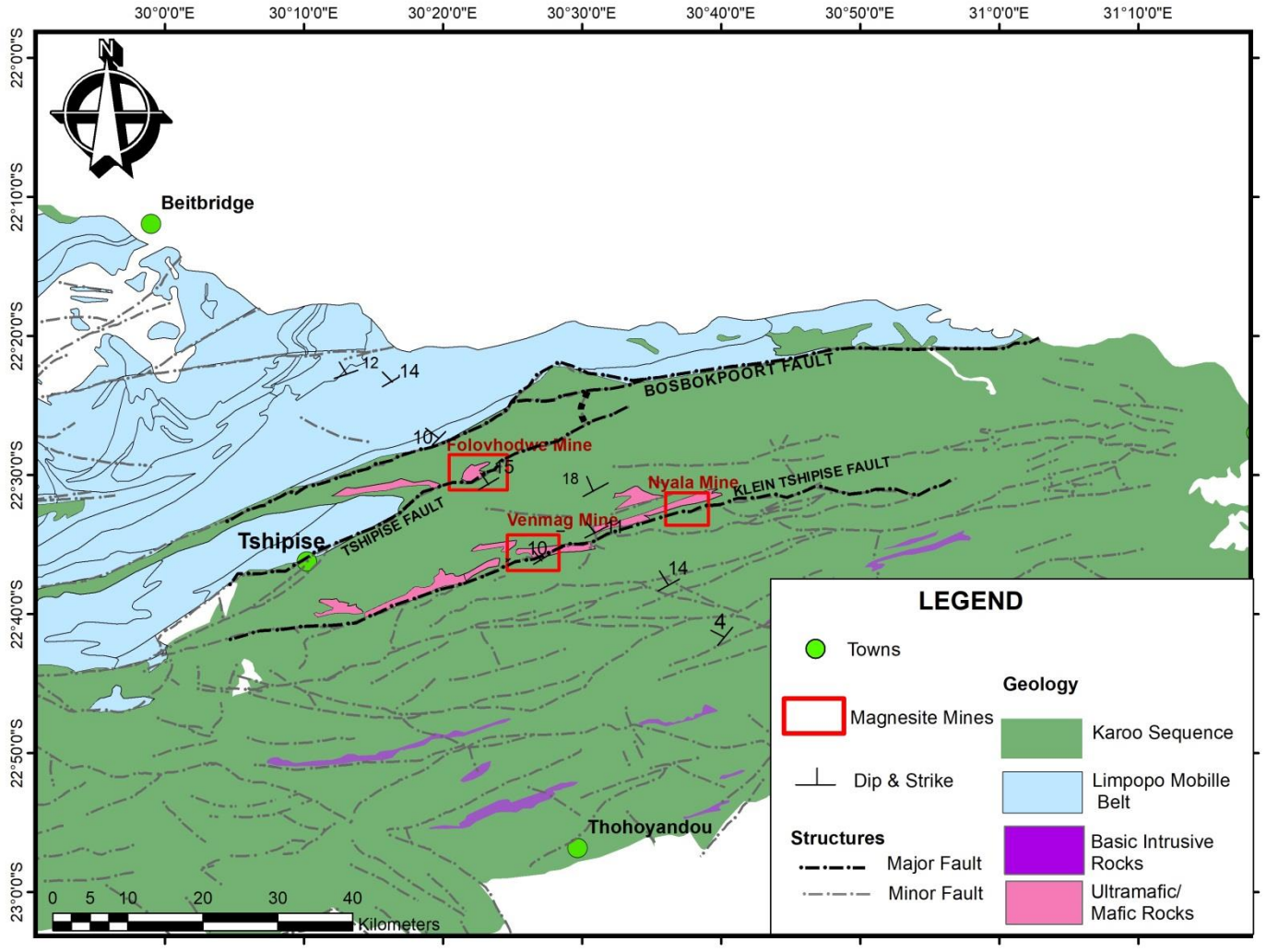


Figure 4.1: Geological map of the Tshipise magnesite mines. Modified from Council for Geoscience.

### 4.1.2 Distribution of magnesite mineralisation

#### 4.1.2.1 Regional distribution of magnesite mineralisation

The magnesite mines in the Tshipise area are situated between the Tshipise and the Bosbokpoort Faults in the north and the Klein Tshipise Fault in the south and a north-east easterly direction from the village of Tshipise. Furthermore, mineralisation occurs in the ultramafic and mafic rocks (pinkish in Figure 4.1) and so any potential mining exploration should target the region rich in ultramafic and mafic rocks situated between the two major faults (Figure 4.1).

#### 4.1.2.2 Local distribution of magnesite

This research focused on the Venmag, Folovhodwe and Nyala Magnesite Mines in order to study their similarities such as the controlling structures of magnesite and mineralisation type within the pits and surrounding lithologies.

**(a) Venmag Mine**

Mapping was conducted in the Venmag Mine on all the lithologies associated with the magnesite mineralisation. All the dolerite dykes and sills were mapped within the mine pit, which showed that dolerite dykes/sills intruded into the ultramafic rocks (Figures 4.2 and 4.3).

Mineralisation in the Venmag Mine appeared to have been controlled by structures such as horizontal and sub-horizontal beddings, and vertical and sub-vertical joints. Major mineralisation occurred in the ultramafic rocks while much minor mineralisation occurred in the dolerite dykes, contacting against the ultramafic rocks. The magnesite deposit occurred as vein type mineralisation within the beddings and joints of the layered ultramafic rocks that might have occurred during thermal water circulation due to the intrusion of the dolerite dykes and sills (Figures 4.3 and 4.4).

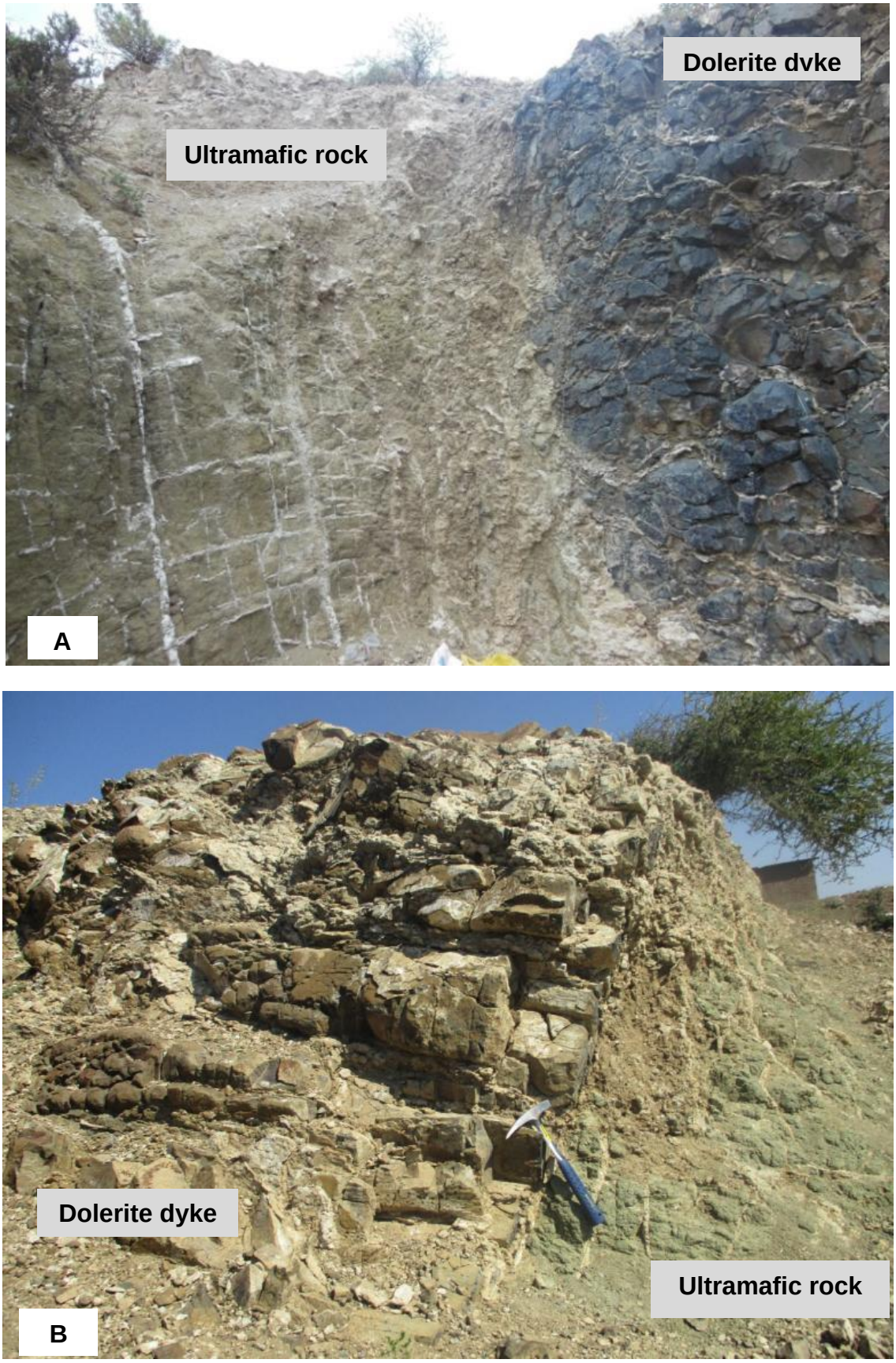


Figure 4.2: Dolerite dykes (A & B) intruded into the ultramafic rocks in the Venmag Mine. Photographs were taken by the candidate.



Figure 4.3: Sills (A & B) intruded into the ultramafic rocks in the Venmag Mine. Photographs were taken by the candidate.

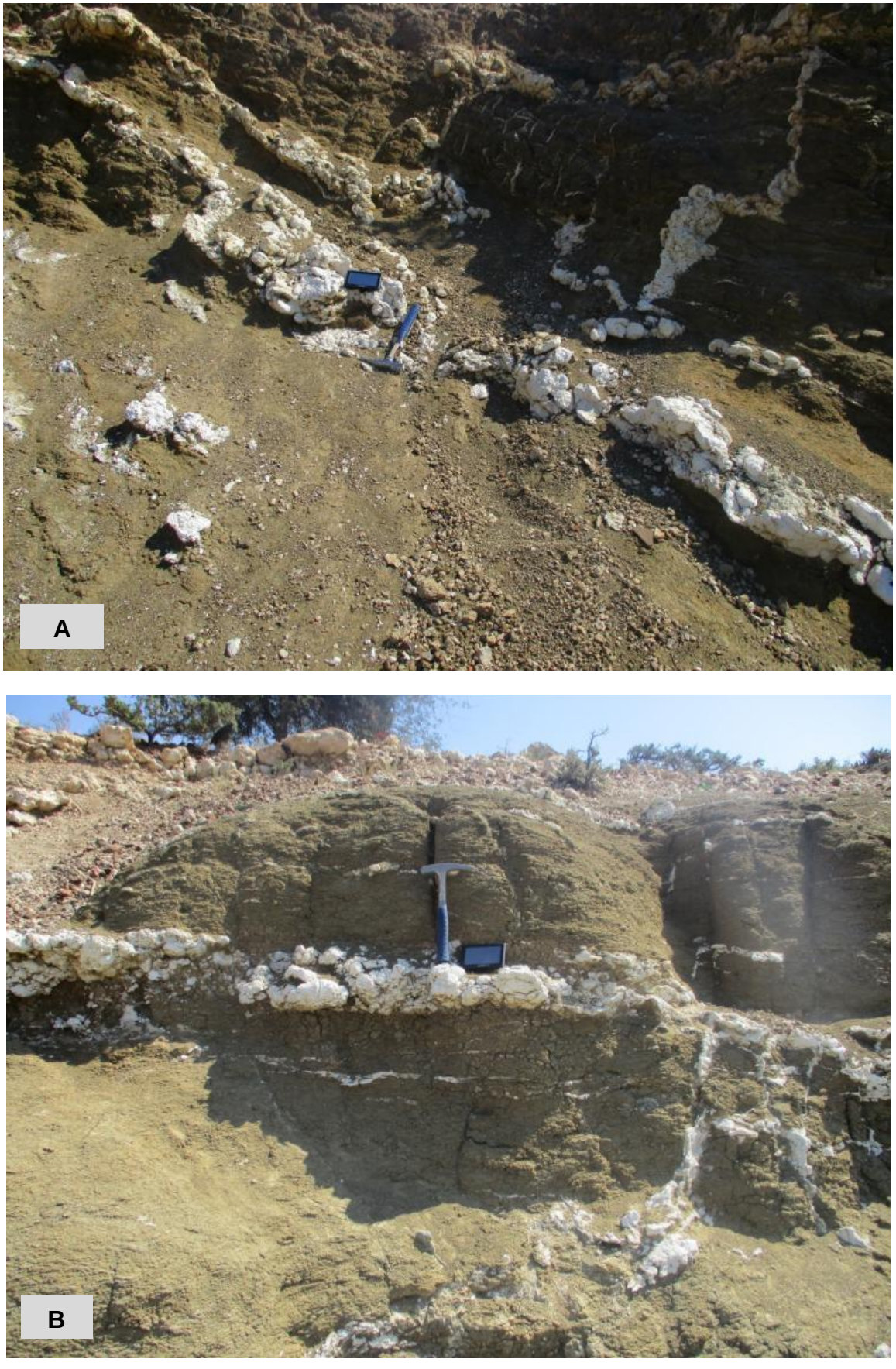


Figure 4.4: Magnesite veins (white in colour) (A & B) in the Venmag Mine. Photographs were taken by the candidate.

**(b) Folovhodwe magnesite mine**

Pit mapping for the Folovhodwe Mine showed similar results to those at the Venmag Mine. Deformed major and minor structures showed that the host ultramafic rocks were subjected to deformation due to compressive stress (Figure 4.5).

Figure 4.5: Magnesite veins in the horizontal beddings in the Folovhodwe Mine. The photograph was taken by the candidate.

Figure 4.6: Magnesite veins (white in colour) in sub-horizontal beddings and sub-vertical joints in the Folovhodwe Mine. The photograph was taken by the candidate.

Figure 4.7 interpreted the principal stress $\sigma_1$, maximum stress and $\sigma_3$, the minimum stress while the intermediate principal stress is horizontal as $\sigma_1$. The ultramafic rocks had been subjected to vertical tension and horizontal compression resulting in their being deformed in horizontal and sub-horizontal beddings compared to the joints resulting from lesser movement. The beddings were more mineralised compared to the joints.

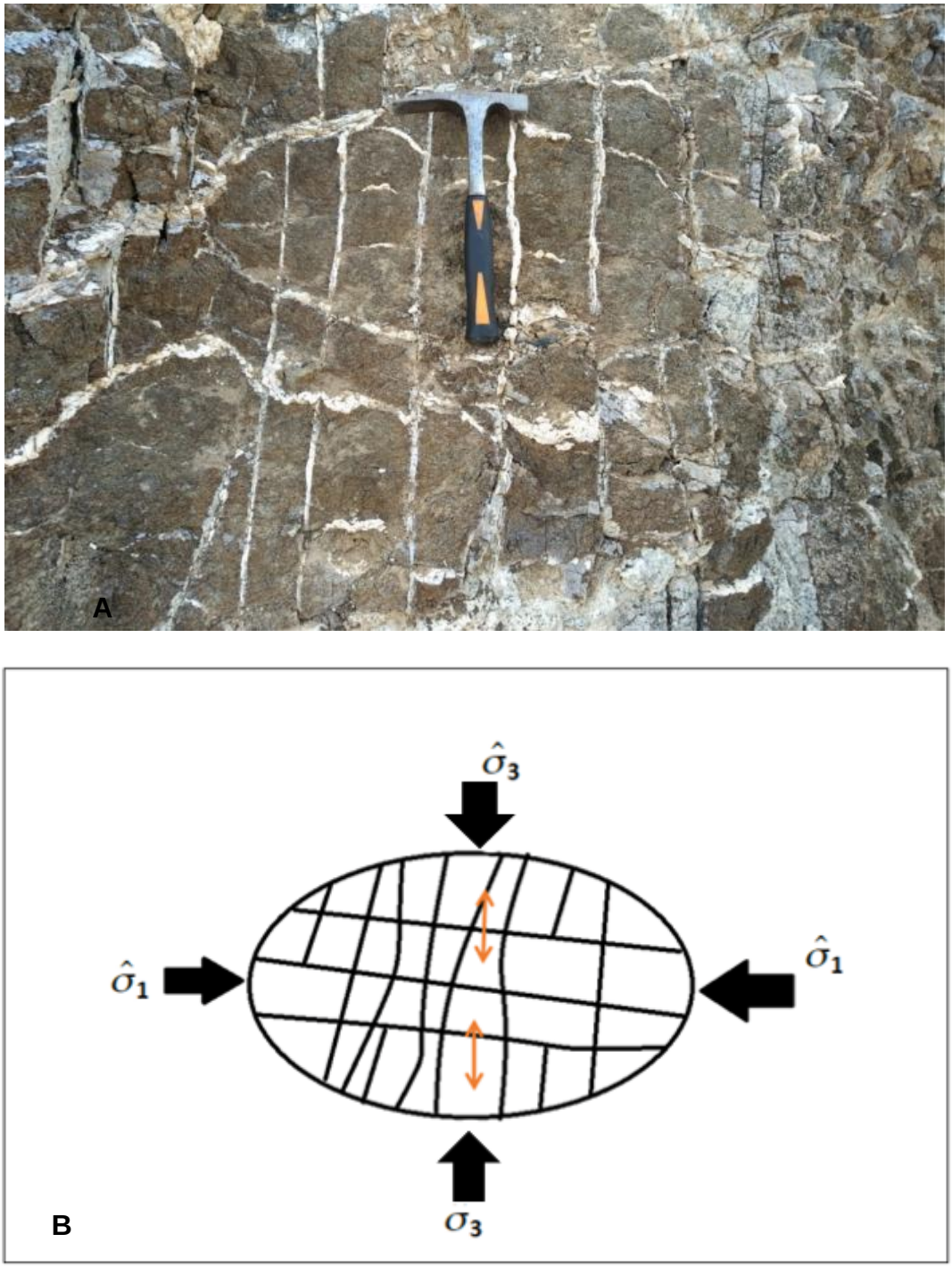


Figure 4.7: Field photo of magnesite veins (A) and sketch of ellipses of stress fields (B) in the Folovhodwe Mine ($\sigma_3$ vertical and $\sigma_1$ horizontal). The photograph was taken by the candidate.

**(c) Nyala Mine**

Nyala Magnesite Mine pit mapping showed similar results to that obtained at the Venmag and Folovhodwe Magnesite Mines in relation to the occurrence of magnesite in the ultramafic rocks and controlling structure (Figure 4.8).

Figure 4.8: Massive magnesite vein in the Nyala Mine. The photograph was taken by the candidate.

### 4.1.3 Host rock petrography, mineralogy and geochemistry

Petrographic, mineralogical and geochemical analysis was conducted for rocks demonstrating magnesite mineralisation, i.e., the ultramafic and dolerite rock samples collected from the Venmag (VR1, VR2 and VR3), Folovhodwe (FR1, FR2 and FR3) and Nyala (NR1 and NR2) Mines.

#### 4.1.3.1 Petrology

**(a) Venmag Mine ultramafic rocks**

The ultramafic rocks in the Venmag Mine showed a coarse-grained texture ranging from euhedral to subhedral. The major rock-forming minerals in the ultramafic rocks consisted of forsterite (Fo), clinopyroxene (Cpx), magnesite (Mgs) veinlets, augite (Aug), muscovite (Ms) and plagioclase (Pla), together with accessory minerals of ilmenite (Ilm) and (Lz) lizardite. The ultramafic rocks were enriched by veinlets and veins of magnesite mineralisation (Figure 4.9).

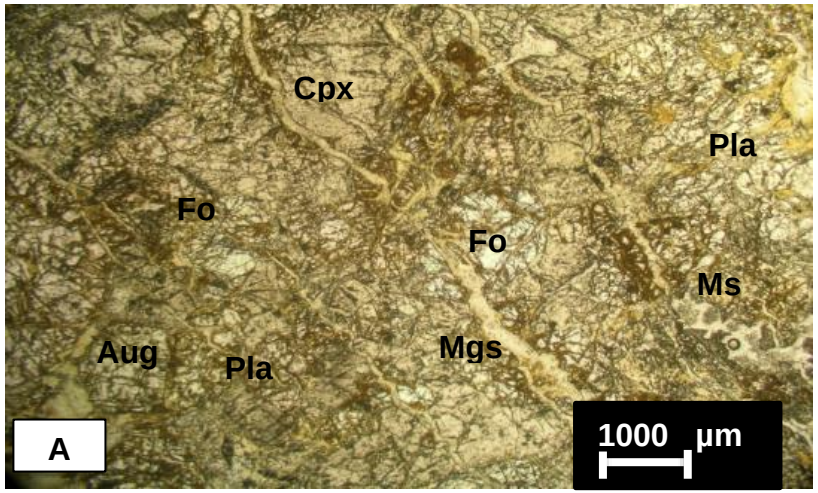


A. Plain polarisation (PPL) sample

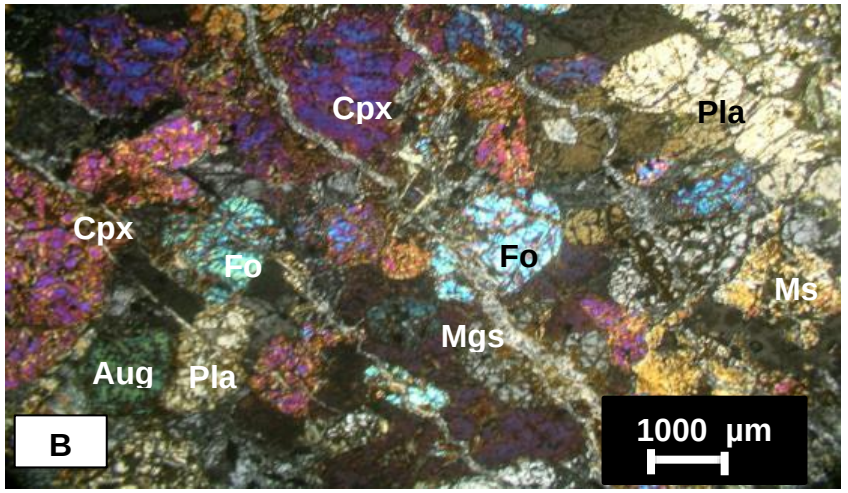


B. Cross polarisation (XPL) sample

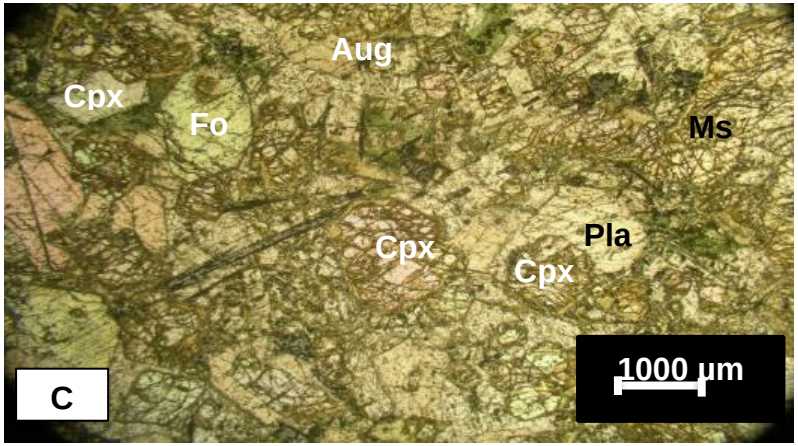


C. Plain polarisation (PPL) sample

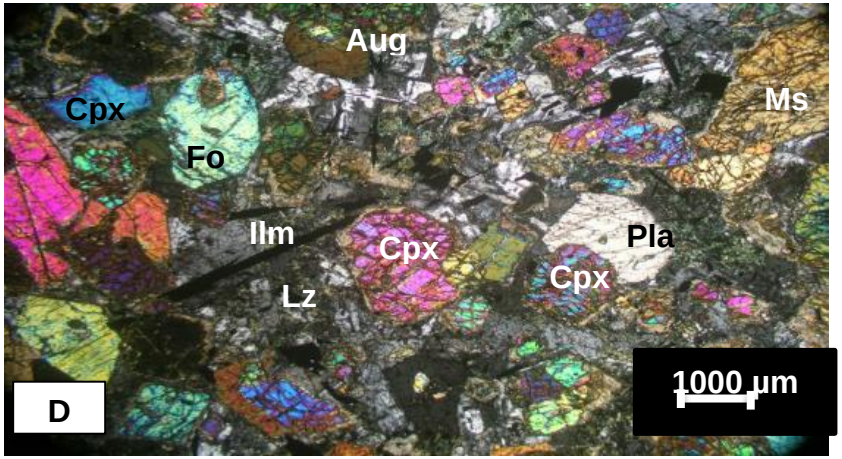


D. Cross polarisation (XPL) sample

Figure 4.9: Photomicrographs of ultramafic rocks (A, B, C & D) in the Venmag Mine VR1 and VR2 samples. Photographs were taken by the candidate. Note: forsterite (Fo), clinopyroxene (Cpx), augite (Aug), plagioclase (Pla), magnesite (Mgs), muscovite (Ms), ilmenite (Ilm) and lizardite (Lz).

### (b) Folovhodwe Mine

In the Folovhodwe Mine, the petrological study showed similarities in texture, mineral composition and alteration and replacement of the minerals in the ultramafic rocks. Major minerals such as forsterite and plagioclase showed alteration by magnesite veins and ilmenite (Ilm) and lizardite (Lz) as accessory minerals (Figure 4.10).

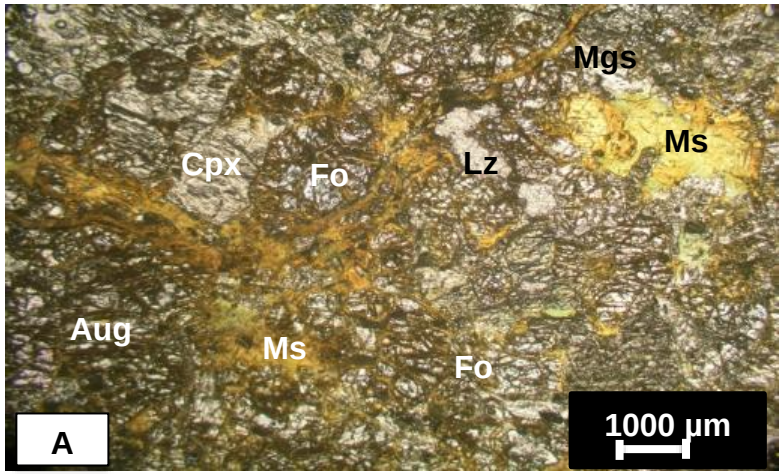


A. Plain polarisation (PPL) sample

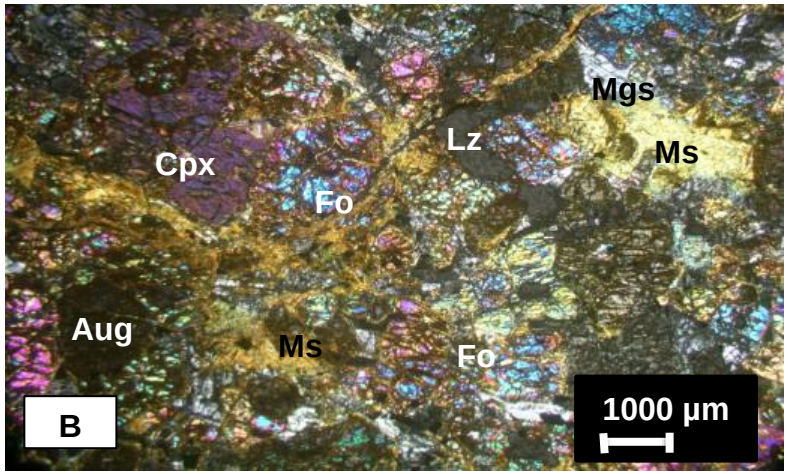


B. Cross polarisation (XPL) sample

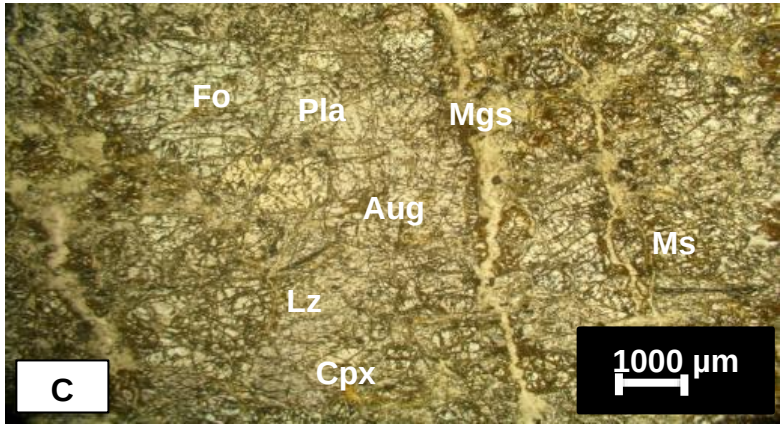


C. Plain polarisation (PPL) sample

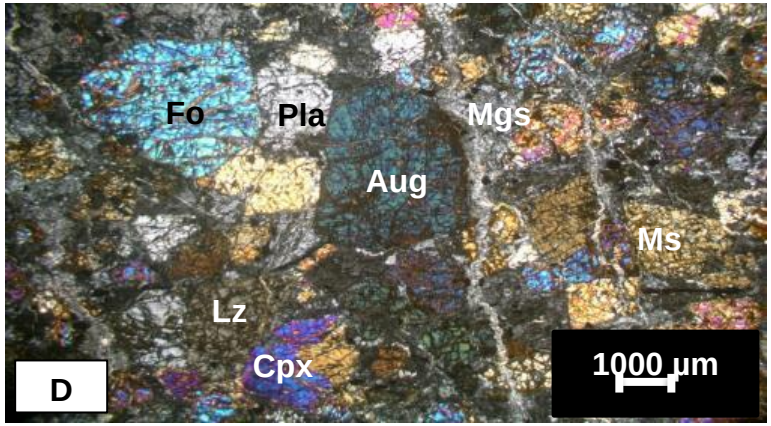


D. Cross polarisation (XPL) sample

Figure 4.10: Photomicrographs of ultramafic rocks (A, B, C & D) in the Folovhodwe Mine FR1 and FR2 samples. Note: Clinopyroxene (Cpx), augite (Aug), forsterite (Fo), magnesite (Mgs), lizardite (Lz) and muscovite (Ms).

### (c) Nyala Mine ultramafic rocks

The ultramafic rocks collected in the Nyala Mine showed similar results to the Venmag and Folovhodwe Mines regarding the texture, mineral composition and replacement and alteration of the forsterite (magnesite veins showing mineralisation along the grains and plagioclase (Figure 4.11).

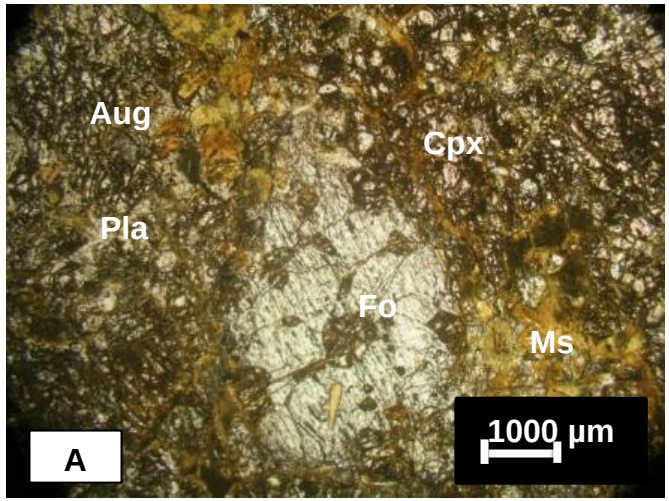


A. Plain polarisation (PPL) sample

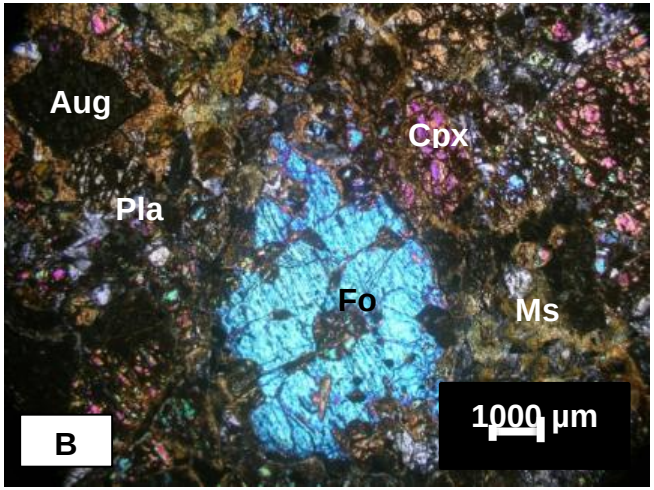


B. Cross polarisation (XPL) sample

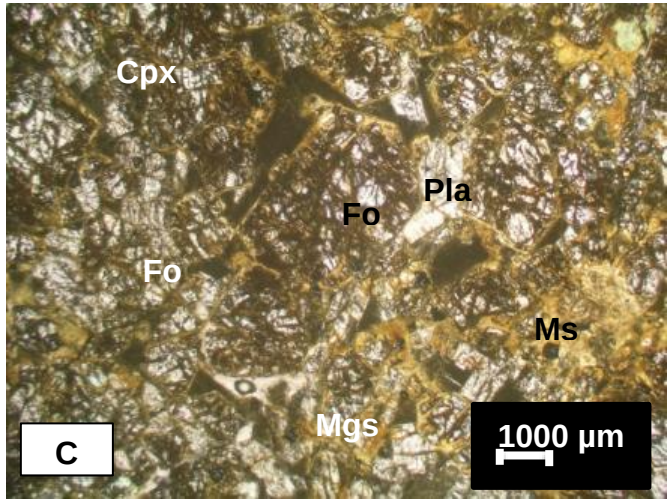


C. Plain polarisation (PPL) sample

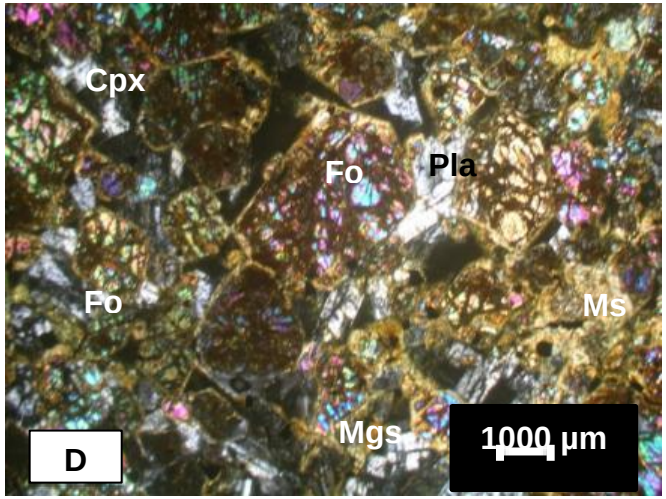


D. Cross polarisation (XPL) sample

Figure 4.11: Photomicrograph of ultramafic rocks (A, B, C & D) in the Nyala Mine NR1 and NR2 samples. Note: forsterite (Fo), plagioclase (Pla), muscovite (Ms), clinopyroxene (Cpx) and magnesite (Mgs).

### (d) Dolerite rock samples

The dolerite soil samples collected in the Venmag and Folovhodwe Mines typically consisted of fine-grained minerals. The major minerals were plagioclase and pyroxene with accessory minerals such as ilmenite and magnetite (Figures 4.15 and 4.16). The plagioclase grains were completely enclosed by pyroxene grains showing an ophitic texture (Figure 4.12).

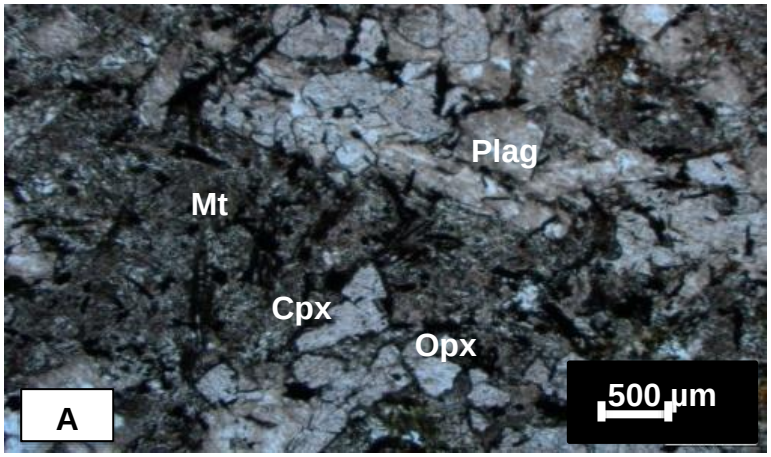


A. Plain polarisation (PPL) sample

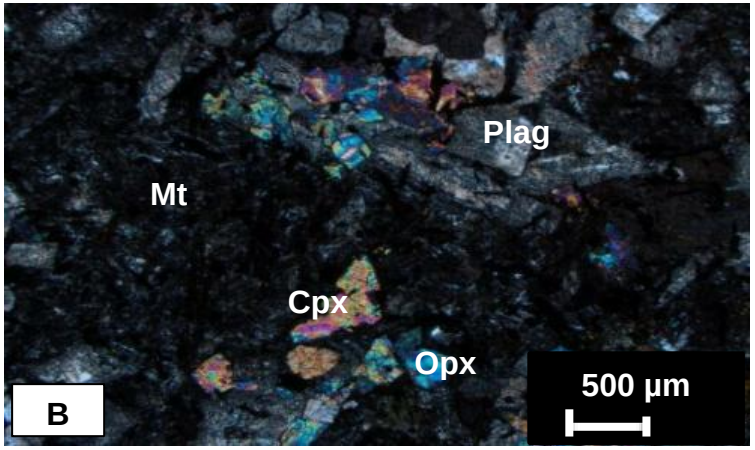


B. Cross polarisation (XPL) sample

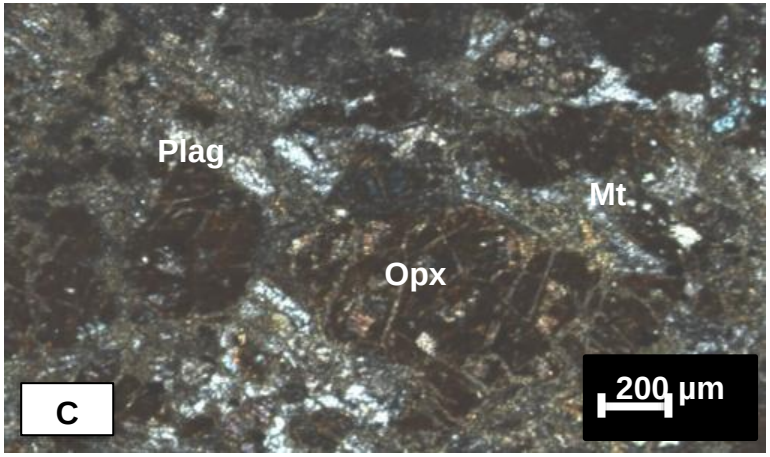


C. Plain polarisation (PPL) sample

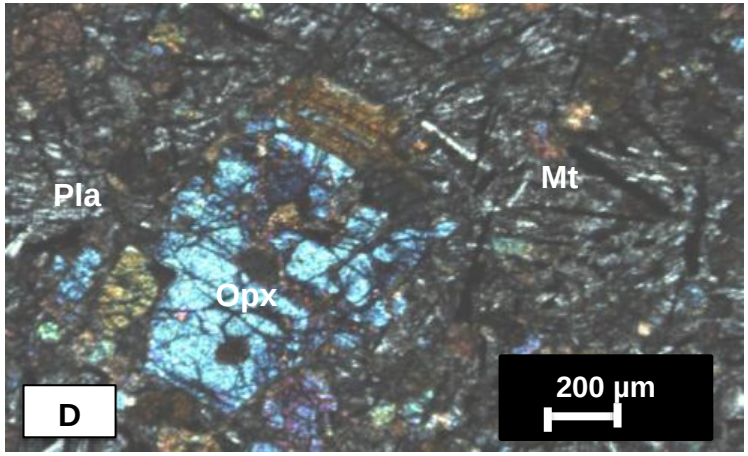


D. Cross polarisation (XPL) sample

Figure 4.12: Photomicrographs of the dolerite rocks (A&B) in the Venmag VR3 and Folovhodwe Mines FR3 samples. Note: plagioclase (Pla), magnetite (Mt), Orthopyroxene (Opx) and clinopyroxene (Cpx).

### 4.1.3.2 Mineralogy

This section presents the classification of the igneous rocks of the Tshipise magnesite area so as to understand the host rock type of the magnesite deposits. Table 4.1 shows the mineralogical composition of ultramafic rock samples collected at the three mines, i.e., FR1, FR2, VR1, VR2, NR1, NR2 and mafic rocks VR3 and FR3 based on the Bowens reaction series (Figure 4.13). According to the Bowens reaction series, igneous rocks are named based on the proportion of different minerals they contain.

The proportions of the mineralogical compositions of the ultramafic and mafic rocks were recalculated for the olivine (forsterite) and pyroxene minerals. The results presented in Figure 4.13 show that rock samples FR1, FR2, VR1, VR2, NR1 and NR2 have higher wt% of the olivine minerals while they have less pyroxene minerals and in the igneous classification Figure 4.13, they fall in the ultramafic rocks category. The silica content (wt%) also showed that samples FR1, FR2, VR1, VR2, NR1 and NR2 fall into the ultramafic rocks category.

The mineral compositions of the VR3 and FR3 showed that they were enriching of the pyroxene minerals while the olivine minerals were very low. The silica contents for samples VR3 and FR3 also showed that they fall in the mafic rock category (Figure 4.13).

Table 4.1: Mineralogical compositions of the ultramafic (FR1, FR2, VR1, VR2, NR1 and NR2) and mafic rock samples (VR3, FR3) collected at three mines

| | **FR1** | **FR2** | **VR1** | **VR2** | **NR1** | **NR2** | **VR3** | **FR3** |
|---|---|---|---|---|---|---|---|---|
| Olivine | 31,35 | 38,68 | 30,11 | 46,70 | 38,90 | 40,10 | 0,28 | 0,59 |
| Pyroxene | 15,15 | 14,04 | 13,36 | 13,94 | 13,80 | 14,10 | 9,89 | 10,03 |
| **Total** | **46,50** | **52,72** | **43,47** | **60,64** | **52,70** | **54,20** | **10,17** | **10,62** |

Recalculated Wt% of the ultramafic/mafic rocks

| | **FR1** | **FR2** | **VR1** | **VR2** | **NR1** | **NR2** | **VR3** | **FR3** |
|---|---|---|---|---|---|---|---|---|
| Olivine | 67,42 | 73,37 | 69,27 | 77,01 | 73,81 | 73,99 | 2,75 | 5,56 |
| Pyroxene | 32,58 | 26,63 | 30,73 | 22,99 | 26,19 | 26,01 | 97,25 | 94,44 |
| **Total** | **100,00** | **100,00** | **100,00** | **100,00** | **100,00** | **100,00** | **100,00** | **100,00** |

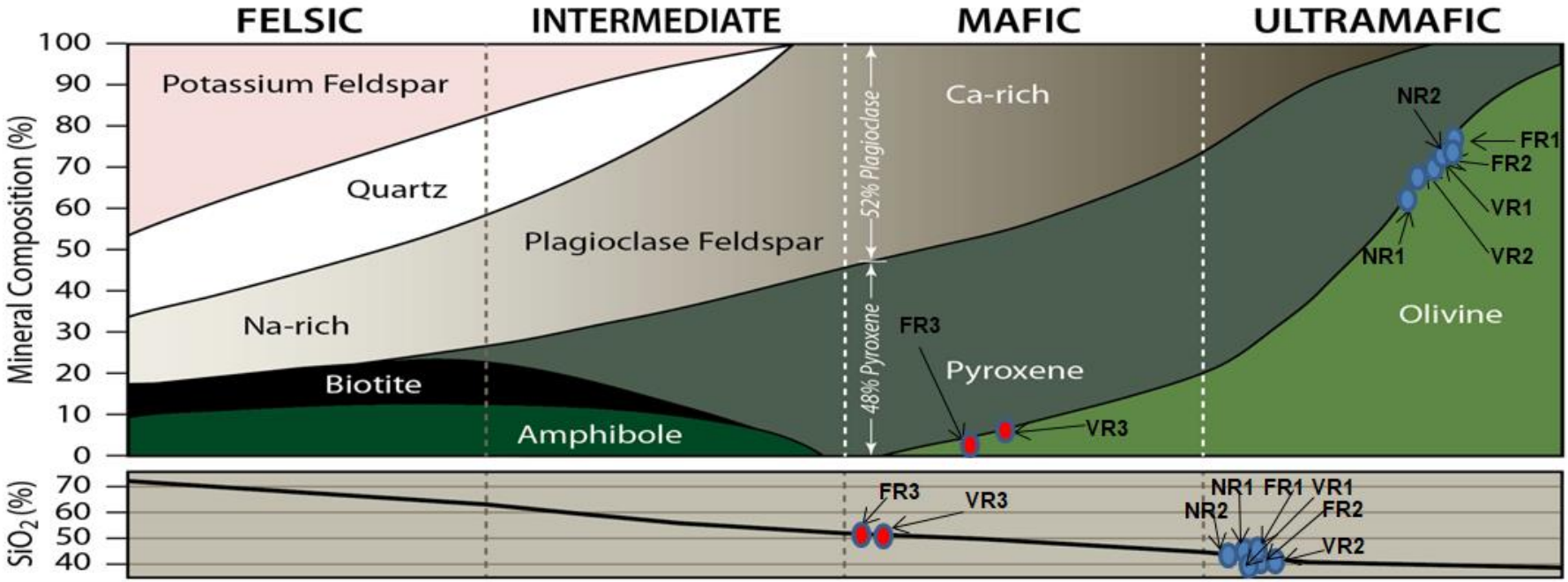


Figure 4.13: Classification of igneous rocks according to mineral composition. Adopted from Bowen (1956).

Note: Mafic rock (red circles) and Ultramafic rock (blue circles).

The classification of ultramafic rocks based on the wt% of olivine, orthopyroxene and clinopyroxene is shown in Figure 4.14. According to this figure, analysis of the ultramafic rock samples collected from the Tshipise magnesite field showed that all samples (FR1, FR2, VR1, VR2, NR1 and NR2) fall in the olivine rich minerals websterite (Wherlite and Lherzolite) while the mafic rock samples (VR3 and FR3) were classified as clinopyroxene as they differed from the ultramafic rock samples by rather being enriched with olivine and Websterite minerals.

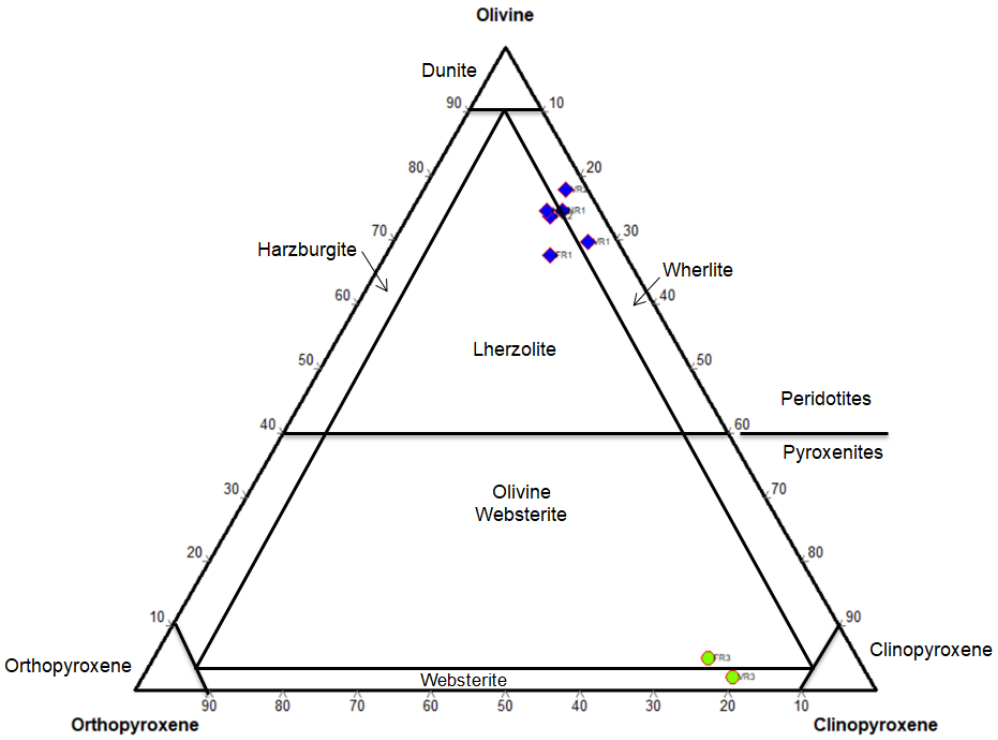


Figure 4.14: Characterisation of the Tshipise ultramafic (blue diamonds) and mafic (green circles) rocks. Modified from Bodinier and Godard (2004).

### 4.1.3.4 Geochemistry

Under this section, the discussion focuses on the geochemical analysis of magnesite ore and its host rock samples from the Venmag, Folovhodwe and Nyala Mines. The dolerite (FR3 and VR3), ultramafic rocks (VR1, VR2, FR1, FR2, NR1, and NR2), and magnesite ore (VM1, FM1, and NM1) samples were analysed for major elements using the ICP-EOS and trace elements using XRF at Geolabs Global (Centurion, South Africa).

### (a) Major oxides

All ten samples of ultramafic (n=6) and dolerite (n=2) rocks, and magnesite ore (n=3) were analysed for major oxides using XRF. The results are presented and discussed in the subsequent sections.

### (i) Ultramafic rocks

The major oxides of ultramafic rock samples that were analysed by XRF are presented in Table 4.2. This shows that the ultramafic rocks from the three magnesite mines consist mainly of silica ranging from 41.14 wt% to 44.20 wt%. The amounts of MgO of all the samples are ranging from 10.90 wt% to 24.75 wt% with an average content of 16.16 wt%. Thus, the ultramafic rocks contained a relatively high proportion of MgO. The silica contents of these rock samples were plotted in the area of ultramafic rocks category and are shown in Figure 4.13.

Table 4.2: Relative percentage compositions of the major oxides in the ultramafic rock samples.

| Sample | VR1 | VR2 | FR1 | FR2 | NR1 | NR2 | Average | Std Dev | Min | Max |
|---|---|---|---|---|---|---|---|---|---|---|
| **$SiO_2$** | 42.10 | 41.14 | 43.90 | 43.10 | 42.99 | 44.20 | **42.91** | 1.14 | 41.14 | 44.20 |
| **$Al_2O_3$** | 9.14 | 4.16 | 6.68 | 4.20 | 7.90 | 8.48 | 6.76 | 2.16 | 4.16 | 9.14 |
| **$Fe_2O_3$** | 11.60 | 15.08 | 13.32 | 14.70 | 12.78 | 11.33 | **13.14** | 1.55 | 11.33 | 15.08 |
| **$TiO_2$** | 3.15 | 1.43 | 1.59 | 2.13 | 2.40 | 2.91 | 2.27 | 0.69 | 1.43 | 3.15 |
| **FeO** | 8.09 | 7.10 | 5.99 | 6.70 | 5.97 | 7.09 | 6.82 | 0.80 | 5.97 | 8.09 |
| **CaO** | 7.41 | 2.98 | 5.31 | 9.10 | 6.65 | 4.32 | 5.96 | 2.21 | 2.98 | 9.10 |
| **MgO** | 12.30 | 24.75 | 16.97 | 10.90 | 16.10 | 15.80 | **16.14** | 4.84 | 10.90 | 24.75 |
| **$Na_2O$** | 2.01 | 0.79 | 0.73 | 1.45 | 1.70 | 0.93 | 1.27 | 0.53 | 0.73 | 2.01 |
| **$K_2O$** | 2.99 | 1.05 | 1.22 | 1.99 | 1.24 | 1.98 | 1.74 | 0.73 | 1.05 | 2.99 |
| **MnO** | 0.15 | 0.17 | 0.16 | 1.50 | 0.91 | 0.29 | 0.53 | 0.56 | 0.15 | 1.50 |
| **$P_2O_5$** | 0.58 | 0.25 | 0.65 | 0.43 | 0.25 | 0.37 | 0.42 | 0.17 | 0.25 | 0.65 |
| **L.O.I.** | 0.70 | 1.23 | 3.37 | 3.90 | 0.90 | 2.21 | 2.05 | 1.34 | 0.70 | 3.90 |
| **Total** | 100.00 | 100.00 | 100.00 | 100.00 | 100.00 | 100.00 | 100.00 | 0.00 | 100.00 | 100.00 |

NB: Determined using XRF analysis.

### (ii) Dolerite Rocks

Dolerite rock samples only were collected from Venmag and Folovhodwe Mines. The major oxides (chemical components) from the dolerite rock samples were analysed using XRF (Table 4.3). These rocks were composed of a higher content of silica

ranging from 50.70 wt% to 51.00 wt%, with a relatively higher $Al_2O_3$ content between 10.92 wt% and 11.60 wt% compared to the tested ultramafic rock samples. The next most common oxide was $Fe_2O_3$ (between 9.21 wt% and 10.90 wt%). These rocks contained a relatively lower proportion of MgO (ranging from 3.11 wt% to 3.61 wt%) compared to the content of MgO tested in the ultramafic rock samples (Table 4.2).

Table 4.3: Relative percentage compositions of the major oxides in the mafic rock samples.

| Sample | VR3 | FR3 | Average |
|---|---|---|---|
| **$SiO_2$** | **50,7** | **51** | **50,85** |
| **$Al_2O_3$** | **11,6** | **10,92** | **11,26** |
| **$Fe_2O_3$** | **9,21** | **10,9** | **10,055** |
| **$TiO_2$** | 3,84 | 4,26 | **4,05** |
| **FeO** | 6,44 | 5,3 | **5,87** |
| **CaO** | 6,35 | 7,1 | **6,725** |
| **MgO** | 3,11 | 3,61 | **3,36** |
| **$Na_2O$** | 2,63 | 2,77 | **2,7** |
| **$K_2O$** | 4,42 | 2,76 | **3,59** |
| **MnO** | 0,11 | 0,12 | **0,115** |
| **$P_2O_5$** | 0,78 | 0,73 | **0,755** |
| **L.O.I.** | 1,06 | 0,82 | **0,94** |
| **Total** | 100 | 100 | **100** |

NB: Determined using XRF analysis.

**(b) Trace elements**

**(i) Ultramafic rocks**

The ultramafic rock samples collected from the Venmag, Folovhodwe and Nyala Mines were analysed for trace elements using XRF (Table 4.4). The relative amounts of the trace elements of these ultramafic rocks collected from the three mines were very low.

Table 4.4: Trace elements concentrations of the ultramafic rock samples.

| Sample | VR1 | VR2 | FR1 | FR2 | NR1 | NR2 |
|---|---|---|---|---|---|---|
| **Ba** | 1300 | 1200 | 1400 | 1300 | 1100 | 1000 |
| **Cr** | **900** | 500 | 300 | 200 | 400 | 500 |
| **Cu** | 100 | 200 | 100 | **1000** | 200 | 100 |
| **Ni** | **500** | 100 | 300 | 200 | 100 | 200 |
| **V** | 300 | 300 | 100 | 100 | 100 | 400 |
| **Zn** | 200 | 100 | 200 | **900** | 100 | 200 |
| **Li** | 0 | 100 | **900** | 0 | 0 | 100 |
| **Nb** | 100 | 0 | 100 | 100 | 100 | 100 |
| **Sn** | 100 | 100 | 100 | 100 | 100 | 100 |
| **Ta** | 100 | 100 | 100 | 100 | 100 | 100 |
| **Rb** | **400** | 100 | 100 | 100 | 100 | 100 |
| **W** | 100 | 100 | 100 | 100 | 100 | 100 |

NB: Concentration figures presented in parts per million (ppm).

### (ii) Dolerite rocks

The trace elements from the dolerite rock samples were analysed by XRF as shown in Table 4.5. Although there were significant variations in the relative amounts of Ba and Rb between the two rock samples, the trace elements in the dolerite samples were detected at a very low concentration.

Table 4.5: Trace elements concentrations in the dolerite rock samples.

| Sample | VR3 | FR3 |
|---|---|---|
| **Ba** | **1700** | 300 |
| **Cr** | 100 | 300 |
| **Cu** | 200 | 200 |
| **Ni** | 100 | 200 |
| **V** | 300 | 300 |
| **Zn** | 100 | 100 |
| **Nb** | 100 | 100 |
| **Sn** | 100 | 100 |
| **Ta** | 100 | 100 |
| **Rb** | **500** | 100 |
| **W** | 100 | 100 |

NB: Concentration figures presented in parts per million (ppm).

**(ii) Magnesite ore**

A total of three samples of magnesite ore were collected from the magnesite mines as follows: Venmag sample (VM1), Folovhodwe sample (FM1) and Nyala sample (NM1). The magnesite ore samples were analysed for trace elements using XRF and the results are shown in Table 4.6.

Table 4.6: Trace elements concentrations in the magnesite ore samples.

| Sample | VM1 | FM1 | NM1 |
|---|---|---|---|
| **Ba** | **160** | 40 | 10 |
| **Cr** | **70** | 10 | 10 |
| **Cu** | 10 | 10 | 10 |
| **Ni** | 110 | 50 | 130 |
| **V** | 10 | 10 | 10 |
| **Zn** | 10 | 10 | 10 |
| **Li** | **23.2** | 14.3 | 14.3 |
| **Nb** | 100 | 100 | 100 |
| **Sn** | 100 | 100 | **200** |
| **Ta** | 100 | 100 | 100 |
| **Rb** | 100 | 100 | 100 |

NB: Concentration figures presented in parts per million (ppm).

### 4.1.3.4 Geochemical data analysis

### AFM diagram

The ternary plots of the AFM (Tables 4.7 and 4.8) showed that the ultramafic rocks contained more MgO compared to the dolerite rock samples, whereas the dolerite samples contained more FeO compared to the ultramafic rocks (Figure 4.15).

Table 4.7: AFM ternary diagrams representing ultramafic rocks.

| Sample | A | F | M | t | A% | F% | M% |
|---|---|---|---|---|---|---|---|
| VR1 | 9.30 | 8.90 | 12.30 | 30.50 | 30.49 | 29.18 | 40.33 |
| VR2 | 4.16 | 7.10 | 24.75 | 36.01 | 11.55 | 19.71 | 68.73 |
| FR1 | 6.68 | 5.99 | 16.97 | 29.64 | 22.54 | 20.21 | 57.25 |
| FR2 | 4.20 | 6.70 | 10.90 | 21.80 | 19.27 | 30.73 | 50.00 |
| NR1 | 7.90 | 5.97 | 16.10 | 29.97 | 26.35 | 19.92 | 53.72 |
| NR2 | 8.48 | 7.09 | 15.80 | 31.37 | 27.03 | 22.60 | 50.37 |

Table 4.8: AFM ternary diagrams representing dolerite rocks.

| **Sample** | **A** | **F** | **M** | **t** | **A%** | **F%** | **M%** |
|---|---|---|---|---|---|---|---|
| VR3 | 11.60 | 6.44 | 3.11 | 21.15 | 54.85 | 30.45 | 14.70 |
| FR3 | 10.92 | 5.30 | 3.61 | 19.83 | 54.81 | 26.61 | 18.12 |

NB: AFM calculations for Table 4.7 and 4.8 are represented in Appendix A.

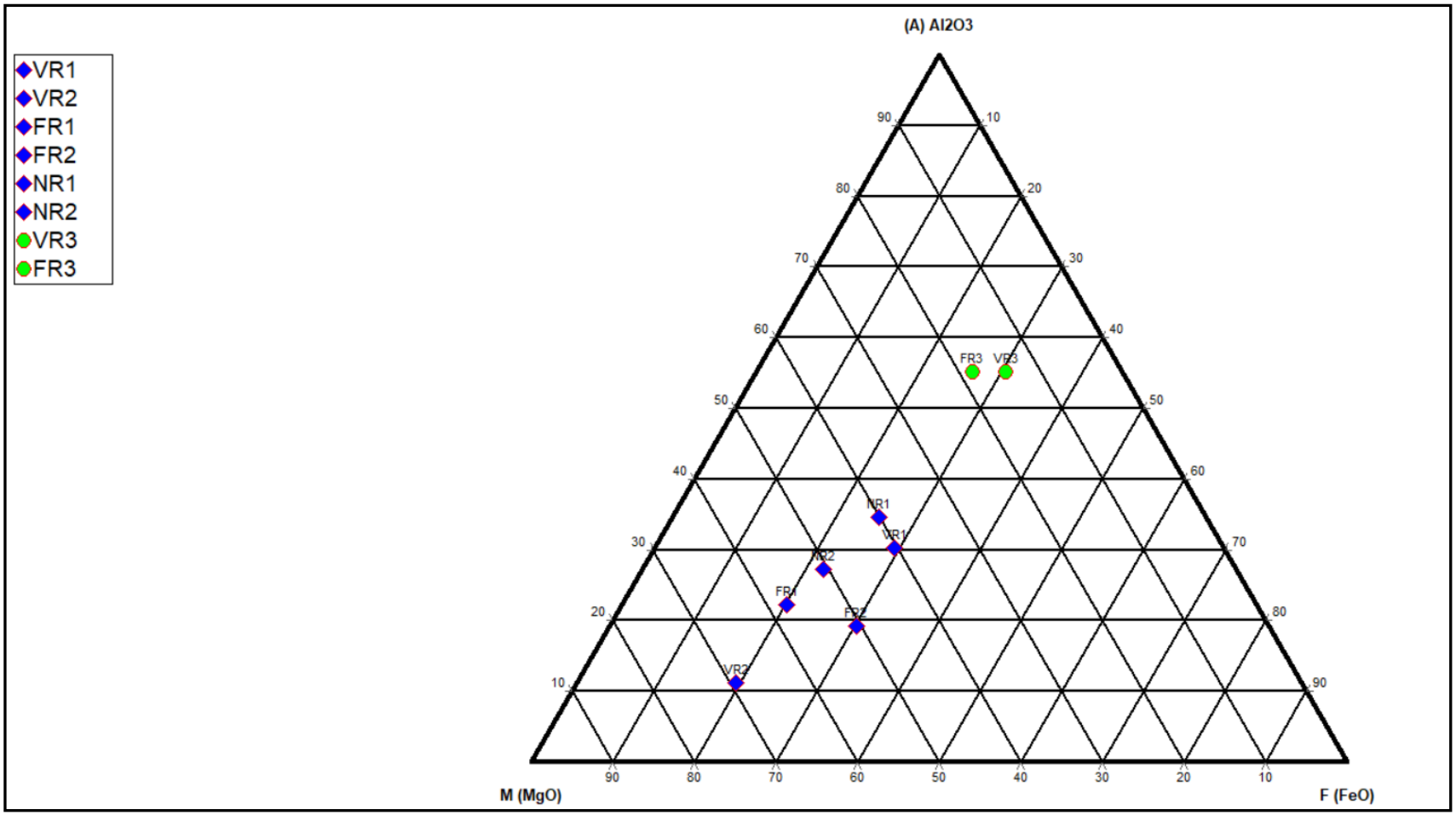


Figure 4.15: AFM plot showing magnesium, aluminium and iron proportions in the ultramafic (blue diamonds) and dolerite (green circles) rocks samples.

## 4.2 Preliminary magnesite resources evaluation

The preliminary magnesite resource evaluation was estimated based on the measurement of pits from Google Earth© in terms of geometry such as areas and depths for the Venmag, Folovhodwe and Nyala Mines. For this study, two resources were assessed, i.e., the waste rock dump and the virgin ground ore (Abzalov, 2016).

### 4.2.1 Venmag Mine

Only one type of resource was assessed, i.e., waste rock dumps because there was no detailed work done in the pits and virgin ground. The total calculated resource of magnesite was based on the volume of the materials in the waste rock dumps and the density of the magnesite ore. The waste rock dumps exist in Venmag mine, namely Dump 1, Dump 2, Dump 3, Dump 4, Dump 5 and Dump 6 (Appendices E and F). The major evaluation parameters were as follows:

(a) Waste rock dumps

| | |
|---|---|
| *Volume ($m^3$)* | *151 912* |
| *Tonnages (t)* | *270 403* |
| *Resources based on grade 2 % (tonnes)* | *135 202* |

Thus, the magnesite resource was preliminarily estimated to be 135 202 tonnes.

### 4.2.2 Folovhodwe Mine

Two types of resources were assessed, i.e., waste rock dumps, the virgin ground and mine pits. Calculations were based on the preliminary data obtained from the Google Earth© geometry and an assumed average depth of 30 m for all three of the Venmag, Folovhodwe and Nyala Mines.

(a) Waste rock dumps

Two waste rock dumps exist in Folovhodwe Mine, namely Dump 1 and Dump 2 (Appendices E and F). The major evaluation parameters were as follows:

| | |
|---|---|
| *Volume ($m^3$)* | *1 098 020* |
| *Tonnages (t)* | *208 233* |
| *Resources Based on grade 2 % (tonnes)* | *104 117* |

(b) Virgin Ground Ore (Unmined)

There are two types of virgin ground ores:

Mined ores located at a shallow depth left by open pit mining, such as Pits 1, 2, 3 that were only mined to depths of 7 m, 7 m and 5 m, respectively, while 30 m in depth can be mined in a dry environment and large pits; and unmined or touched virgin ground with magnesite mineralisation (Appendices E and F).

(i) Deepening the Pits

The major parameters are as follows:

| | |
|---|---|
| *Volume ($m^3$)* | *1 126 220* |
| *Tonnages (t)* | *3 356 136* |
| *Resources based on grade 6.5% (tonnes)* | *258 164* |

(ii) Virgin Ground

| | |
|---|---|
| *Volume ($m^3$)* | *1 820 460* |
| *Tonnages (t)* | *5 424 971* |
| *Resources based on grade 6.5% (tonnes)* | *417 305* |

(iii) Total Resources

| | |
|---|---|
| *Volume ($m^3$)* | *4 044 700* |
| *Tonnages (t)* | *8 989 340* |
| *Resources based on grade 6.5% (tonnes)* | *691 488* |

### 4.2.3 Nyala Mine

Three types of the resource were assessed, i.e., waste rock dumps, mine pits and virgin ground (Appendix E and F).

The major parameters are as follows:

(a) Waste rock dumps

| | |
|---|---|
| *Volume ($m^3$)* | *123 915* |
| *Tonnages (t)* | *220 569* |
| *Resources based on grade 2 % (tonnes)* | *110 284* |

*(b) Deepening the Pits*

| | |
|---|---|
| *Volume ($m^3$)* | *813 320* |
| *Tonnages (t)* | *2 423 694* |
| *Resources based on grade 6.5% (tonnes)* | *186 438* |

(ii) Virgin Ground (Unmined ground)

| | |
|---|---|
| *Volume ($m^3$)* | *2 742 600* |
| *Tonnages (t)* | *8 172 948* |
| *Resources based on grade 6.5% (tonnes)* | *628 688* |

(iii) Total Resources

| | |
|---|---|
| *Volume ($m^3$)* | *3 679 835* |
| *Tonnages (t)* | *10 817 210* |
| *Resources based on grade 6,5 % (tonnes)* | *832 093* |

NB: All resources estimated for the above mines are indicated in Appendix D.

## 4.3 Environmental impact assessment at Venmag Mine

This section discusses the results from the analysis of soil and waste rock dumps of the Venmag Mine. Figure 4.16 shows the location for the soil samples and waste rock dumps samples from the Venmag Mine.

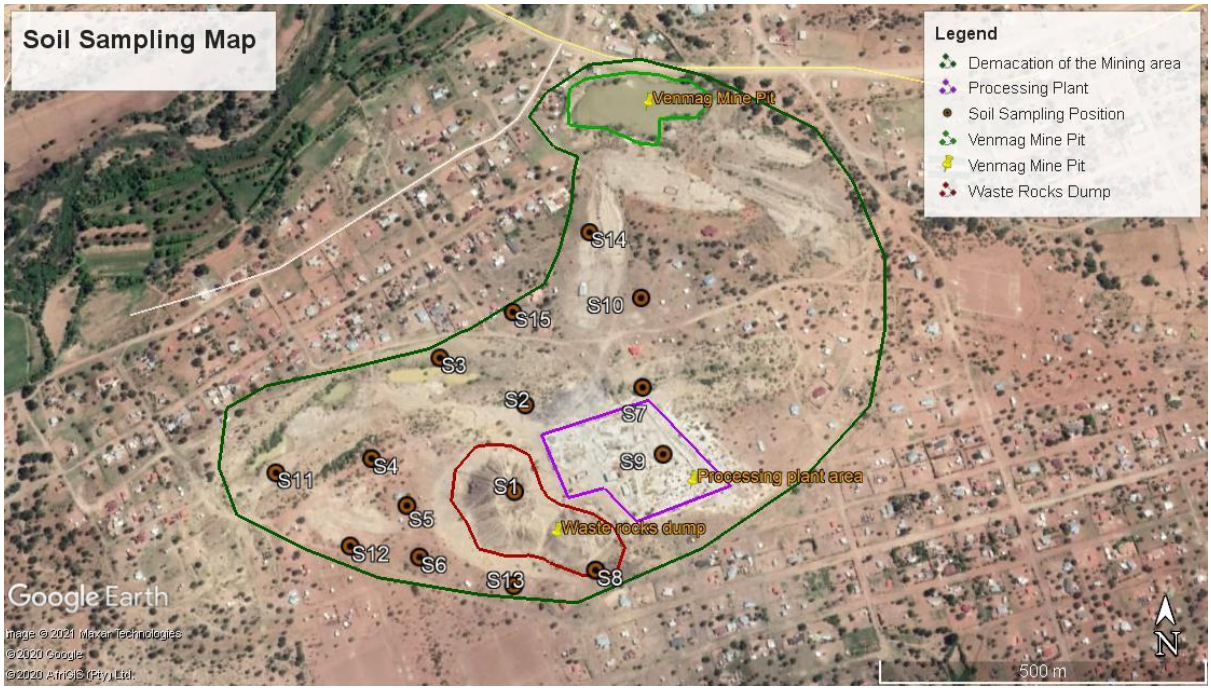


Figure 4.16: Venmag soil sampling positions (Maroon circles) (Pit, waste rock dumps and demarcation line affected by mining). NB the green colour - Venmag pit, dark green colour - demarcation mine area, Maroon colour - Waste rock dumps, and purple colour - processing plant area.

### 4.3.1 Analysis of soil and waste rock samples from the Venmag Mine

A total of 15 samples were collected from the Venmag Mine and the surrounding waste rock dump area to understand the environmental impact of trace element and heavy metal pollution originating from the Venmag mine dumps. The following labelled samples were collected from the waste rock dumps, i.e., S1, S2, S6, S11, S12, and S14 while samples labelled S3, S4, S5, S7, S8, S9, S10, S13, and S15 were collected from areas surrounding the dumps (Figure 4.16).

#### 4.3.1.1 Trace elements

Trace elements that were detected in samples collected from the surrounding area of the waste rock dumps were compared with the WHO (2007) guidelines for vegetation and soil as well as the SASV (2010) for land use. This was done to understand the level of leaching of trace elements from the waste rock dumps to the surrounding environment. The distribution of trace elements in different soil samples was: (ppm) Ba 0.02-0.14, Cr 0.02-0.07, Cu 0.00-0.001, Ni 0.00-0.03, and Zn 0.00-0.01 (Tables 4.9 and 4.10).

All the soil samples analysed for heavy metals showed low concentrations below the WHO (2007) standards and the SASV (2010) guideline for permissible limits for soil heavy metals. The soil chemical analysis indicated that the soil was not contaminated with trace elements originating from the mine dumps.

Iron (Fe) was noted at relatively very high levels, at up to 100x the concentration of the next most prevalent element (Cr). Copper (Cu) was often not detected and Ni was detected at low levels. The highest concentration of Ni (0,03 ppm) was obtained from sample S5 and the lowest (0,0001 ppm) was obtained from S8, S9, and S13. The concentrations of the Cu were found to be below the detection limits for all samples (Table 4.9).

Table 4.9: Trace elements concentrations in the soil samples of the Venmag Mine.

| ID | Fe | Cr | Cu | Ni |
|---|---|---|---|---|
| **WHO (Soil)** | 50,00 | 1,00 | 2,00 | 0,07 |
| **South African Screening values for standard residential** | n.a | 13,00 | 2,300 | 1,200 |
| **S3** | 3,14 | 0,06 | 0,00 | 0,02 |
| **S4** | 3,88 | 0,04 | 0,00 | 0,01 |
| **S5** | 6,41 | 0,05 | 0,01 | 0,03 |
| **S7** | 3,43 | 0,05 | 0,00 | 0,02 |
| **S8** | 3,03 | 0,03 | 0,00 | 0,00 |
| **S9** | 4,91 | 0,02 | 0,00 | 0,00 |
| **S10** | 3,73 | 0,02 | 0,01 | 0,01 |
| **S13** | 2,45 | 0,03 | 0,00 | 0,00 |
| **S15** | 3,72 | 0,07 | 0,01 | 0,02 |
| **Mean** | 3,86 | 0,04 | 0,00 | 0,01 |

Note: Concentration of trace elements presented in parts per million (ppm).

Table 4.10 shows the internal background values compared with metals from the waste rock dumps and soil samples. The highest concentration of Ni (0,08 ppm) was obtained from S1 and S6 samples and the lowest was obtained from (0,02 ppm) S11, S15, and S13. The concentrations of the Cu (0,01 ppm) were found to be below the detection limits for all samples.

The results that were obtained from both internal and external control samples were further used to evaluate the pollution levels due to anthropogenic activities within the

study area. This study revealed that all soil samples complied with the WHO (2007) and SASV (2010) guidelines.

Table 4.10: Trace elements concentrations of waste rock dump samples of the Venmag Mine.

| ID | Fe | Cr | Cu | Ni |
|---|---|---|---|---|
| **WHO (Soil)** | 50,00 | 1,00 | 2,00 | 0,07 |
| **South African Screening values for standard residential** | n.a | 13,00 | 2,300 | 1,200 |
| **S1** | 7,30 | 0,12 | 0,01 | **0,08** |
| **S2** | 6,88 | 0,11 | 0,01 | 0,07 |
| **S6** | 7,62 | 0,15 | 0,01 | **0,08** |
| **S11** | 3,33 | 0,03 | 0,00 | 0,02 |
| **S12** | 6,60 | 0,15 | 0,00 | 0,06 |
| **S14** | 4,30 | 0,08 | 0,00 | 0,03 |
| **S15** | 3,72 | 0,07 | 0,01 | 0,02 |
| **Average** | 5,68 | 0,10 | 0,01 | 0,05 |

Note: Concentration of trace elements is presented in parts per million (ppm).

### Evaluation of soil pollution

The results of the quantification of the metal contamination of the soil samples using the contamination index are shown in Table 4.11. The pictorial impression of trends in the mutual pollution effect of the studied metals in the study area is presented in Figure 4.17.

Table 4.11: Determination of pollution index of the Venmag Mine soil and waste rock dumps samples.

| Sample type | Metal | External Background values (ppm) | Internal background values (ppm) | Sample level (ppm) | Contamination index | Pollution grade |
|---|---|---|---|---|---|---|
| **Soil** | **As** | 0,009 | 0,00 | 0,086 | 0,00 | Low |
| | **Cu** | 0,0418 | 0,00 | 0,04 | 0,00 | Low |
| | **Pb** | 0,007 | 0,00 | 0,036 | 0,00 | Low |
| | **Zn** | 0,0688 | 0,01 | 0,053 | 5,3 | High |
| | **Ni** | 0,0606 | 0,01 | 0,144 | 14,4 | Super High |
| **Waste rock dumps** | **As** | 0,009 | 0,00 | 0,086 | 0,00 | Low |
| | **Cu** | 0,0418 | 0,01 | 0,04 | 4 | High |
| | **Pb** | 0,007 | 0,00 | 0,036 | 0,00 | Low |
| | **Zn** | 0,0688 | 0,01 | 0,053 | 5,3 | Very High |
| | **Ni** | 0,0606 | 0,05 | 0,144 | 2,9 | High |

The results of the determination of As, Cu, Pb, Zn, and Ni contamination in the soil show that pollution at Venmag Mine was ranging from low to super high (Figure 4.17) with Zn and Ni being the main polluters. Contamination at this mine was higher than the background values provided by the Council for Geoscience (Column 3, Table 4.11).

From these results, land use values were found to be very low as high for Super High pollution grades were associated with Ni and Zn. Figure 4.17 also indicates a relative variation in the distribution of metals between the mine soil and the waste rock dumps. Thus, the fourfold increase in the concentration of Ni in the mine soils and a similar concentration of Zn between the two sample types suggests that these metals have leached from the mine waste rock dumps. On the other hand, the relatively high concentration of Cu in the waste rock dumps compared to the surrounding soil suggests that this metal is fairly recalcitrant and is retained within the mine waste rock dumps.

The pollution ranges were as follows: Ni<Zn<As<Cu<Pb in the surrounding soil and the waste rock dumps was as follows: Zn<Cu<Ni<As<Pb (From these statistics, one can deduce that surroundings are relatively is pristine condition and but with a marginal contaminated area such as the waste rock dumps compared to surrounding soil samples.

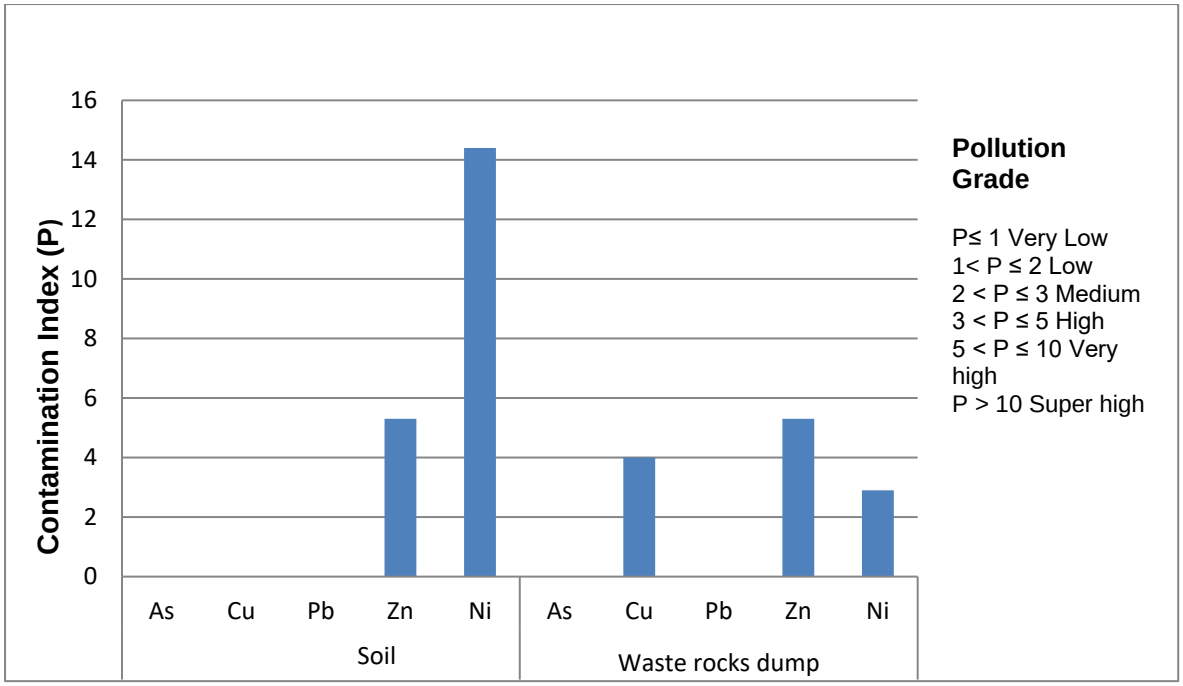


Figure 4.17: Variations of pollution index for selected metals in the Venmag Mine soil and rock samples. Adopted from Singo, (2014).

### 4.3.2 Water quality analysis

Figure 4.18 below indicates the water sampling positions along the Nwanedi River (W04 to W10) and the Venmag Mine pit (W01 and W02).

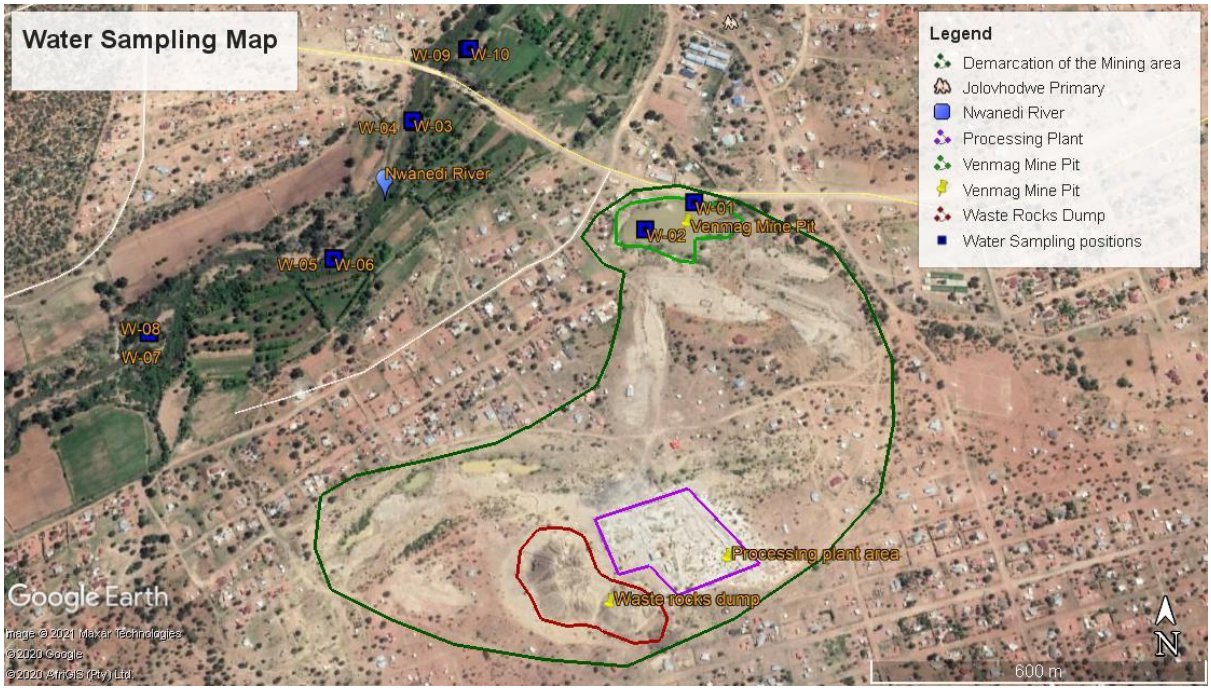


Figure 4.18: Location of surface water sampling (green boxes) positions in the Nwanedi River and Venmag Mine pit. NB the green colour - Venmag pit, dark green colour - demarcation mine area, Maroon colour - Waste rock dumps, and purple colour - processing plant area.

#### 4.3.2.1 Venmag Mine

The water quality results for the Nwanedi River and Venmag pit is presented in the section below.

**(a) Analysis of water quality parameters for river and mine pit water samples**

**(i) Physical water quality parameters**

With the exception of temperature, all of the physical water quality parameters (pH, TDS, EC, hardness) pertaining to the Venmag Mine Pit were raised in comparison to the values obtained for these parameters in the river water samples.

**pH**

The pH of the water samples from the Nwanedi River (W03, W04, W05, W06, W07, W08, W09 and W10) were ranging from 6.99 (neutral) to 7.49 (near neutral) with an average pH of 7.37, whereas the pH of water from the two mine pit water samples (W1

and W2) were ranging from 7.21 - 7.28 with an average of 7.25 (Figure 4.19). The site of a collection of river sample W10 was obtained downstream of the Nwanedi River and those samples showed the lowest pH (pH 7) of all the water samples (Figure 4.18).

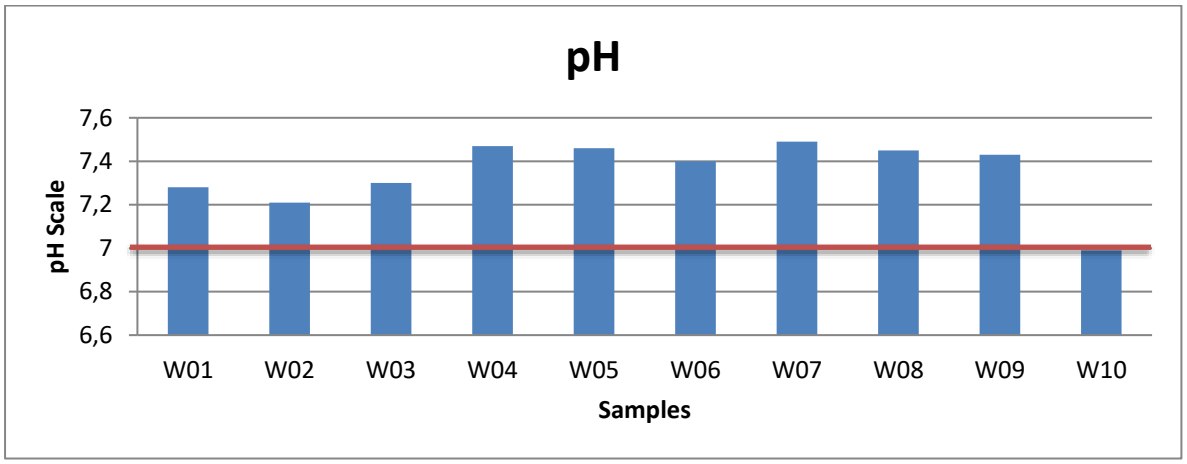


Figure 4.19: pH analysis of the Nwanedi River and Venmag Mine pit water quality samples. Note that the red line indicates neutral pH and that the mine water samples are W01 and W02 and Nwanedi River samples are W03 to W10

**Total dissolved solids (TDS)**

The TDS of the water samples collected in the Venmag Mine pit were 324.00 mg/L and 348.00 mg/L, respectively, and those samples collected from the Nwanedi River were ranging from 92.00 mg/L to 128.00 mg/L. These results attest to low concentrations of dissolved solutes in the water. Based on the best standards for drinking water by the DWA (<450 mg/L) and the WHO (2007) guidelines (1000 mg/L), the TDS of the water samples falls within the permissible limits for drinking water and is suitable for lifetime domestic use (DWA, 1998) (Table 4.12). W01 and W02 from the Venmag Mine pit had higher concentrations of TDS and these elevated figures may be associated with the dissolution of compounds from the mine waste rocks. Overall, the TDS of the studied water falls within the domestic drinking water limits, set by local and international bodies (DWA, 1998; WHO, 2007).

Table 4.12: Analysis of water quality parameters in the Nwanedi River and Venmag Mine.

| SAMPLE ID | WHO | DWS | W01 | W02 | W03 | W04 | W05 | W06 | W07 | W08 | W09 | W10 |
|---|---|---|---|---|---|---|---|---|---|---|---|---|
| **pH** | 6.5-8.5 | 5-9.5 | **7,28** | **7,21** | 7,3 | 7,47 | 7,46 | 7,4 | 7,49 | 7,45 | 7,43 | 6,99 |
| **Total conductivity (µS/m)** | - | <70 | **49,2** | **52,1** | 16,8 | 17 | 16,7 | 16,7 | 17 | 17 | 18,7 | 18,6 |
| **Sample temp. (ºC)** | - | - | 23,7 | 23,7 | 24,2 | 24,2 | 24,2 | 24,3 | 24,4 | 24,6 | 24,6 | 24,5 |
| **TDS (mg/L)** | 1000 | <450 | **324** | **348** | 108 | 112 | 92 | 106 | 128 | 114 | 122 | 116 |
| **TH (mg/L)** | - | 0-200 | **62,5** | **78,8** | 45,8 | 46,1 | 44,8 | 39,2 | 41,9 | 42,1 | 38,9 | 44 |
| **Ca (mg/L)** | - | - | **0,6** | **0,8** | 0,3 | 0,3 | 0,3 | 0,3 | 0,3 | 0,3 | 0,3 | 0,3 |
| **Mg (mg/L)** | - | - | 0,7 | 0,8 | 0,6 | 0,6 | 0,6 | 0,5 | 0,6 | 0,6 | 0,5 | 0,6 |
| **Na (mg/L)** | - | 70 | **2,7** | **3,9** | 0,7 | 0,7 | 0,7 | 0,9 | 0,7 | 0,9 | 1,00 | 0,7 |
| **K (mg/L)** | - | - | **0,3** | **0,3** | 0,00 | 0,00 | 0,00 | 0,00 | 0,00 | 0,00 | 0,00 | 0,00 |
| **$SO_4$ (mg/L)** | - | - | 0,1 | 0,1 | 0,1 | 0,1 | 0,1 | 0,1 | 0,1 | 0,1 | 0,1 | 0,1 |
| **Cl (mg/L)** | - | 100 | 0,9 | 0,9 | 0,8 | 0,8 | 0,7 | 0,7 | 0,7 | 0,8 | 0,9 | 0,8 |
| **$NO_3$ (mg/L)** | - | - | 0,2 | 0,2 | 0,2 | 0,2 | 0,2 | 0,2 | 0,2 | 0,2 | 0,1 | 0,1 |
| **F (mg/L)** | - | 2.0 | 0,00 | 0,00 | 0,00 | 0,00 | 0,00 | 0,00 | 0,00 | 0,00 | 0,00 | 0,00 |
| **Alk ($CaCO_3$)** | - | - | **4,7** | **5,8** | 0,9 | 0,9 | 0,9 | 0,9 | 0,9 | 0,9 | 1,00 | 1,00 |
| **TH ($CaCO_3$)** | - | - | **2,09** | **2,63** | 1,53 | 1,54 | 1,5 | 1,31 | 1,4 | 1,41 | 1,3 | 1,47 |
| **EC (µS/m)** | - | - | **49,2** | **52,1** | 16,8 | 17 | 16,7 | 16,7 | 17 | 17 | 18,7 | 18,6 |
| **Ambient temp (ºC)** | - | - | 25 | 25 | 25 | 25 | 25 | 25 | 25 | 25 | 25 | 25 |

Note: The concentration of each parameter is presented in mg/L.

**(ii) Chemical water quality parameters**

Comparison of the results of chemical water quality parameters showed that the concentration of $Na^{+}$, $K^{+}$ and the $Ca^{++}$ cations were raised relative to the figures obtained from the river water samples. No difference was noted for the other tested water quality chemical parameters. The results of these analyses are shown in Table 4.12 and the differences between the mine pit and the river water samples are highlighted in bold.

**(b) Water Chemistry**

The concept of hydrochemical facies can be used to denote the diagnostic chemical character of water in hydrologic systems. The facies reflect the effect of complex hydrochemical chemical processes in the subsurface (Kumar, 2013) occurring between the minerals of lithologies formation and groundwater to investigate the spatial variability of groundwater chemistry in terms of hydrochemical evolution.

A Piper trilinear diagrams (Piper, 1944) are used to evaluate the evolution of the river water and the relationship between rock types and water composition while a Durov diagram is advantageous over the Piper diagrams in revealing some geochemical processes that could affect the groundwater genesis (Lloyd and Heathcoat, 1985).

Stiff and Piper diagrams were used to determine the hydrogeochemical facies of the studied water samples. The water samples from the Nwanedi River and Venmag Mine showed significant variations in their water chemistry (Table 4.12).

Based on the Stiff diagram, water samples collected from the Venmag Mine pit were dominated by the $HCO_3^{-}+CO_3^{2-}$ anions with fewer $Na^{+}+K^{+}$ cations. The Nwanedi River was mostly dominated by the $HCO_3^{-}+CO_3^{2-}$ and $Mg^{2+}$ with fewer $Na^{+}+K^{+}$ cations and $SO_4^{2-}$ and Nwanedi River water is much less of anion $Cl^{-}$ for sample ID W03, W04, W05, W06, W07, W08, W09, and W10 (Figure 4.20).

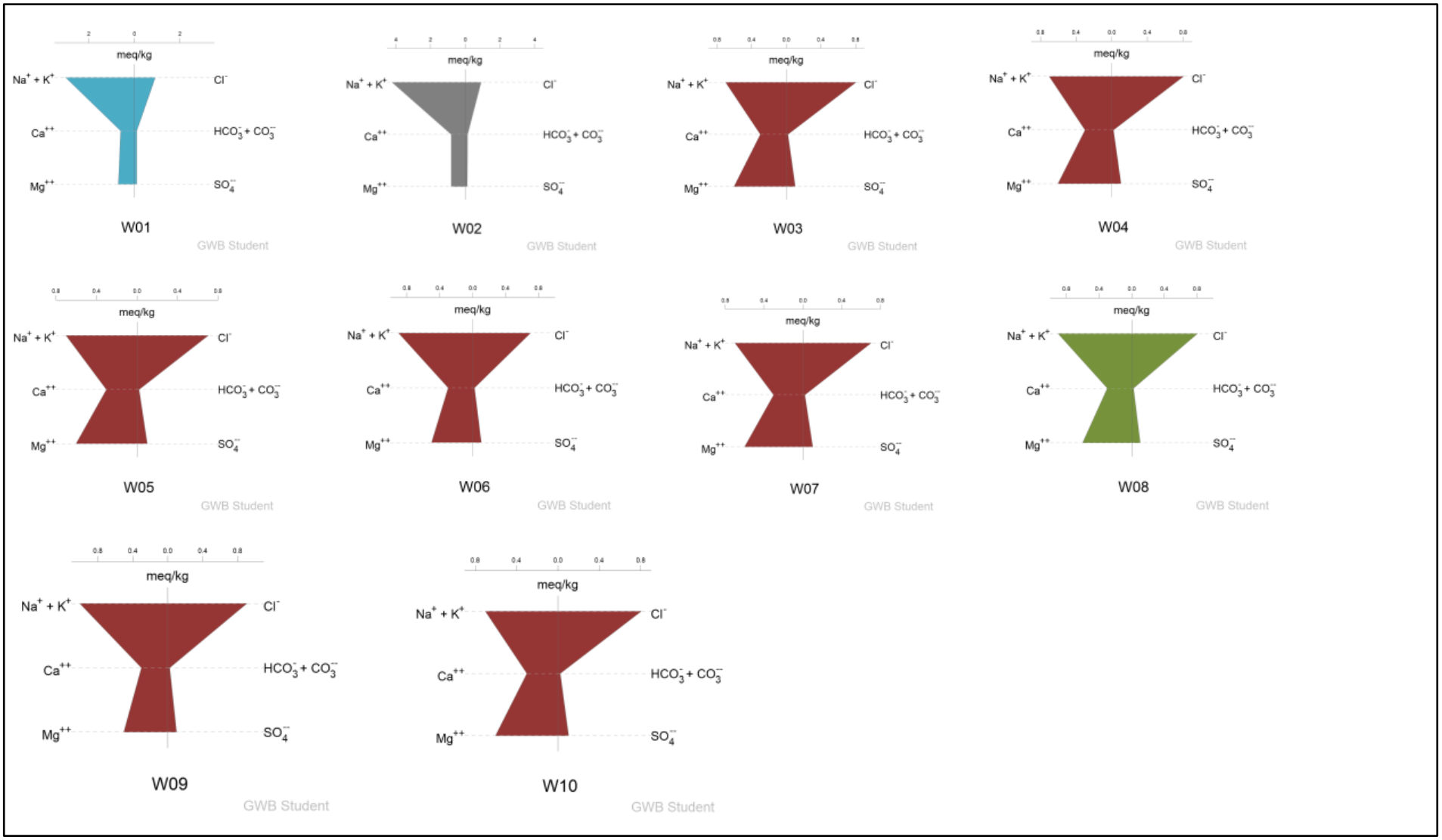


Figure 4.20: Stiff diagrams representing Venmag and Nwanedi River water quality samples (Created by GWB 14 software).

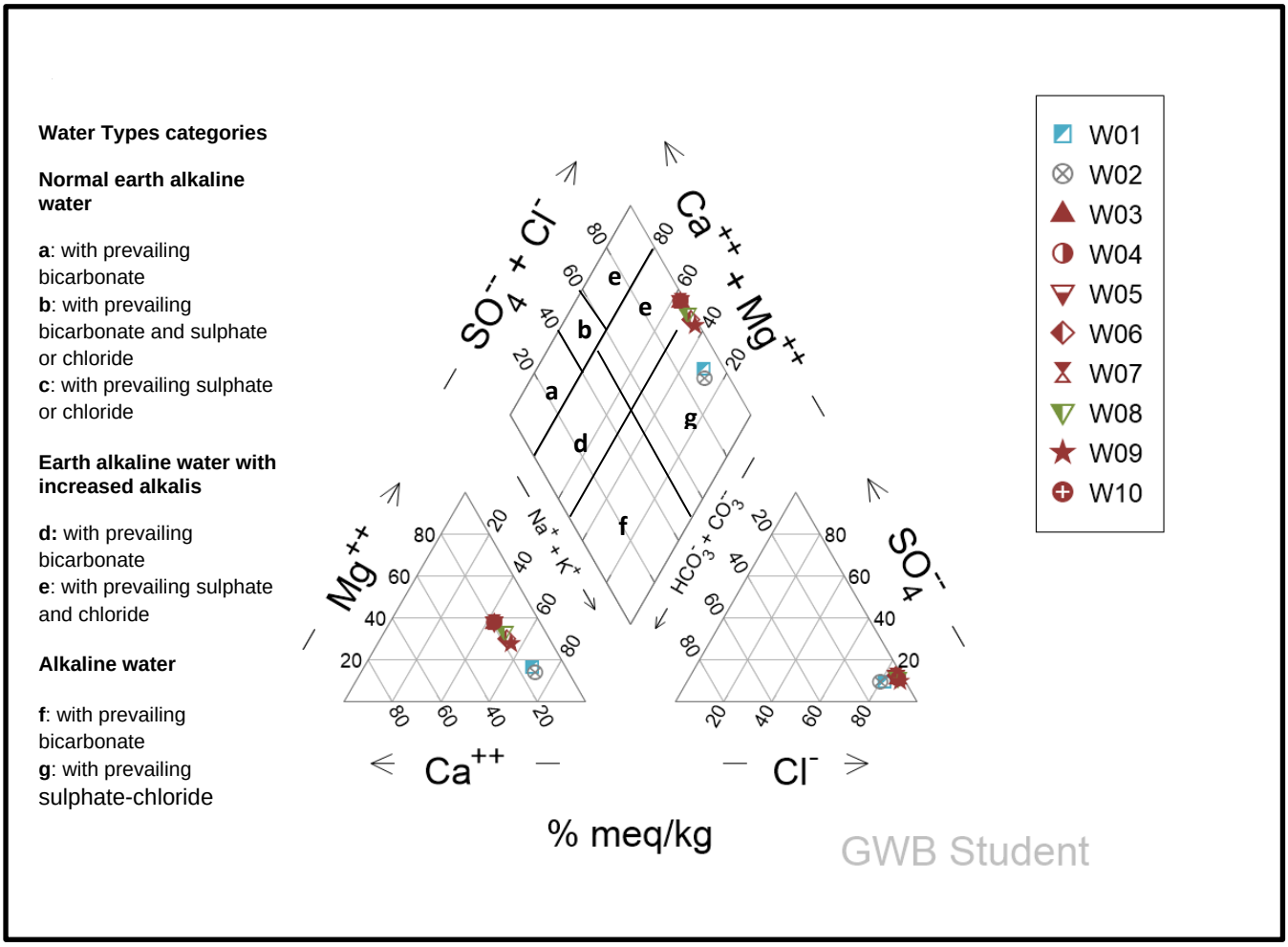


Figure 4.21: Piper diagrams representing Venmag Mine and Nwanedi River water quality samples (created by GWB Student software).

The results of the chemical analysis for the Nwanedi River and Venmag Mine were plotted on a Piper diagram as indicated in Figure 4.21 above. The water samples identified as WO3, W04, W05, W06, W07, W08, W09, and W10 were collected from along the Nwanedi River while the mine pit water samples were tagged W01 and W02. These diagrams were developed to investigate the source of its dissolved salts, and explain the different processes affecting the surface water characters. The subdivisions of the diamond field represent seven water-type categories of natural waters.

The surface water types of the Nwanedi River and Venmag Mine in the study area are represented by two categories (Figure 4.21). The first category (e) (Table 4.21) was characterized by alkaline earth, water showing an increase in alkali with prevailing

sulphate and chloride ions. The second category (g) (Table 4.21) was characterised by alkaline water with prevailing sulphate chloride ions from Venmag Mine.

In summary, the water quality of the Nwanedi River and Venmag Pit results showed that the water was slightly alkaline and the results obtained during this study suggest that there has been no impact on water quality from mine runoff or leaching. Furthermore, the results show that low sulphate concentration and the pH of the water were found to be slightly neutral.

# CHAPTER 5 - DISCUSSION

This chapter discusses (1) the host rock of magnesite mineralisation, (2) vein type of mineralisation of magnesite, (3) the role of the dolerite dyke, sills and structures, (4) the economic potential of the *in situ* magnesite, (5) waste rock dumps reuse, and (6) water quality.

## 5.1 Host rock of magnesite mineralisation

Previous researchers (Van Zyl *et al.,* 1942; Wilke, 1965; Michael and Carey, 1989; Strydom, 1998; Mbedzi, 2014) reported that magnesite in the Tshipise area was formed within the mafic rock, i.e., dolerite dykes and sills, of the Karoo Supergroup. Eglington and Armstrong (2004) reported depositions of ultramafic (with mafic and pelitic) rocks in the Banderlierkop Formation of the Limpopo Mobile Belt (LMB). Furthermore, Brandl (1981) conducted a petrological study of the ultramafic rocks in the Banderlierkop Formation and reported that these are characterised by olivine (peridotite), pyroxenite, dunite and hornblendite, and most of which are serpentinised. Moreover, previous researchers reported that magnesite deposits in the Mooketsi in the Giyani area are associated with Greenstone Belt formed about 3.5 Ga (Hamilton *et al.,* 1977; Kamo and Davis, 1994; Lahaye *et al.,* 1995; De Ronde and Kamo, 2000) while the Malelane magnesite deposits have been deposited within the ultramafic rocks of the Bushveld Complex formed at 2.0 Ga (Hamilton *et al.,* 1977; Walraven *et al.,* 1990; Cawthorn *et al.,* 1981).

Pit mapping in the Venmag, Nyala, and Folovhodwe Magnesite Mines revealed that magnesite deposits in the Tshipise area are hosted by ultramafic rocks rather than mafic rocks as previously indicated by researchers (Van Zyl *et al.*, 1942; Wilke, 1965; Michael and Carey, 1989; Strydom, 1998); Mbedzi, 2014). Such ultramafic rocks (peridotite) are enriched in forsterite (olivine), orthopyroxene, clinopyroxene, and plagioclase in the order of abundance (Figures 4.11 to 4.12).

In the current study, the AFM plot depicted that all the host rocks are rich in magnesium and deficient in iron and, based on the petrological and mineralogical studies of the ultramafic rocks of the Tshipise area, these results are in line with the magnesite mineralisation in the Bushveld Complex in the Malelane area as presented by Viljoen and Viljoen (1969).

A Bowen's reaction method was applied to classify the igneous rocks in the Tshipise area and the results confirmed that the dolerite rocks fall in the category of mafic rocks while the ultramafic rocks fall in the olivine-rich, ultramafic rocks category. Furthermore, the classification of the ultramafic rocks based on the wt% of olivine, orthopyroxene and clinopyroxene, revealed that the ultramafic rocks fall in the category of Peridotites websterite (Wherlite and Lherzolite) being enriched with olivine minerals (Figure 4.14).

## 5.2 Magnesite mineralisation type

Researchers have indicated that magnesite may occur during regional metamorphism; or hydrothermal metamorphism of peridotite or serpentine rocks; or during regional metamorphism of limestone where magnesium-rich solutions cause alteration of carbonate rocks, i.e., limestone; or may occur in sedimentary environments through solutions of carbonic acid forming magnesite within the regolith of rocks rich in magnesium environment of the ultramafic rocks; and may occur during the precipitation of the thermal water forming veins within the fissures and fractures (Zachmann and Johannes, 1989; Scott *et al.,* 2013).

In the current study, structural mapping was conducted within the Nyala, Folovhodwe, and Venmag Magnesite Mine pits to understand the mineralisation of the Tshipise magnesite deposits and found that magnesite mineralisation occurred within the horizontal and sub-horizontal beddings; and vertical and sub-vertical joints of the ultramafic rocks while minimum mineralisation occurred in the contact of dolerite dykes (Figure 4.2). Further, this study also found that magnesite mineralisation in Tshipise occurs as a veined type as described by Zachmann and Johannes (1989) and Scott (2013).

## 5.3 Regional structures controlling mineralisation

Van Zyl *et al.* (1942) indicated that the exposures of both the intrusive and extrusive (volcanic) rocks in the Tshipise area are controlled by three major east-northeast-striking fault systems, namely the Klein Tshipise, the Bosbokpoort and the Tshipise

Faults which might have contributed during the mineralisation of Tshipise magnesite deposits (Figure 4.3).

## 5.4 Role of doleritic intrusives

Olivier *et al.* (2011) reported that the existence of the thermal springs might suggest that the Tshipise magnesite deposits occurred in the same period.

This study, however, found that the sequences of geological events are as follows:

(1) At first, ultramafic rocks intruded at fair depth (10 m) and exposed to the surface at present;

(2) Secondly, the dolerite dykes and sills intruded into the ultramafic rocks, and further drove, heat up and circulate groundwater along the weak zones, fractures, beddings and joints of the ultramafic rock; and

(3) Thirdly, magnesite precipitated from the hydrothermal alteration of the magnesium-rich olivine, forming vein-type magnesite mineralisation in the ultramafic rocks, which is illustrated by the Formula 1 (such as chrysotile) (Van Zyl, 1942; Wilke, 1965).

$$2\ Mg_3Si_2O_5(OH)_4 + 3\ CO_2 \rightarrow Mg_3Si_4O_5(OH)_4 + 3\ MgCO_3 + 3\ H_2O \quad (1)$$

Chrysotile Serpentine Magnesite

## 5.5 Economic potential of magnesite *in situ* and waste rock dumps

Sibanda *et al.* (2013) reported that the Venmag, Nyala, and Folovhodwe Magnesite Mines left several waste rock dumps within the communities of Zwigodini and Folovhodwe, being dormant since 2012 due to economic challenges. Nevertheless, there are still mineable magnesite ore resources that can be recovered, although most of the magnesite ore has been mined out at the Fallershall farm of the Folovhodwe Mine (Strydom, 1998).

Before their closure, the mines were operated on a small scale through excavating using machines and by hand sorting of > 25 mm valuable magnesite ore (Paul *et al.,* 1997).

The current study attempted to preliminarily assess the ore resources based on the *in situ* in the pits and virgin ground ores, and the remaining magnesite within the waste rock dumps of the Venmag, Nyala and Folovhodwe Mines.

It was found that the magnesite estimations resources were as follows;

**(a) Folovhodwe Magnesite Mine**

691 488 tonnes for grade 6.5 wt% (for virgin ground)

4 494 670 tonnes for 2 wt% (for waste rock dumps)

**(b) Nyala Magnesite Mine**

832 093 tonnes grade 6.5 wt% (for virgin ground)
5 408 605 tonnes for grade 2 wt% (for waste rock dumps)

**(c) Venmag Mine resource**

135 202 tonnes for grade 2 wt% (for waste rock dumps)

## 5.6 Reuse of waste rock dumps

In the north-western parts of Rwanda, local industry uses volcanic rocks for building materials and so the employment offered in their reuse has benefited the local community, which have high compressive strength and improved permeability, essential characteristics for road construction as subsurface layers, and for brick making (El-Mahllawy, 2008; Radwan *et al.,* 2011; De Dieu *et al.,* 2016).

According to Sibanda *et al.* (2013), waste rock dumps in the Tshipise area are unrehabilitated within the communities of Zwigodini and Folovhodwe, in turn, reducing settlement size and causing air pollution during the windy season. Although these researchers noted that the mine dumps have a negative impact on the environment, nonetheless the waste rock dumps of magnesite might be considered for road construction materials and brick making which makes them beneficial to the community. In addition, the current assessment of the mine waste rock dumps noted

they were highly alkaline, which could make these rocks useful for neutralising acid mine drainage.

## 5.7 Soil geochemistry

This study on the waste rock dumps found that trace elements in different soil samples are: Ba, Cr, Cu, Ni and Zn (Tables 4.18 and 4.19), which are below the WHO (2007) and the SASV (2010) guidelines of permissible limits for the heavy metals in the soil. There is no previous study identified on soil geochemistry. Therefore, this study concludes that there is no impact associated with the heavy metals from within the waste rock dumps.

## 5.8 Water quality

Jeleni *et al.* (2012) reported that the water in the Nyala Mine pit is very saline together with alkaline compounds that result in a pH between 9.4 and 9.8, and high concentration levels of fluoride (F), chloride (Cl), magnesium (Mg), and potassium (K).

The current study conducted limited water quality analysis for both the Venmag Mine pit and the nearby Nwanedi River. The results showed that the water is characterised by low concentrations of dissolved solutes. The TDS in the water of the Venmag Mine pit and the Nwanedi River are low (Table 4.19). Based on the best guidelines for drinking water (DWA, 1998; WHO, 2007), the water falls within the permissible limits for drinking water. This, therefore, implies that the water is suitable for domestic use.

Based on the Stiff diagram, water samples collected from the Venmag Mine pit and Nwanedi River are dominated by $HCO_3^-+CO_3^{2-}$ anions and $Mg^{2+}$ (Figure 4.25). Based on the Piper diagrams, the surface water types of the Nwanedi River and Venmag Mine in the study area are represented by two categories alkaline water together with sulphate and chloride ions (Figure 4.26).

In summary, the current study suggests there are no issues with the extremely high pH and high concentrations of F, Cl, Mg and K that there is a possibility due to the sampling conducted during the dry season.

# CHAPTER 6 - CONCLUSIONS AND RECOMMENDATIONS

## 6.1 Conclusions

This study set out to determine the mineralisation of magnesite in the selected mines. Field mapping, petrological and mineralogical studies as well as water and soil geochemistry analyses were conducted. To determine whether this study suitably addressed the study objectives set down on page 5 of this dissertation, this concluding chapter will examine each objective in relation to the study findings.

Objective 1 was **to characterise the geology and formation of magnesite, including the ore bodies, the host rocks and the source of metals, and hydrothermal fluids and mechanism of magnesite mineralisation**.

In addressing this objective, field mapping and observation of the Venmag, Folovhodwe Mine pits investigated structural control and the type of mineralisation of magnesite. Research determined that the mineralisation of magnesite in the Tshipise area appears to have been hosted by ultramafic rocks which are characterised by orthopyroxene, clinopyroxene, and plagioclase, rather than the mafic rocks, specifically dolerite dykes, as previously thought.

The mineralisation of the magnesite order was determined as follows: Firstly, the layered ultramafic rocks occurred, then the dolerite dykes and magnesite mineralisation at the last stage. Such mineralisation in the Tshipise area appears to have been controlled by structures such as horizontal and sub-horizontal along with beddings, and vertical and sub-vertical in the joints. Major mineralisation occurred in the ultramafic rocks and minimum mineralisation occurred in the dolerite dykes contact against the ultramafic rocks. The magnesite deposits occurred as vein-type mineralisation within the beddings and joints of the layered ultramafic rocks that might have occurred during the thermal water along with the intrusion of the dolerite dykes and sills.

Thus Objective 1 was suitably addressed as the research provided clarity as to the host rock of the magnesite, type of mineralisation, structural control and an understanding of geological sequences.

Objective 2 was **to evaluate the magnesite deposit in the Tshipise Mines waste rock dumps, *in situ* (in and outside pits) and identify magnesite resources along the mineral belt, and potentially reprocessing of the waste rock dumps**.

In achieving this objective, a preliminary magnesite resources evaluation was estimated based on the measurement of pits from Google Earth© in terms of geometry such as areas and depths for the Venmag, Folovhodwe and Nyala Mines. The total tonnage of the waste rock dumps as well as *in situ* magnesite content was calculated for those magnesite mines and results showed that there are still mineable magnesite resources (virgin ground) for reprocessing of the waste rock dumps that is worthy of further investigation as its exploitation might be feasible for economic beneficiation.

Assessment of waste dump rocks within the selected mines indicated that the waste rock dumps have a high concentration of alkaline, which might be used as a lime for neutralising acid mine drainage and further might be considered for road construction materials and brick making to create local employment.

Thus, objective 2 was appropriately addressed as this study estimated the economic potential of the magnesite ore remaining in the waste rock dumps and provided a preliminary positive assessment regarding the reuse and repurposing of the mine waste from those magnesite mines.

Objective 3 was **to assess the impact of magnesite mining on the soil and surface water in the area**.

In addressing this objective, soil samples (n=15) were collected from the waste rock dumps and the surrounding areas and they were sent for analysis to determine minerals and heavy metals contamination. Heavy metals in the waste rock dumps of the Venmag Mine were low in Cu, Ni, Pb, Zn and As. Thus, these test results indicated that the soil surrounding the mine as well as from the waste dump rocks complied with the WHO guidelines and SASV guidelines for heavy metals. Additional field work was conducted by collecting water samples (n=8) from the Nwanedi River and the Venmag Mine pit (n=2) for laboratory analysis of minerals, metals and heavy metals. All samples were sent for analysis and the results showed that the water from the river and mine pit complied with the WHO guidelines and DWS standards. Thus, as it was noted that different seasons affect the quality of water for both the Venmag Mine pit and Nwanedi River, such water may be used for domestic use during the wet season.

These results support the assertion that objective 3 was suitably addressed - analysis of the Venmag waste rock dumps as well as the soil surrounding the mine together with the surrounding water sources such as rivers indicated that there were no significant impacts from the mine waste rock on the surrounding environment.

## 6.2 Recommendations

Based on the discussion and conclusions drawn in this study, the researcher recommends the following:

- Field mapping be conducted within a spacing of 50 m from the eastern to the western part of the Tshipise area to cover the Venmag, Folovhodwe, and Nyala Magnesite Mines for the exploration of magnesite ore deposit along the Folovhodwe valley;
- Age dating should be conducted on the ultramafic rocks, the dolerite dykes and the magnesite veins which help to solve the origin of the mineralisation;
- A study be done on the distribution of magnesite along the Folovhodwe valley in the easterly to the westerly direction to cover the Nyala, Venmag, and Folovhodwe Mines and the extension along the three major faults;
- Further studies should be conducted on the reprocessing of the magnesite waste rock dumps using the new technology in the Venmag, Nyala, and Folovhodwe Mines to recover the remaining magnesite ore; and
- Further laboratory test work should be done on the reuse of the waste rocks for making bricks, road construction and treatment materials for mine acid drainage.

# REFERENCES


Abu-Jaber, N.S. and Kimberley, M.M. 1992. Origin of ultramafic-hosted vein magnesite deposits. *Ore Geology Reviews*, 7(3), 155-191. Accessed at: https://doi.org/10.1016/01691368(92)90004-5.

Abzalov, M. 2016. Resource Estimation Methods. In: Applied Mining Geology. Modern Approaches in Solid Earth Sciences. 221-230. Accessed at: https://doi.org/10.1007/978-3-319-39264-6_16.

Appelo, C.A. and Postma, D. 2005. Geochemistry, groundwater and pollution. In: Earth Sciences, Engineering & Technology: Second Edition. (C.A.J. Appelo, & D. Postma, editors. *CRC Press*, 683. Accessed at https://doi.org/10.1201/9781439833544.

Artioli, G. 2017. X-ray Diffraction (XRD). In: Gilbert A.S. (Eds) Encyclopedia of Geoarchaeology. Encyclopedia of Earth Sciences Series. *Springer, Dordrecht*. Accessed at: https://doi.org/10.1007/978-1-4020-4409-0_29.

Ashton, P.J. and Schoeman, F.R. 1986. Southern African thermal springs. *The Naturalist*, 30(1), 32-34.

Bahnemann, K.P. 1972. A review of the structure, stratigraphy, and metamorphism of the Basement rocks in the Messina District, Northern Transvaal. Unpublished D.Sc. Thesis, University of Pretoria, 156.

Balamurugan, B. and Balakumaran, B. 2015. Soil quality assessment around Magnesite Mines and Salem Township using GIS techniques. *International Journal of Advances in Engineering & Technology*, 8, 1–30.

Barton, J.M. Jr., Doig, R., Smith, C.B., Bohlender, F. and Van Reenen, D.D. 1992. Isotopic and REE characteristics of the intrusive charnoenderbite and enderbite geographically associated with the Matok Pluton, Limpopo Belt, Southern Africa. *Precambrian Research*, 55, 451–467.

Bodinier, J.L. and Godard, M. 2004. Orogenic, ophiolitic, and abyssal peridotites, in Carlson, R., editors. Treatise on Geochemistry. The Mantle and Core: Amsterdam, 2, 103-170.

Boss, C. and Fredeen, K. 2004. 3rd Edition Concepts, instrumentation and techniques in Inductively Couple Plasma Optical Emission Spectrometry, 1–50.

Bowen, N.L. 1956. The Evolution of the Igneous Rocks. *New York Dover Publications*, 60–62.

Brandl, G. 1981. The geology of the Messina area. *Explanation of the Sheet 2230, Geological Survey of Africa*, 35.

Brandl, G. and De Wit, M.J. 1997. The Kaapvaal Craton. In: De Wit, M. and Ashwal, L.D, editors. Greenstone belts. *Oxford University Press*, 581-607.

Bumby, A.J., Eriksson, P.G., Van Der Merwe, R. and Steyn, G.L. 2002. A half-graben setting for the Proterozoic Soutpansberg Group (South Africa): Evidence from the Blouberg area. *Sedimentary Geology*, 147, 37–56.

Cawthorn, R.G., Davies, G., Clubley-Armstrong, A. and McCarthy, T.S. 1981. Sills associated with the Bushveld Complex, South Africa: an estimate of the parental magma composition. *Lithos*, 14, 1–15.

Coetzee, H., Nengobela, N.R., Vorster, C., Sebake, M.D., Heath, G., Hansen, R., Foya, S., Croukamp, L., Mthethwa, S. and van Tonder, D. 2008. Strategy for the management of derelict and ownerless mines in South Africa. In: Proceedings of the Third International Seminar on Mine Closure. *Council for Geoscience to the Department of Minerals and Energy,*110.

De Dieu, M.J., Pranesh, M.R. and Wali, U.G. 2016. Engineering characteristics of volcanic rock aggregates of Rwanda. *International Journal of Civil Engineering and Technology,* 7, 81-90.

DWAF. Department of Water Affairs and Forestry. 1996. South African Water Quality Guidelines for domestic use (Volume 1).

De Ronde, C.E.J. and Kamo, S.L. 2000. An Archaean arc-arc collisional event: A short-lived (ca 3 Myr) episode, Weltevreden area, Barberton greenstone belt, South Africa. Journal of African Earth Sciences, 30, 219–248. Accessed at: https://doi.org%2F10.1016%2FS0899-5362(00)00017-8.

De Wit, M.J. and Roering, C. 1990. Episodes of formation and stabilization of the Kaapvaal craton in the Archean: an overview based on some selected recent data. In: The Limpopo Belt: A field workshop on granulites and deep crustal tectonics, Extended Abstract. J. M. Barton, editors. *Rand Afrikaans University, Johannesburg and Foundation for Research and Development, Pretoria,* 42-52.

Diamond, R.E. and Harris, C. 2000. Oxygen and hydrogen isotope geochemistry of thermal springs of the Western Cape, South Africa: Recharge at high altitude, *Journal of African Earth Sciences*, 31(3-4), 467-481. Accessed at: https://doi.org/10.1016/S0899-5362(00)80002-0.

Du Toit, M.C., Van Reenen, D.D. and Roering, C. 1983. Some aspects of the Geology, Structure and Metamorphism of the Southern Marginal Zone of the Limpopo Metamorphic Complex. *Special Publication of the Geological Society of South Africa,* W. J. Van Biljon and J. H. Legg, editors. 121.

El-Mahllawy, M.S. 2008. Characteristics of acid resisting bricks made from quarry residues and waste steel slag. *Construction and Building Materials.* 22 (8), 1887-1896. Accessed at: https://doi.org/10.1016/j.conbuildmat.2007.04.007

Emmons, W. H. and Harlington, G. L. 1913. A comparison of waters of mines and of hot springs. *Economic Geology*, 8 (7), 653–669. Accessed at: https://doi.org/10.2113/gsecongeo.8.7.653.

Fripp, R. E. P. 1981. The ancient Sand River gneisses, Limpopo mobile belt, South Africa. *Special Publication, Geological Society of Australia*, 7, 329–335.

Fripp, R.E.P. 1983. The Precambrian Geology of the area around the Sand River near Messina, central zone, Limpopo Mobile Belt. *Special Publication of the Geological Society of South Africa*, 89.

Fu, S., & Li, P., Feng, Q., Xiaojun, l., & Li, P., Sun, Y. and Yang, C. 2011. Soil Quality Degradation in a Magnesite Mining Area. *Pedosphere*, 21, 98-106. Accessed at: https://doi.org%2F10.1016%2FS1002-0160(10)60084-7.

Hamilton, J.O. 1977. Sr isotope and trace element studies of the Great Dyke and Bushveld mafic phase and their relation to early Proterozoic magma genesis in southern Africa. *Journal of Petrology*, 18, 24–52. Accessed at: https://doi.org/10.1093/petrology/18.1.24.

Hess, F.L. 1908. The magnesite deposits of California. *Washington Government Printing Office*, 23-34. Accessed at: https://doi.org/10.3133/b355.

Hill, R.A. 1940. Geochemical patterns in Coachella Valley. *Eos, Transactions American Geophysical Union*, 21(1), 46–53. Accessed at: https://doi.org/10.1029/TR021i001p00046.

Hoffmann, J.R.H. 1979. Die Chemiese Samestelling van Warmwaterbronne in Suid- en Suidwes-Afrika. *CSIR Report No. WAT 56A, Pretoria,* 21.

Jeleni, M.N., Gumbo, J., Muzerengi, C. and Dacosta, F.A. 2012. An Assessment of Toxic Metals in Soda Mine Tailings and a Native Grass: A Case Study of an Abandoned Nyala Magnesite Mine, Limpopo, South Africa. *WIT Transactions on Ecology and the Environment,* 164. Accessed at: https://doi.org%2F10.2495%2FWP120361.

Kamo, S.L. and Davis, D.W. 1994. Reassessment of Archaean crustal development in the Barberton Mountain Land, South Africa, based on U-Pb dating. *Tectonics*, 13(1), 167–192. Accessed at: https://doi.org/10.1029/93TC02254.

Kent, L.E. 1949. The thermal waters of the Union of South Africa and South West Africa. *Transactions of the Geological Society of South Africa,* 52, 231-264.

Kent, L.E. 1969. The thermal waters in the Republic of South Africa. Report of the 23rd session of the International Geological Conference. In: Proceedings of Symposium II on mineral and thermal waters of the world, B - overseas countries. *Academia, Prague*, 19, 143-164.

Kumaresan, M. and Riyazuddin, P. 2006. Major ion chemistry of environmental samples around suburban of Chennai city. *Current Science*, 91 (12), 1668.

Lahaye, Y., Arndt, N., Byerly, G., Chauvel, C., Fourcade, S. and Gruau, G. 1995. The influence of alteration on the trace-element and Nd isotopic compositions of komatiites. *Chemical Geology*, 126, 43–64.

Lamoreaux, P.E. and Tanner, J.T. (editors) 2001. Springs and Bottled Waters of the World: Ancient History, Source, Occurrence, Quality and Use. Accessed at: https://doi.org%2F10.1007%2F978-3-642-56414-7.

Lavina, B., Przemyslaw, D. and Robert, D. 2014. Modern X-ray Diffraction Methods in Mineralogy and Geosciences. *Reviews in Mineralogy and Geochemistry,* 78 (1), 1–31. Accessed at: https://doi.org/10.2138/rmg.2014.78.1.

Lloyd, J. W. and Heathcote, J. A. 1985. Natural inorganic hydrochemistry in relation to groundwater: an introduction. Oxford [Oxfordshire]: New York: Clarendon Press; *Oxford University Press.*

Masindi, V. 2016. A novel technology for neutralizing acidity and attenuating toxic chemical species from acid mine drainage using cryptocrystalline magnesite tailings. *Journal of Water Processing and Engineering*, 10, 67–77.

Mbedzi, A. 2014. Investigation of the Mode of Magnesite Mineralisation within the Host Rocks at Folovhodwe Mine, Limpopo Province, South Africa.

McCourt, S. and Van Reenen, D.D. 1992. Structural geology and tectonic setting of the Sutherland greenstone belt, Kaapvaal Craton, South Africa. *Precambrian Research*, 55(1-4), 93–110. Accessed at: https://doi.org/10.1016/03019268(92)90017I.

Mhlongo, S. and Amponsah-Dacosta, F. 2014. Assessment of Safety Status of Open Excavations and Water Quality of Pit Lake at Abandoned Nyala Mine in Limpopo Province of South Africa. *Published in An Interdisciplinary Response to Mine Water Challenges - Sui, Sun & Wang, editors, China University of Mining and Technology Press*, *Xuzhou*, 395–399.

Michael, G. and Carey, W. 1989. A Preliminary Appraisal of the Mineral Potential of Venda Based on a Reconnaissance Geochemical Soil Sampling Survey and Literature Review. *Rhodes University*, 266.

Möller, P. 1989. Magnesite: geology, mineralogy, geochemistry, formation of Mg-carbonates*. Publisher Gebrüder Borntraeger*, 300.

Murphy, C.P. 1986. Thin section preparation of soils and sediments. *Publisher A.B. Academic*. 1, 181-182. Accessed at: https://doi.org/10.1002/jqs.3390010207.

Narayanan, M. and Devarajan, N. 2011. Assessment of Physiochemical and Heavy Metals. *Electronic Journal of Environmental, Agricultural and Food Chemistry*, 10(11), 3076-3082.

Nham, T.T. 1991. Analysis of potable water for trace elements by ICP-AES. Agilent Technologies.

Olivier, J., van Niekerk, H.J. and van der Walt, I.J. 2008. Physical and chemical characteristics of thermal springs in the Waterberg area in Limpopo Province, South Africa. *Water South Africa*, 34(2), 163-174.

Parente, C.V., Ronchi, L.H., Sial, A.N., Guillou, J.J., Arthaud, M.H., Fuzikawa, K. and Veríssimo, C.U.V. 2004. Geology and geochemistry of Paleoproterozoic magnesite deposits (~1.8Ga), state of Ceará, northeastern Brazil. *Carbonates and Evaporites*, 19(1), 28–50. Accessed at: https://doi.org/10.1007/BF03175194.

Piper, A.M. 1944. A graphic procedure in the geochemical interpretation of water analyses. *American Geophysical Union Transactions*, 25, 914–928.

Paul, R., Guest, R. and Nel, P. 1997. The Mintek small mine case study - Venmag. *Journal of the South African Institute of Mining and Metallurgy*, 97(1), 1–6.

Ramulwela, N., Ramudzuli, V.K., Mudzuli, T., Nageli, M.R., Nemukomlome, M.R. and Manager, R. 2013. Five-year Strategic Plan for the Nwanedi Nature Reserve, Limpopo Province, South Africa.

Rindl, M.R. 1916. The Medicinal Springs of South Africa (Supplement). *South African Journal of Science,* (13), 528-552.

Rollinson, H.R. and Lowry, D.L. 1992. Early basic magmatism in the evolution of the North Marginal Zone of the Archean Limpopo belt. *Precambrian Research, 55,* 33-45. Accessed at: https://doi.org/10.1016/0301-9268(92)90012-D.

Radwan, A.M., Osman, R.M. and Abu-El-Naga, H. 2011. Characteristics of Building Bricks Made from Altered Basalt and De-Aluminated Kaolin. *InterCeram: International Ceramic Review*, 60 (2), 130-133.

Kumar, S.P.J. 2013. Interpretation of groundwater chemistry using Piper and Chadha´s diagrams: a comparative study from perambalur taluk. *Elixir Geoscience* 54. 12208-12211.

SASV. South African Screening Values. 2007. Framework for the management of contaminated land.

Scott, H.P. 2013. Magnesite Formation from MgO and $CO_2$ at the Pressures and Temperatures of Earth's Mantle. *American Mineralogist*, 98(7), 1211–18. Accessed at: https://doi.org%2F10.2138%2Fam.2013.4260.

Shackley, M.S. 2018. X-Ray Fluorescence Spectrometry (XRF). In The Encyclopedia of Archaeological Sciences, S.L. López Varela, editors. Accessd at: https://doi.org/10.1002/9781119188230.saseas0620.

Shand, M.A. 2006. The Chemistry and Technology of Magnesia. 304. Wiley. ISBN: 978-0-471-65603-6.

Sibanda, Z., Amponsah-Dacosta, F. and Mhlongo, S.E. 2013. Characterization and evaluation of magnesite tailings for their potential utilization: A case study of Nyala magnesite mine, Limpopo Province of South Africa. *ARPN Journal of Engineering and Applied Sciences*, 8, 1–20.

Singo, N.K. 2013. An Assessment of Heavy Metal Pollution near an old Copper Mine Dump in Musina, South Africa. (MSc in Environmental Management submitted to the University of South Africa).

South African Weather Services, 2017. Seasonal Climate Watch February to June 2017. 9(3), 23.

Strydom, J.H. 1998. Magnesite. In: The Mineral Resources of South Africa*:* Handbook (sixth edition)*.* M.G.C. Wilson and C.R. Anhaeusser (editors)*. Publisher Council for Geoscience.* 16*,* 447–449.

Van Reenen, D.D., Roering, C., Ashwal, L.D. and De Wit, M.J. 1992. The Archean Limpopo granulite belt: Tectonics and deep crustal processes. *Precambrian Research,* 55, 587.

Van Zyl, J.S., Broadman, L.G., Brandt, J.W. and De Villiers, J. 1942. Magnesite in the Union of South Africa: *Memorandum Geological Survey Africa*, 38.

Vearncombe, J.R., Cheshire, P.E., de Beer, J.H., Killick, A.M., Mallinson, W.S., McCourt, S. and Stettler, E.H. 1988. Tectonophysics: Structures related to the Antimony Line, Murchison Schist Belt, Kaapvaal Craton, South Africa. 154, 285-308. Accessed at: https://doi.org/10.1016/0040-1951(88)90109-6.

Viljoen, R.P. and Viljoen, M.J. 1969. The geological and geochemical significance of the upper formations of the Onverwacht Group. *Specification Publication Geological Society South Africa*, 2, 113–151.

Visser, D.J.L. 1989. The Geology of the Republics of South Africa, Transkei, Bophuthatswana, Venda and Ciskei and the Kingdoms of Lesotho and Swaziland. *Department of Mineral and Energy, Pretoria, South Africa*.

Walraven, F., Armstrong, R.A. and Kruger, F.J. 1990. A chrono-stratigraphic framework for the north-central Kaapvaal Craton, Bushveld Complex and Vredefort Structure, South Africa. *Tectonophysics*, 171, 23–48.

Wang, H., Zhao, Q., Zeng, D., Hu, Y. and Yu, Z. 2015. Remediation of a Magnesium-contaminated soil by chemical amendments and leaching. *Land Degradation & Development*, 26(6). Accessed at: https://doi.org%2F10.1002%2Fldr.2362.

Wei, Z., Wang, D., Zhou, H. and Qi, Z. 2011. Assessment of soil heavy metal pollution with Principal component analysis and Geoaccumulation index. *In: Procedia Environmental Sciences*, 10(C), 1946-1952.

Wilke, D.O. 1965. Magnesite deposits north of Soutpansberg, Transvaal. *Bulletin, Geological Survey of South Africa*, 55.

Wilson, M.G.C. and Anhaeusser, C.R. 1998. The Mineral Resources of South Africa. In: *Handbook, Council for Geoscience,* 16, 447– 448.

WHO. World Health Organisation. 2007. Health risks of heavy metals from long-range transboundary air pollution.

Zachmann, D. and Johannes, W. 1989. Cryptocrystalline Magnesite. Magnesite. Geology, Mineralogy, Geochemistry, Formation of Mg-Carbonates, 15–28.

# APPENDIX A: TERNARY CALCULATIONS

A ternary diagram is ideally suited for a three-component system. However, rocks are complex chemical systems, containing 10 to 13 components. Nevertheless, ternary diagrams can be constructed for any rock by making some assumptions. Clearly, the usefulness of the ternary diagram will depend on the validity of these assumptions. It is, therefore, necessary to first identify the compositional group to which the rock in question belongs, make your assumptions and select the type of compositional ternary to be used.

For this study, the AFM ternary diagram was used to calculate the wt% of the mafic and ultramafic rocks in order to classify those in terms of MgO, FeO and $Al_2O_3$. The AFM diagram is used to represent the phase relations in igneous rocks, i.e., the mineralogical content of the ultramafic and mafic rocks obtained from the Tshipise area. Mathematically this can be expressed as follows:

**A= $Al_2O_3$ F= FeO M= MgO.**

Ternary diagram for AFM

**A** = [$Al_2O_3$] **F** = [FeO] **M** = [MgO]

**Ultramafic rocks**

**VR1 SAMPLE**

**A** = 9.30

**F** = 8.90

**M** = 12.30

**Total:** (A + F + M) = 30.50

Plotting values:

**A:** 9.30/30.50 x 100 = **30.49**

**F:** 8.90/30.50 x 100 = **29.18**

**M:** 12.30/30 x 100 = **40.33**

**VR2 SAMPLE**

**A** = 4.16

**F** = 7.10

**M** = 24.75

**Total:** (A + F + M) = 36.01

**A** = 4.16/36.01 x 100 = **11.55**

**F** = 7.10/36.01 x 100 = **19.71**

**M** = 24.75/36.01 x 100 = **68.73**

**FR1 Sample**

**A** = 6.68

**F** =5.99

**M** =16.97

**Total:** (A + F + M) = 29.64

**A** = 6.68/29.64 x 100 = **22.54**

**F** = 5.99/29.64 x 100 = **20.21**

**M** = 16.97/29.64 x 100 = **57.25**

**FR2 SAMPLE**

**A** = 4.20

**F** = 6.70

**M** = 10.90

**Total:** (A + F + M) = 21.80

**A** = 4.20/21.80 X 100 = **19.27**

**F** = 6.70/21.80 x 100 = **30.73**

**M** = 10.90/21.80 x 100 = **50.00**

**NR1 sample**

**A** = 7.90

**F** = 5.97

**M** = 16.10

**Total:** (A + F + M) = 29.97

**A** = 7.90/29.97 x100 = **26.35**

**F** = 5.97/29.97 x 100 = **19.92**

**M** = 16.10/29.97 x 100 = **53.72**

**NR2 Sample**

**A** = 8.48

**F** = 7.09

**M** = 15.80

**Total:** (A + F + M) = 31.37

**A** = 8.48/31.37 x 100 = **27.03**

**F** = 7.09/31.37 x 100 = **22.60**

**M** = 15.80/31.37 X 100 = **50.37**

**Dolerite samples**

**VR3 Sample**

**A** = 11.60

**F** = 6.44

**M** = 3.11

**Total:** (A + F + M) = 21.15

**A** = 11.60/21.15 x 100 = **54.85**

**F** = 6.44/21.15 x 100 = **30.45**

**M** = 3.11/21.15 x 100 = **14.70**

**FR3 sample**

**A** = 10.92

**F** = 5.30

**M** = 3.61

**Total:** (A + F + M) =19.83

**A** = 10.92/19.92 x 100 = **54.81**

**F** = 5.30/19.92 x 100 = **26.61**

**M** = 3.61/19.92 x 100 = **18.12**

## APPENDIX B: PALEOSTRESS ANALYSIS USING THE WINTENSOR PROGRAM DEVELOPED BY DELVAUX, 2012

Win-Tensor is the Windows version of the Tensor program (Win-Tensor) developed originally in DOS. The program has been developed in order to meet the needs of field geologists active in brittle fault analysis and paleostress reconstructions, an emerging standard method in structural geology. The program uses the Right-Dihedral method, followed by the Rotational Optimization. The following figures illustrate the procedure.

The data digitization and processing sheet

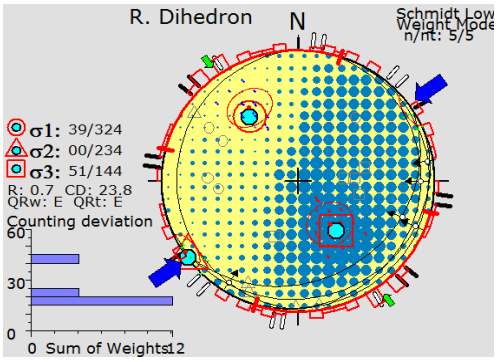


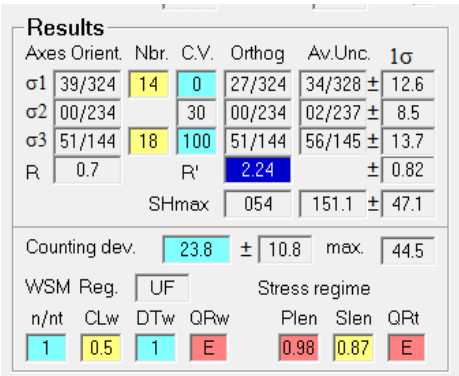


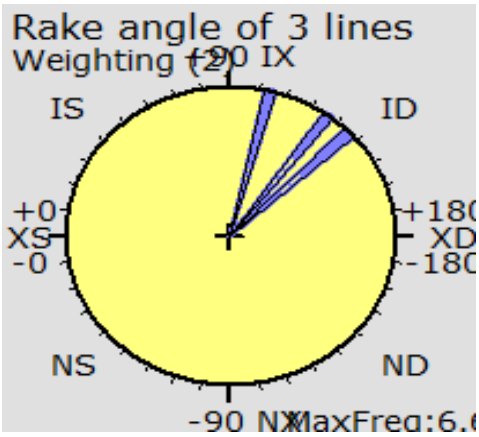

# APPENDIX C: COORDINATES OF SOIL, WATER, ORE AND ROCK SAMPLING SITES

| Soil Samples | | |
|---|---|---|
| **Sample ID** | **Y** | **X** |
| **S1** | -22.594 | 30.427 |
| **S2** | -22.593 | 30.427 |
| **S3** | -22.594 | 30.425 |
| **S4** | -22.596 | 30.425 |
| **S5** | -22.596 | 30.427 |
| **S6** | -22.595 | 30.429 |
| **S7** | -22.593 | 30.43 |
| **S8** | -22.591 | 30.429 |
| **S9** | -22.59 | 30.428 |
| **S10** | -22.593 | 30.425 |
| **S11** | -22.595 | 30.422 |
| **S12** | -22.596 | 30.422 |
| **S13** | -22.597 | 30.424 |
| **S14** | -22.597 | 30.426 |
| **S15** | -22.595 | 30.429 |

Venmag Mine Soil and Waste rock dumps sampling position

| Water samples | | |
|---|---|---|
| **Sample ID** | **Y** | **X** |
| W01 | -22.591 | 30.427 |
| W02 | -22.591 | 30.427 |
| W03 | -22.59 | 30.421 |
| W04 | -22.59 | 30.421 |
| W05 | -22.591 | 30.419 |
| W06 | -22.591 | 30.419 |
| W07 | -22.589 | 30.422 |
| W08 | -22.589 | 30.422 |
| W09 | -22.586 | 30.422 |
| W10 | -22.586 | 30.422 |

Venmag Mine and Nwanedi River water sampling points (Google coordinates)

| Rock Samples | | |
|---|---|---|
| **Sample ID** | **Y** | **X** |
| **VR1** | -22.592 | 30.427 |
| **VR2** | -22.594 | 30.425 |
| **VR3** | -22.596 | 30.425 |
| **FR1** | -22.3021 | 30.2210 |
| **FR2** | -22.3022 | 30.2211 |
| **FR3** | -22.30.19 | 30.2218 |
| **NR1** | -22.3142 | 30.3750 |
| **NR2** | -22.3148 | 30.3742 |
| **NR3** | -22.3140 | 30.3754 |

Tshipise rocks sampling points

| Magnesite Ore Samples | | |
|---|---|---|
| **Samples ID** | **Y** | **X** |
| **VM1** | -22.594 | 30.427 |
| **FM1** | -22.596 | 30.422 |
| **NM1** | -22.594 | 30.429 |

Tshipise magnesite ore sampling points

## APPENDIX D: EQUATIONS USED TO ESTIMATE ORE RESERVES

The following equations were used to estimate the ore reserves at the Venmag Mine. Equation variables include volume, area, height, tonnage, the density of waste, total tonnage, dump tonnage, pit tonnage, estimated tonnage (dump recovery as well as total mining area), the density of magnesite, total mining tonnage and mineralisation of magnesite (Abzalov, 2016).

1. *Volume = Area X Height*
2. *Tonnage = Volume X Density of waste*
3. *Total Tonnage = Dump Tonnage + Pit tonnage*
4. *Estimated tonnage (Dump recovery) = Dump tonnage X Density of Magnesite*
5. *Estimated tonnage (Total mining area) = Volume (50 m) X Density of Magnesite*
6. *Estimated ore resource = Total mining tonnage X Mineralisation Magnesite*

## Calculation of estimated ore reserve at Venmag Mine

| Venmag Dump | Area (m2) | Height (m) | Volume (m3) | Specific Gravity | Tonnages (t) | Waste 2% | Magnesite (t) |
|---|---|---|---|---|---|---|---|
| Dump 1 | 15 909 | 7 | 111 363 | 1,78 | 198 226 | 2 | 99 113 |
| Dump 2 | 2 130 | 5 | 10 650 | 1,78 | 18 957 | 2 | 9 479 |
| **Subtotal** | **18 039** | | **122 013** | | **217 183** | | **108 592** |
| Dump 3 | 1 578 | 3 | 4 734 | 1,78 | 8 427 | 2 | 4 213 |
| Dump 4 | 1 232 | 5 | 6 160 | 1,78 | 10 965 | 2 | 5 482 |
| **Subtotal** | **2 810** | | **10 894** | 1,78 | **19 391** | 2 | **9 696** |
| Dump 5 | 2 123 | 5 | 10 615 | 1,78 | 18 895 | 2 | 9 447 |
| Dump 6 | 1 678 | 5 | 8 390 | 1,78 | 14 934 | 2 | 7 467 |
| **Subtotal** | **3 801** | | **19 005** | | **33 829** | | **16 914** |
| **Grand Total** | **24 650** | | **151 912** | | **270 403** | | **135 202** |

## Calculation of estimated ore reserve at Folovhodwe Mine

| Folovhodwe Mine | Area (m2) | Depth (m) | Volume (m3) | Specific Gravity | Tonnages (t) | Waste 2% | Magnesite Resource (t) | Virgin 6,5% | Magnesite Resource (t) |
|---|---|---|---|---|---|---|---|---|---|
| Dump1 | 15 607 | 5 | 78 035 | 1,78 | 138 902 | 2 | 69 451 | 6,5 | 10 685 |
| Dump2 | 7 790 | 5 | 38 950 | 1,78 | 69 331 | 2 | 34 666 | 6,5 | 5 333 |
| **Subtotal** | **23 397** | | **1 098 020** | | **208 233** | | **104 117** | | **16 018** |
| Pit 1 | 15 280 | 20 | 305 600 | 2,98 | 910 688 | 2 | 455 344 | 6,5 | 70 053 |
| Pit 2 | 12 585 | 20 | 251 700 | 2,98 | 750 066 | 2 | 375 033 | 6,5 | 57 697 |
| Pit 3 | 28 446 | 20 | 568 920 | 2,98 | 1 695 382 | 2 | 847 691 | 6,5 | 130 414 |
| **Subtotal** | **56 311** | | **1 126 220** | | **3 356 136** | | **1 678 068** | | **258 164** |
| Virgin Ground to Mine | **60 682** | 30 | **1 820 460** | 2,98 | **5 424 971** | 2 | **2 712 485** | 6,5 | **417 305** |
| **Total Resources** | | | **4 044 700** | | **8 989 340** | | **4 494 670** | | **691 488** |

## Calculation of estimated ore reserve at Nyala Mine

| Nyala Mine | Area (m2) | Depth (m) | Volume (m3) | Specific Gravity | Tonnages (t) | Waste 2% | Magnesite Resources (t) | Virgin 6,5% | Magnesite Resources |
|---|---|---|---|---|---|---|---|---|---|
| Dump1 | 15 851 | 5 | 79 255 | 1,78 | 141 074 | 2 | 70 537 | 6,5 | 10 852 |
| Dump2 | 8 932 | 5 | 44 660 | 1,78 | 79 495 | 2 | 39 747 | 6,5 | 6 115 |
| **Subtotal** | **24 783** | | **123 915** | | **220 569** | | **110 284** | | **16 967** |
| **Mine pit** | | | | | | | | | |
| Pit 1 | 15 003 | 20 | 300 060 | 2,98 | 894 179 | 2 | 447 089 | 6,5 | 68 783 |
| Pit 2 | 21 904 | 20 | 438 080 | 2,98 | 1 305 478 | 2 | 652 739 | 6,5 | 100 421 |
| Pit 3 | 3 759 | 20 | 75 180 | 2,98 | 224 036 | 2 | 112 018 | 6,5 | 17 234 |
| **Subtotal** | **40 666** | | **813 320** | | **2 423 694** | | **1 211 847** | | **186 438** |
| Virgin Ground | 91 420 | 30 | **2 742 600** | 2,98 | **8 172 948** | 2 | **4 086 474** | 6,5 | **628 688** |
| **Total resources** | | | **3 679 835** | | **10 817 210** | | **5 408 605** | | **832 093** |

# APPENDIX E: RESOURCE MAPS (Adopted from Google Earth)

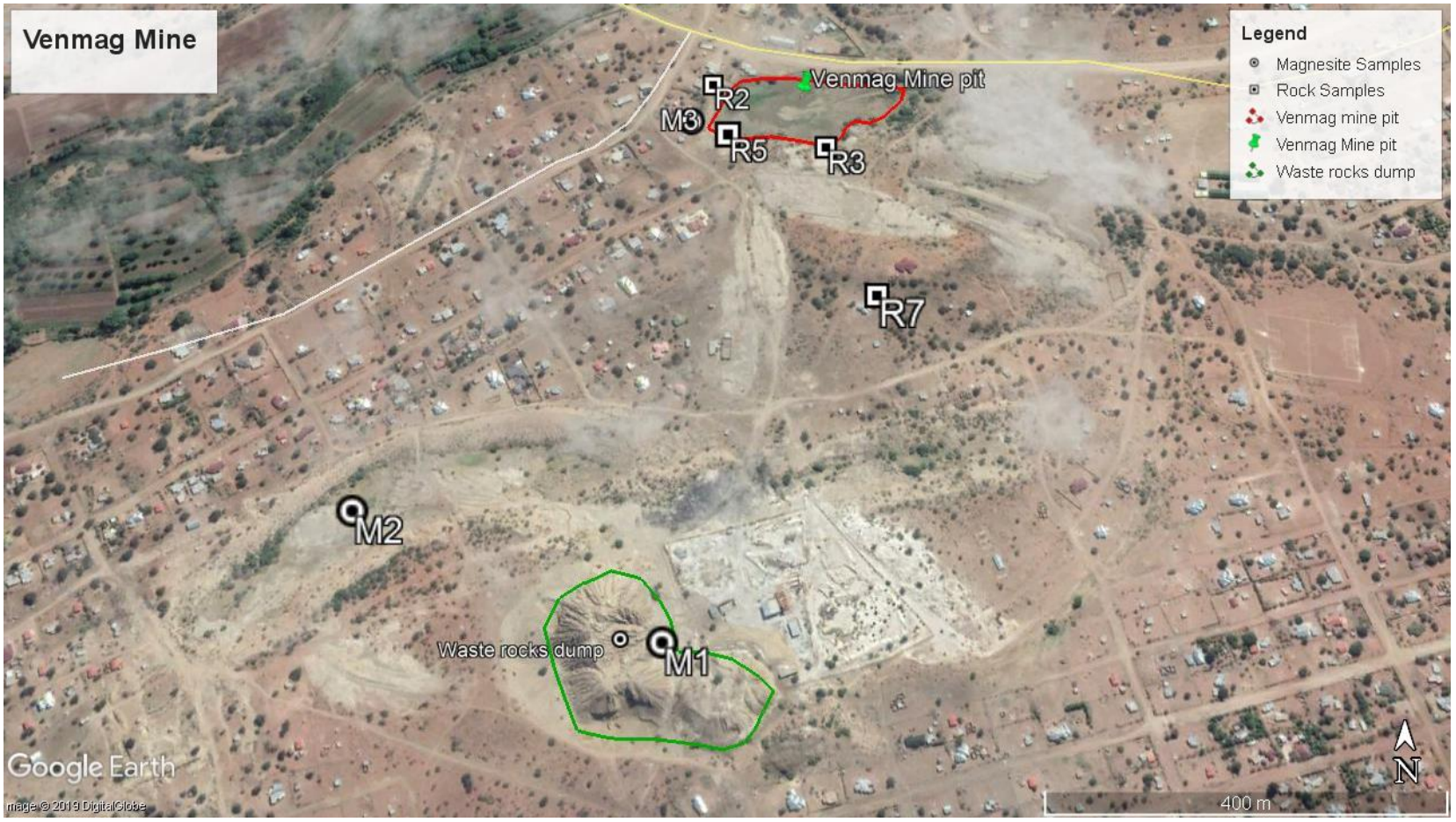


Venmag Mine

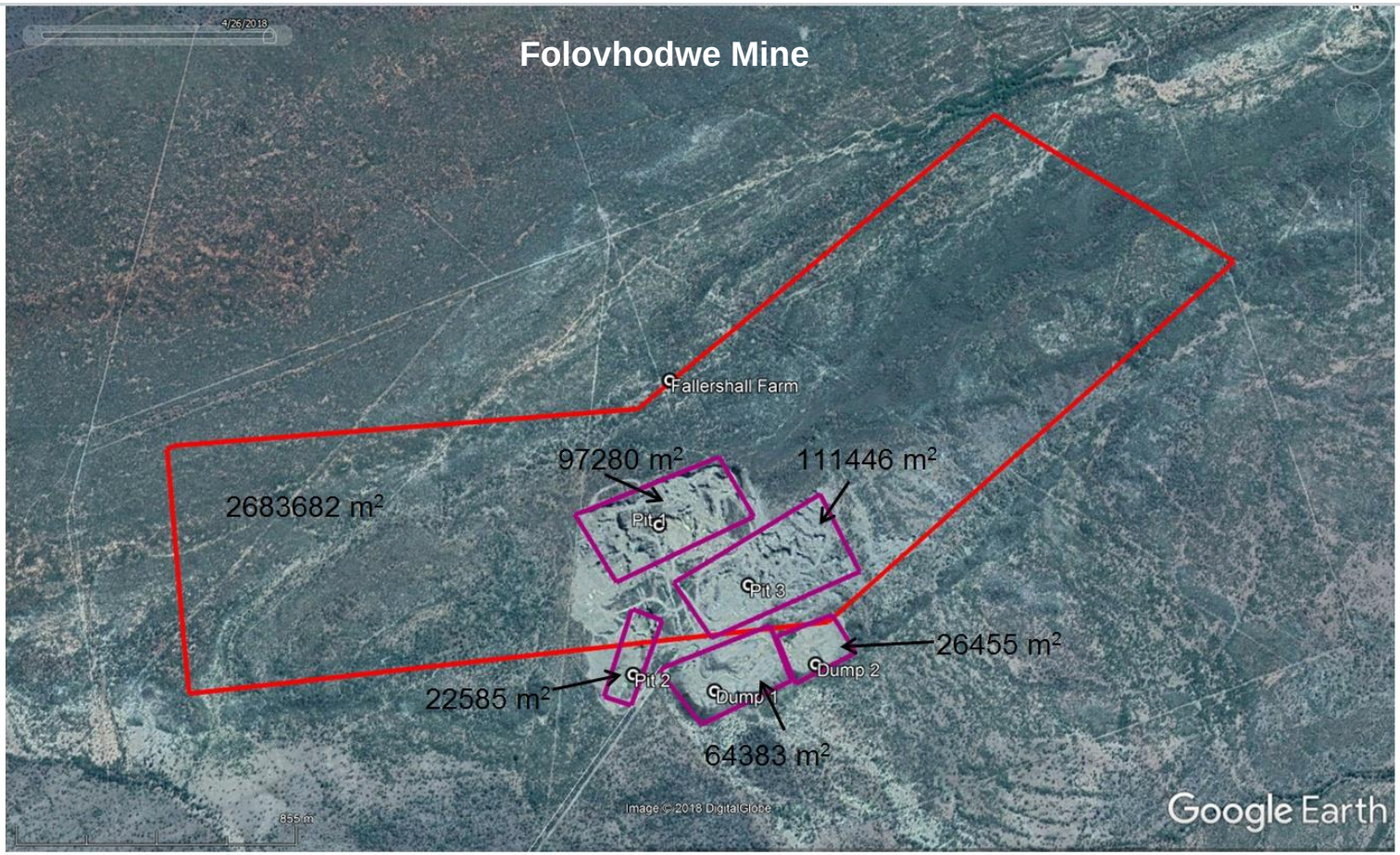


Folovhodwe Magnesite

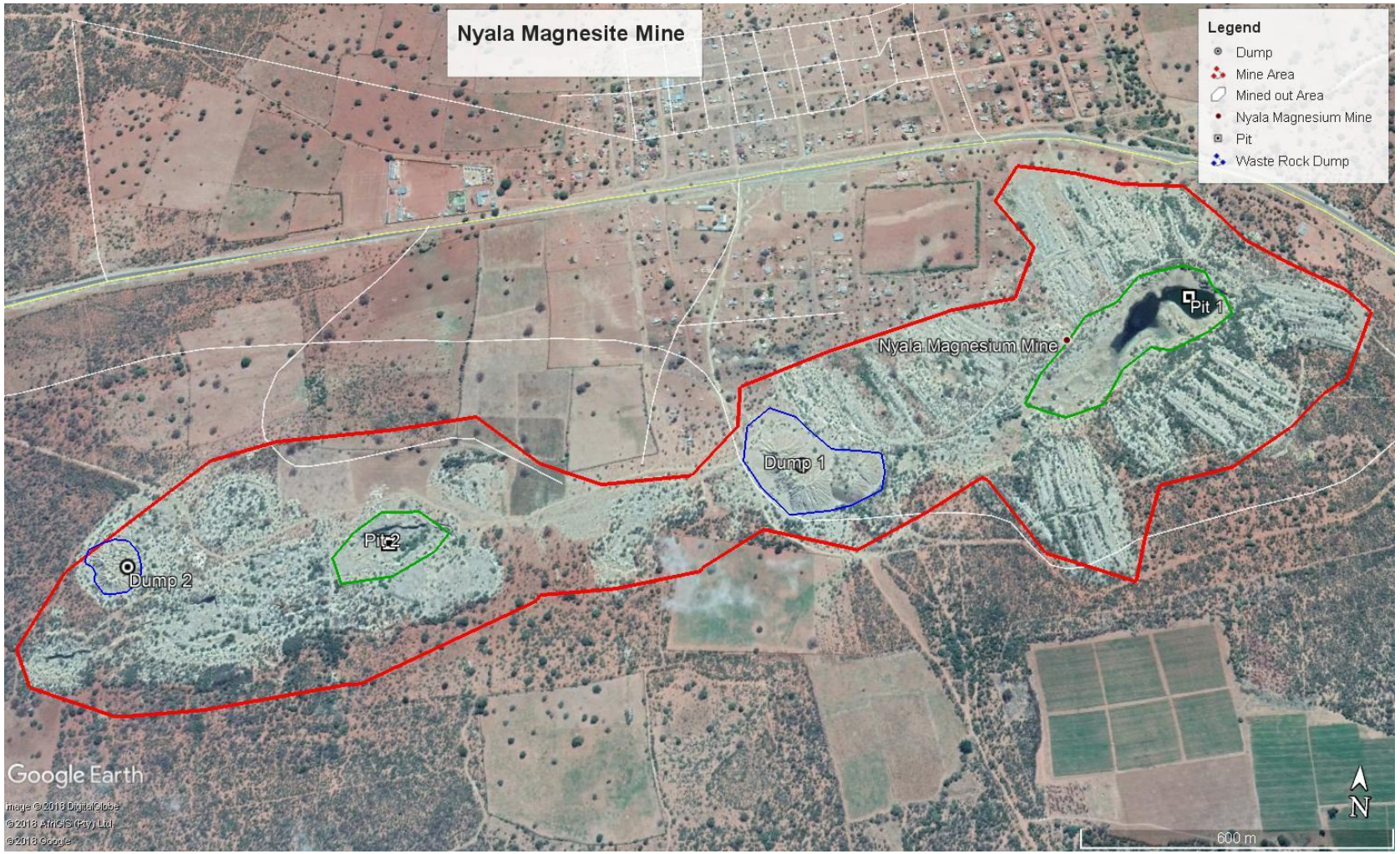


Nyala Magnesite

# APPENDIX F: CHEMICAL FORMULAE OF MINERALS

| | |
|---|---|
| **Dolomite** | $CaMg(CO_3)_2$ |
| **Augite** | $Ca(Mg,Fe)Si_2O_6$ |
| **Enstatite** | $(Mg,Fe)SiO_3$ |
| **Forsterite** | $(Mg,Fe)_2SiO_4$ |
| **Muscovite** | $KAl_2[AlSi_3O_{10}](OH)_2$ or $Al_2K_2O_6Si$ |
| **Goethite** | FeO.(OH) |
| **Lizardite** | $Mg_3Si_2O_5(OH)_4$ |
| **Magnetite** | $Fe_3O_4$ |
| **Plagioclase** | $(Na,Ca)(Si,Al).4O_8$ |
| **Magnesite** | $MgCO_3$ |
| **Smectite** | $(Na,Ca)_3(Al,Mg)_2Si_4O_{10}(OH)_2n(H_2O)$ |
| **Montmorillonite** | $MgNaAl_5(Si_4O_{10})_3(OH)_6$ or $Al_2H_2O_{12}Si_4$ |
| **Talc** | $Mg_3Si_4O_{10}(OH)_2$ |

## APPENDIX G: HYDROCHEMICAL FACIES DIAGRAMS

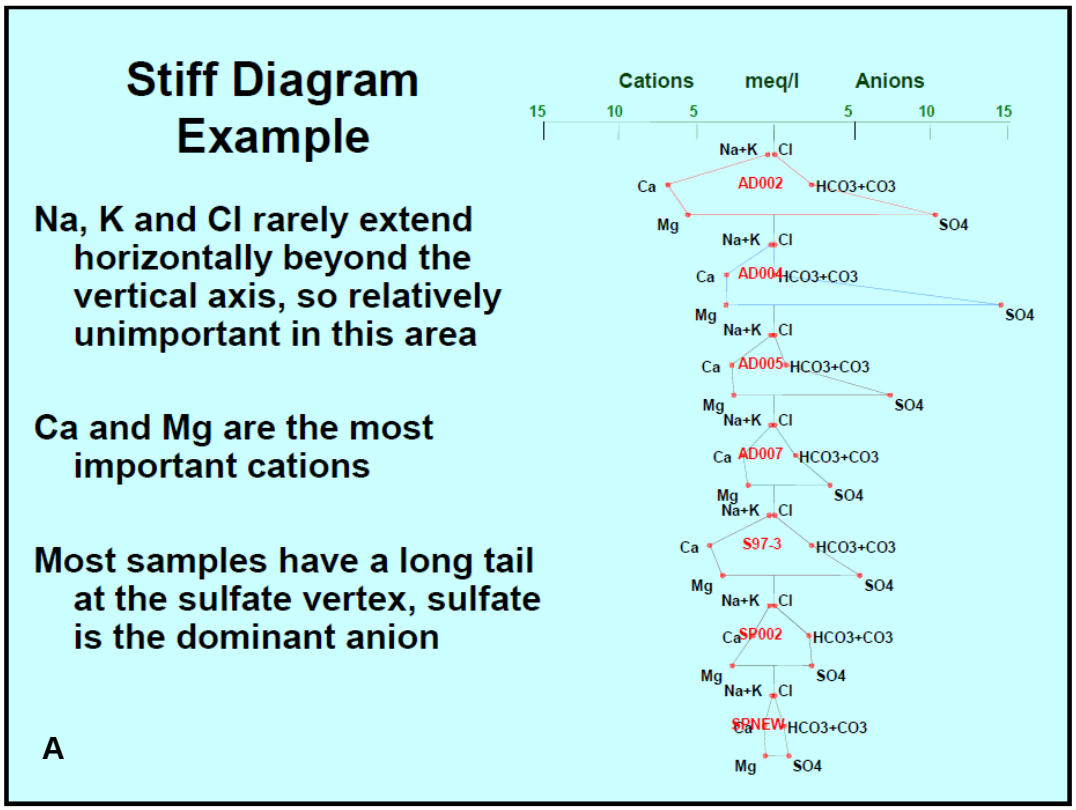


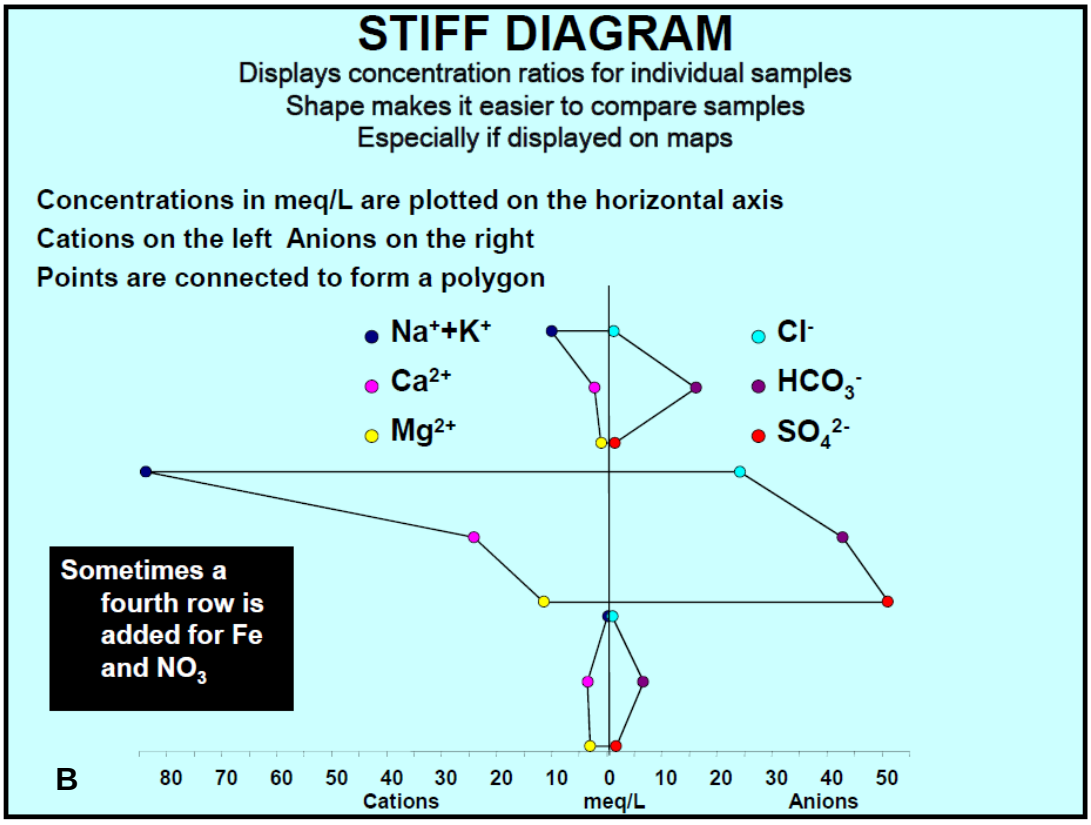


A-B: Stiff diagram adopted from water chemistry 2 documents

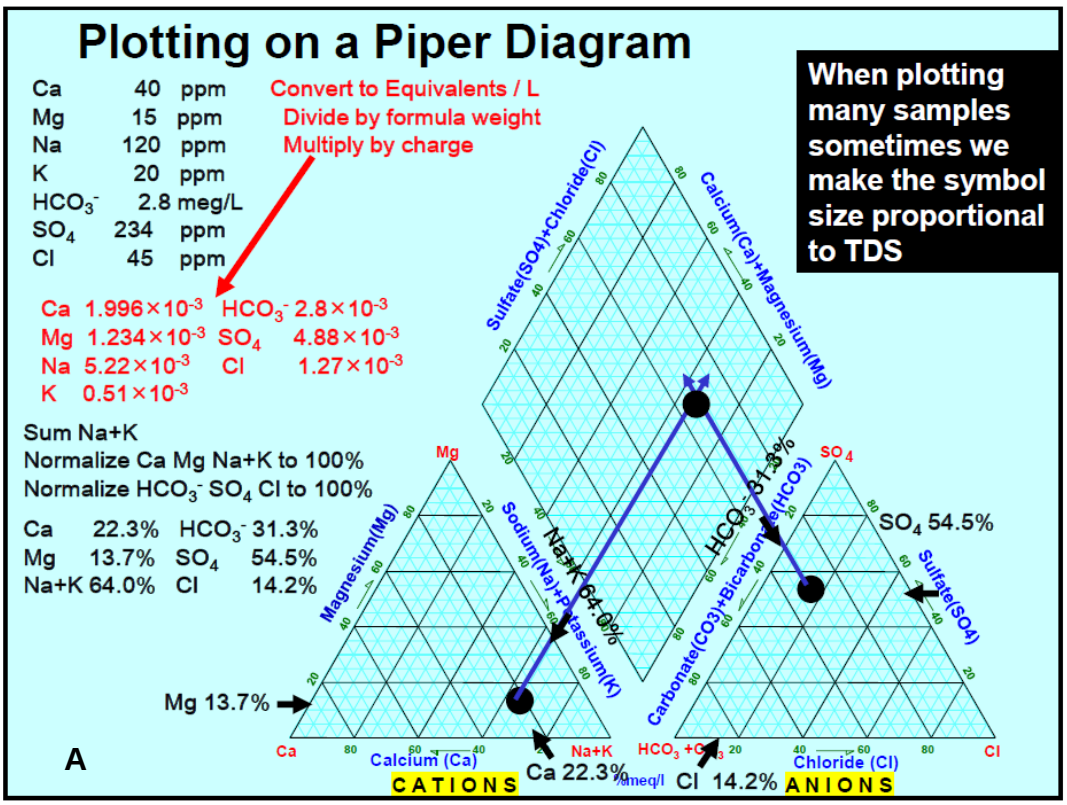


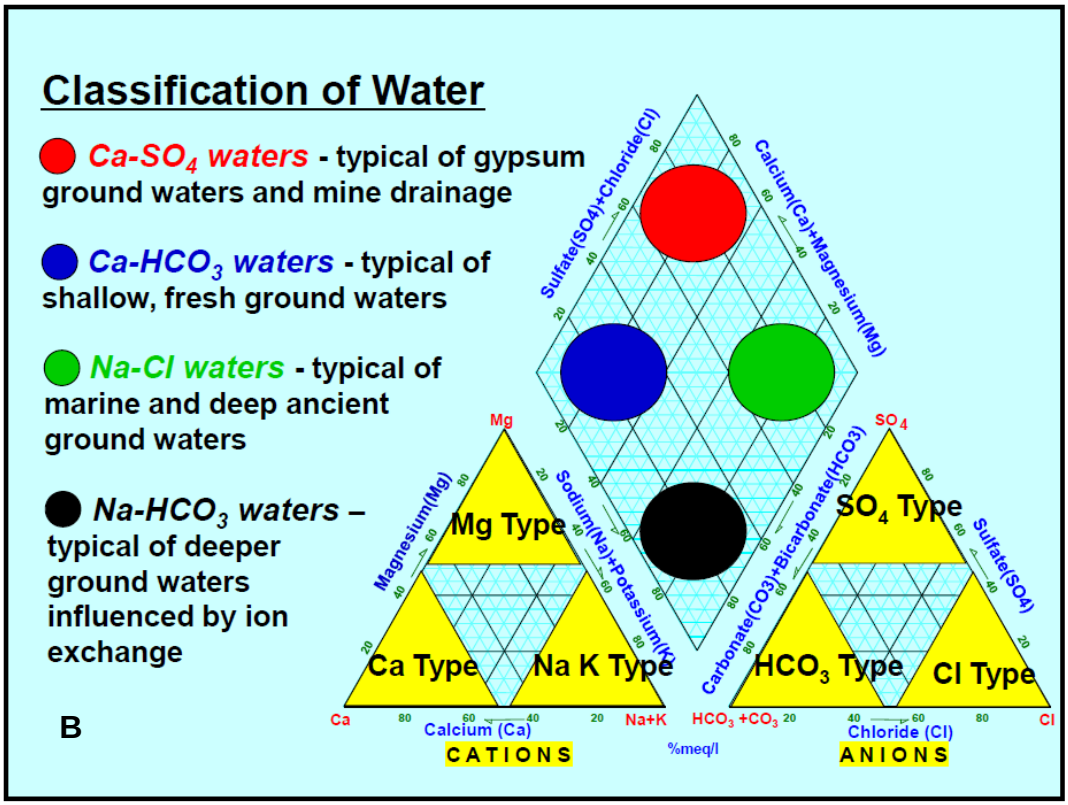


A-B: Piper diagrams adopted from water chemistry 2 documents